NTNU

Norwegian University of
Science and Technology

Application of Monte Carlo Simulation to Power System Adequacy Assessment

Øystein Stake Laengen

Master of Energy and Environmental Engineering
Submission date: June 2018
Supervisor: Vijay Vadlamudi, IEL

Norwegian University of Science and Technology
Department of Electric Power Engineering

Abstract

This thesis examines three Monte Carlo Simulation methods that can be used in power system reliability studies. Through application of the methods to both generation- and composite system adequacy assessment, an understanding of the methods was built. The field of probabilistic methods in power system reliability studies is a highly developed field with a lot of written material. However, it can be difficult for an inexperienced reader in the field to understand the small, but important, steps along the path for building Monte Carlo Simulation based applications for generation- and composite system adequacy assessment. Thus, the motivation for this thesis has been to present a transparent and detailed methodology for both levels of adequacy assessment.

The thesis elaborates on the details of obtaining power system adequacy indices through three fundamental Monte Carlo Simulation methods: state sampling, state duration and state transition methods. All the three simulation methods are applied to generation system adequacy assessment, while only the state sampling and the state transition methods are applied to composite system adequacy assessment. A detailed methodology on how to create a DC based contingency solver and an AC based contingency solver for composite system state evaluation, is also proposed in the thesis. The developed scripts created by implementation of the proposed methodology are tested on two test systems (Roy Billinton Test System and IEEE-Reliability Test System). Comparisons of three adequacy indices, viz. loss of load expectation, expected energy not served and loss of load frequency, are made against corresponding benchmark results from literature.

It was observed that the state sampling method provides estimates with a higher precision than the two sequential methods when equal sample sizes are used. The state sampling method, however, is unable to provide distributions of the indices. It was also observed that the state transition method requires less computation time than the two other methods to simulate a year.

A dependency for the bus indices on choice of load curtailment philosophy was observed in the study. The Roy Billinton Test System is found to be more reliable than the IEEE-Reliability Test System. It was also observed that the estimates of the latter's indices are more influenced by the choice of DC based or AC based system representation.

Sammendrag

Denne avhandlingen har undersøkt hvordan tre Monte Carlo simuleringsmetoder kan brukes til å utføre pålitelighetsstudier av kraftsystemer. Metodene ble implementert i pålitelighetsstudier av både kraftproduksjon alene og i kombinasjon med overføringsnettet. Det er skrevet mye litteratur om hvordan pålitelighetsstudier kan gjennomføres, men til tross for dette kan det være vanskelig å sette seg inn i temaet og forstå de grunnleggende detaljene som er nødvendig for å benytte metodene. Motivasjonen for å skrive denne oppgaven har derfor vært å identifisere disse detaljene, for videre å presentere metodologien på en transparent og detaljert måte.

I pålitelighetsstudiene av kraftproduksjonen ble det brukt tre Monte Carlo simuleringsmetoder; *state sampling*, *state duration* og state *transition*. I studiene der overføringsnettet er inkludert i analysene, ble kun to av metodene brukt; *state sampling* og *state transition*. Når overføringsnettet er inkludert i studiene, er det behov for et verktøy som kan analysere systemtilstandene. Avhandlingen presenter et forslag til to slike verktøy, der det ene er basert på DC lastflyt og det andre er basert på AC lastflyt. Programmene som ble utviklet gjennom arbeidet med avhandlingen er testet på to testsystemer. Disse er *Roy Billinton Test System* og *IEEE-Reliability Test System*. Resultatene fra testene er deretter sammenlignet med tilsvarende resultater fra andre studier.

Av de tre Monte Carlo metodene, leverer *state sampling* metoden estimater med høyere presisjon enn de to andre metodene gitt at prøvestørrelsen er lik (likt antall simuleringsår). *State sampling* metoden er imidlertid ikke i stand til å gi de underliggende fordelingene av pålitelighetsindeksene. *State transition* metoden bruker mindre tid på å simulere et år enn de to andre metodene.

Det ble også observert at pålitelighetsindeksene til en samleskinne var avhengige av prioriteten som en samleskinne har når laster i systemet må kuttes. Av de to test systemene ble det observert at *Roy Billinton Test System* er mer pålitelig enn *IEEE-Reliability Test System*. Pålitelighetsindeksene til *Roy Billinton Test System* er i tillegg mindre avhengige av om det er DC eller AC som brukes sammenliknet med *IEEE-Reliability Test System*.

Acknowledgement

I would like to express my greatest appreciation to my supervisor Associate Professor Vijay Venu Vadlamudi at the Department of Electric Power Engineering, NTNU, for valuable guidance and help during the last year. He has been a great source of inspiration and knowledge. Through him I have gained a solid foundation in the field of power system reliability. For that I am sincerely grateful.

Trondheim, 07 June 2018

Øystein Stake Laengen

Table of Contents

Abbreviations

CYPL	Constant Yearly Peak Load
CDF	Cumulative Distribution Function
CI	Confidence Interval
CV	Coefficient of Variation
DPL	Daily Peak Load
EENS	Expected Energy Not Served
FOR	Forced Outage Rate
HL	Hierarchical level
HPL	Hourly Peak Load
IEAR	Interrupted Energy Assessment Rate
RTS	IEEE-Reliability Test System
LDC	Load Duration Curve
LOEE	Loss of Energy Expectation
LOL	Loss of Load

LOLE	Loss of Load Expectation
LOLP	Loss of Load Probability
MTTR	Mean Time to Repair
MCS	Monte Carlo Simulation
OPF	Optimal Power Flow
PSR	Power System Reliability
RBTS	Roy Billinton Test System
SD	Standard Deviation
TRM	Transition Rate Matrix
TTF	Time to Failure
TTR	Time to Repair

List of Figures

List of Tables

1 Introduction

1.1 Background

Electric power utilities worldwide are under increased pressure, due to the society's increasing dependence on electric power and inclusion of renewable energy sources. From the end user point of view, the energy supply is expected to be continuously available. Increased reliability comes at an economic cost. Hence, the balancing between reliability and economic criteria, requires tools that are based on objective criteria. In history, deterministic criteria have commonly been used by electric power utilities and are still applied around the world. Such criteria, as the common N-1 security criterion, which says that a system should be able to operate within the limits in the event of an outage of any of its components, may lead to unnecessary redundancy in some parts of a power system, while overlooking critical parts of the system at the same time. Deterministic techniques are unable to capture the random nature of a power system that is significant for a system's reliability [1].

A lot of research has been performed on probabilistic methods, and the field is highly developed. The reliability indices, obtained by probabilistic methods, are quantitative and provide relevant information about the system behavior [2]. However, interpretation of numerical indices provided by probabilistic methods can be difficult, and consequently lead to a reluctant use as well as limited appreciation of the methods. There exist various probabilistic methods, where a division can be made between analytical and simulation based methods. Among the analytical methods, there are a variety of approaches, where the most common are the state space method, contingency enumeration method and minimal cut set method [3]. Analytical methods may require assumptions to simplify the problem when an analytical model of the system is established [4]. Complex system effects and system processes, that may be necessary to approximate when an analytical method is used, could in theory be incorporated in a simulation based method [5]. Most of the simulation based methods are normally based on Monte Carlo Simulation (MCS). The first example where the method is used seems to be by Buffon in the 18th century. Further on, the method had its revival during the second world war, where it was employed in the field of nuclear technology [6]. Later developments in computer resources led to an increased use of the method in other fields. One main advantage of using MCS, compared to analytical methods, is when the system of analysis is complex combined with a relatively large frequency of severe events [7].

The topic of MCS application to power system reliability (PSR) is highly developed and well described. However, it can be difficult for an inexperienced reader in the field to understand the small steps along the path which are necessary for building MCS based applications for generation- and composite system adequacy studies. Therefore, the underlying goal of this master thesis is to highlight these steps, with focus on pedagogical clarity. The steps might seem elementary for the experienced reader, however, the way they are presented in literature is cryptic in style. 'Seemingly troublesome' steps were identified and worked on to provide algorithmic clarity to the methods. In this way it is relatively easier for any power system engineer to replicate the results, while obtaining conceptual clarity to realize a suitable software implementation.

1.2 Contributions

The thesis builds on a specialization project undertaken during Autumn 2017, where the focus was of a detailed literature review on MCS as applied to the domain of PSR. Through extensive literature survey, a conceptual understanding of the fundamentals of power system adequacy assessment and the application of MCS to conduct adequacy studies was laid. The thesis work conducted during Spring 2018, has the main objective as summarized in the following problem statement:

Develop in-house software tools (MATLAB-based) as part of development of a comprehensive framework for conducting power system adequacy studies for generation systems and composite systems, using select-few Monte Carlo Simulation methods.

Adequacy for generation systems and composite systems has been quantified by the following metrics: Loss of Load Expectation (LOLE), Expected Energy Not Served (EENS), and Loss of Load Frequency (LOLF).

- The main investigation centers on how contingency analysis is embedded in the process of accumulating reliability indices (in the optimization subroutines) for composite systems. (Most literature does not clearly explain how the required optimization framework is developed.)
- As a starting point, for illustrative ease, DC optimal power flow (OPF) formulation and solution (linear programming-based) was used. Then an AC OPF formulation and

solution (non-linear programming-based) was used. Accordingly, DC OPF and AC OPF based contingency solvers have been developed.

- MCS was then employed, on the platform of MATLAB, where the developed contingency solvers have been suitably embedded into the process of obtaining the adequacy indices for generation systems and composite systems.
    - In-house programming scripts in MATLAB have been built, and their implementation aspects studied. The scripts have been released for further internal use and research at the Department of Electric Power Engineering, NTNU.
    - In principle, the scripts can be used to conduct adequacy analysis on any other test system. However, it must be pointed out that the focus was not on optimizing the software codes but just getting them to work 'reasonably' faster.
- The procedure for the application of MCS to obtain the various reliability indices has been clearly explained, with emphasis on pedagogical clarity and replicability.

  The application of the developed framework for standard reliability test systems has been investigated. Both Roy Billinton Test System (RBTS) and the IEEE-Reliability Test System (RTS) have been used to conduct generation adequacy studies and composite system adequacy studies.

1.3 Structure of Thesis

Chapter 1 – Introduction: provides the background and motivation behind the thesis work.

Chapter 2 – Conceptual Background: presents the essential concepts of the thesis and gives a brief introduction to reliability indices and MCS methods.

Chapter 3 – Methodological Approach: presents in detail the proposed methodology of the adequacy assessment used for the implementation of MATLAB scripts. Presented first is the illustration of the methodology of generation adequacy assessment, with simple examples, followed by the illustration of the methodology of composite assessment.

For establishing narrative clarity and with an aim to make this thesis a complete and independent unit in and of itself, much of the content from chapter 2 and some from chapter 3 is a replication of the specialization project work, with suitable extensions where deemed necessary.

Chapter 4 – Case Studies: applies the proposed methodology to both generation- and composite system adequacy studies, and presents and discusses the results obtained when the developed scripts are applied to two different test systems.

Chapter 5 – Conclusions: draws conclusions from the work done in the thesis and suggests future work.

2 Conceptual Background

2.1 Introduction

The methodology presented in this master thesis has its theoretical foundation in the PSR framework. When a system is analyzed, the term reliability denotes the system's ability to serve its required function under stated conditions for a given period of time [8]. Due to the complexity involved in PSR assessment, the framework can broadly be divided into two sub-domains, adequacy and security [4], [5], taking different aspects of the reliability analysis into consideration.

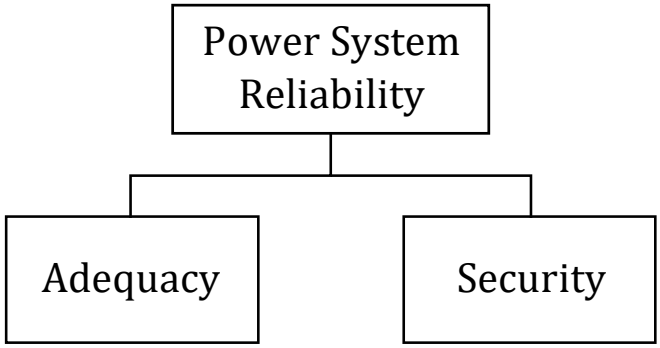

Figure 2.1: Power System Reliability.

The main difference between the two sub-domains is that adequacy studies relate to the static conditions of a system, while security assessment is associated with the dynamic aspects of a system. Adequacy assessment of a power system is in its simplest form an evaluation of whether the generation capacity of a system is sufficient to supply the load requirement of the system. Other considerations can also be included in the assessment, such as whether the transmission and distribution facilities of the system can provide sufficient energy transportation from the generating facilities to the end consumers.

Security assessment relates to the dynamic phenomena that are induced in the system whenever the system is exposed to various disturbances arising inside the system, e.g. line faults or loss of large generating units. Under such disturbances where transient effects are induced, it is of interest whether the system can remain inside its stability limits. In practice, these effects are also present whenever a system enters or departs from any system state. Adequacy studies usually ignore the associated effects and consider only whether the system's steady state requirements are fulfilled for each system state [5]. Both the departure state and the arriving state may be adequate states, but the transition itself may be essential in determining if the

arriving state is a temporary or static state. Hence, it can be argued that the separation in two domains are one of convenience and not one due to the practical system behavior [4]. In this master thesis, the aspects of dynamic security concept are not threated.

2.1.1 Hierarchical Levels

PSR studies are usually divided into hierarchical levels (HL), defined by which functional zones of the power system they include [5]. The first level, HLI, assesses the generation adequacy, while the second level, HLII, includes both generation and transmission facilities into the assessment. Complete system adequacy assessment, HLIII studies, includes the distribution facilities in addition to the two functional zones assessed in HLII studies. The main challenge associated with performing HLIII studies, is that the inclusion of distribution facilities creates large-scale models for most practical systems. However, this challenge is usually overcome by performing isolated studies on the distribution functional zone alone, to reduce the scale of the problem [5]. The focus of this master thesis is solely on the adequacy issues related to HLI and HLII. A representation of the functional zones with their division into HLs is shown in Figure 2.2.

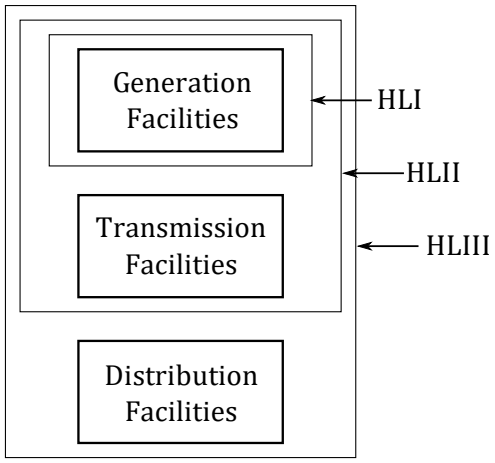

Figure 2.2: Hierarchical levels of the power system.

HLI studies are concerned with the system's generation facilities and their ability to supply the load requirement of the system. In these types of studies, the energy transporting capability of the system is left out of the analysis. A representation of the elements that are needed in a HLI model is shown in Figure 2.3, where the generating units of the system are combined into one equivalent model, and the loads are combined similarly. Various deterministic criteria have been and are still used by the electric utilities to assess the adequacy of a system. Among them are the N-1 contingency criterion and various percentage reserve capacity criteria [5]. The N-1

criterion states that the system should be able to handle the loss of the largest generating unit, while the percentage based criteria state that there should be a specified percentage reserve capacity in a system. These criteria fall under the category of deterministic criteria, because they relate to a "pre-determined" outcome in the case of contingencies. Criteria based on probabilistic methods have gained an increased interest, due to their reflection of actual factors influencing the system reliability [9]. In HLI studies the basic modelling approach is to combine the generation model and the load model to form a probabilistic risk model. The reliability indices of interest are evaluated by comparing the total generation capacity against the total load requirement [5].

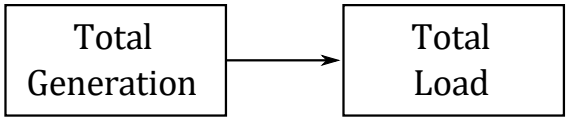

Figure 2.3: HLI model.

HLII studies include the network topology of the transmission system into the adequacy assessment. Hence, additional parameters are considered when the system is analyzed. Even though HLII studies are concerned with the adequacy of a system, steady-state security constraints like voltage limits of the load buses, P-Q buses, are normally included in the evaluation process [10]. It is also possible to obtain the bus indices in addition to the system indices at HLII, since a model of the network topology is included. However, assessment at this level is more cumbersome to perform, because the evaluation of system states involves some sort of load flow analysis. The load flow evaluation can lead to a large increase in computation time. There exist various techniques to overcome this time-consuming stage to improve the speed of the evaluation process. Among them are newer techniques based on the intelligent system methodology, where the system state vectors are classified by algebraic comparisons against pre-solved system state vectors, instead of solving each system state by OPF methods [11]. One suggested method is the use of Self-Organizing Maps in [12].

Two OPF approaches are considered in this thesis, one that is based on DC power flow and one that is based on AC power flow. The DC power flow approach simplifies the OPF problem because reactive power and voltage limit considerations are neglected. The benefit is that a linear OPF problem is obtained instead of the nonlinear OPF problem of an AC based approach. Thus, the optimization process is simplified and a reduction in computation time is achieved compared to the AC based OPF.

The probability based reliability methods can broadly be classified as analytical or simulation based methods. The analytical methods represent the system by a mathematical model, from which the reliability indices are calculated by solving an equation set. Various analytical methods exist, and among the more common are the state space method, contingency enumeration method and the minimal cut set method [3]. The state space method considers all possible system states when the system is assessed. If the size of the system is large, it will lead to a large quantity of system states to be analyzed. Thus, the method depends on simplifications like network reduction techniques, to limit the computational effort involved. The contingency enumeration method assesses only a selected number of contingencies, where it is common to determine a depth of contingencies depending on the desired level of accuracy. In the minimal cut set method, the focus is placed on calculation of the reliability indices at selected load points and not on the complete system. Thus, only contingencies that can affect the load points are evaluated, leading to a reduction in computation time.

The simulation methods, most often with a foundation in the MCS methodology, simulate a series of real experiments on the mathematical model representation of the system [13]. The simulation process can capture the random behavior of the system. In addition to providing average point values, the MCS methods can give distributions for the indices if the method of choice is sequential instead of non-sequential [14]. The sequential methods should also be chosen whenever the system-operation depends on history [13].

2.2 Reliability Indices

The probabilistic PSR indices that are commonly used today are based on loss of load (LOL) events in power systems. These events are associated with insufficient generation, at both HLI and HLII, and/or insufficient transfer capability of the transportation facilities at HLII. A generation model and a load model are needed to create a probabilistic risk model at both levels, while a HLII model is dependent on the inclusion of a network model. By combining the models, a probabilistic risk model as shown in Figure 2.4 for a HLII model, can be obtained. A HLI risk model is similar, only without the network model.

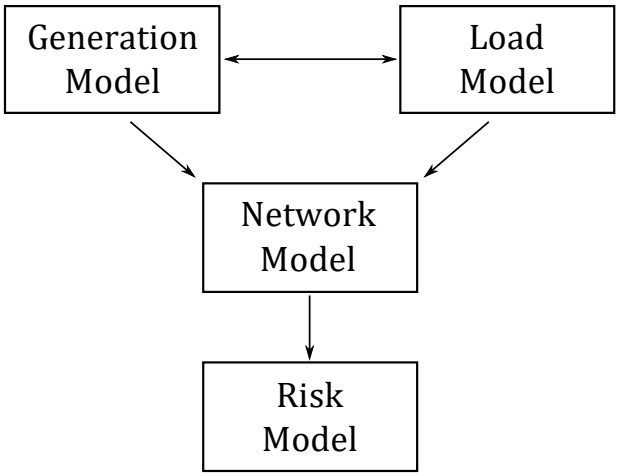

Figure 2.4: Probabilistic HLII risk model.

When PSR assessment is performed, it is usually advantageous to obtain a basic index and a severity based index. Basic indices reflect the frequency and durations of LOL events, but do not quantify the severity of LOL events. Severity based indices, on the other hand, reflect the severity of LOL events. Various indices are described in [4], [7], [15] and [16]. It is important to note, that the interpretation of a calculated index, is dependent on the choice of load model [17]. Common models that are used, are constant yearly peak load (CYPL), daily peak load (DPL) and hourly peak load (HPL) representations. This thesis has based the formulations of the selected indices, which are presented in the following, on the formulations presented in [7] and [16].

It is common to specify the LOLE in hours/year or days/year. A general mathematical representation of the index is given by:

$$\mathrm{LOLE}=\sum_{i\in S} p_i \cdot T \tag{2.1}$$

The index gives the expected number of time units in a period of study that will experience LOL. A system has several possible system states, each of which, has a probability, p_i, of occurrence. The set of system states that have LOL are denoted S. To calculate the index, a summation of the probabilities of the system states in set S is performed. The sum is then multiplied with the period of study T, which should be specified in number of time intervals per period depending on the choice of load model. Normal choices of T are days or hours per year. A days/year expectation is obtained by use of a DPL model, while an hours/year expectation is obtained by using a HPL model. It is worth noting that a direct conversion from

a days/year to an hours/year expectation value cannot be made, since they are obtained by using different load models [17].

This thesis uses MCS methods as tools for sampling the system states, where a system state is obtained for each time increment of a simulation year, and multiple years are simulated. The reliability indices are calculated for each simulation year, before the final indices are obtained as the averages of the yearly indices. Hence, (2.1) is given in a more suitable format:

$$\mathrm{LOLE}=\frac{\sum_{i=1}^{N}\left(\sum_{j=1}^{M} x_j \cdot \Delta t\right)}{N} \tag{2.2}$$

The number of conducted simulation years is given by N. A simulation year consists of M time increments, that are treated as trials by evaluating the time increment's system state. For each trial, there is an outcome, x_j, which is given by a one if a system state has LOL, and a zero if not. The duration of a time increment is denoted Δt. When the LOLE index is calculated, each outcome is multiplied with the duration of the time increment, before a summation of all the products is performed. The sum is then divided by the number of simulation years.

A probability based index is the loss of load probability (LOLP). In some applications, this is a "re-engineered" LOLP, which is obtained by dividing the LOLE index by the number of considered time increments per year. However, a general representation of the index, which is not re-engineered, is given by:

$$\mathrm{LOLP}=\sum_{i \in S} p_i \tag{2.3}$$

The index is calculated in a similar manner as the LOLE index, except that probabilities are not weighted with the period of study, i.e. it is given as the sum of probabilities of failure states. As for the LOLE index, a LOLP obtained by a DPL model may differ from a LOLP obtained by a HPL model. The only time an equal LOLP can be obtained is whenever the load requirement is constant through the period of study. This thesis uses the "re-engineered" LOLP' index, by simply dividing the LOLE index by the number of time increments, M, per year.

$$\mathrm{LOLP'}=\frac{\sum_{i=1}^{N}\left(\sum_{j=1}^{M} x_j \cdot \Delta t\right)}{N \cdot M} \tag{2.4}$$

A severity based index commonly used, is the EENS. This index is equal to the loss of energy expectation (LOEE) in HLI studies. The index is calculated in a similar manner as the LOLE index, except that the severity of the energy deficit, C_i, is included in the weighting of the probabilities. Hence, the mathematical expression is given by (2.5), where T must be given in hours per year to obtain a normal energy quantity.

$$\mathrm{EENS}=\sum_{i\in S} p_i \cdot C_i \cdot T \tag{2.5}$$

This thesis uses an expression, given in (2.6), for the calculation of an EENS index from the MCS samples. When the index is calculated, the outcomes of the trials are weighted by the severity of energy deficits and the duration of time increments. If a system state has no LOL, the energy deficit is zero.

$$\mathrm{EENS}=\frac{\sum_{i=1}^{N}\left(\sum_{j=1}^{M} x_j \cdot C_j \cdot \Delta t\right)}{N} \tag{2.6}$$

The last index used in this thesis, is the loss of load frequency (LOLF). It is a frequency based index, which gives the number of system failures per period of study. A new system failure should only be counted whenever the transition to a LOL state crosses the boundary between the set of healthy system states and the set of LOL states. The mathematical expression for the index is given in (2.7). It is defined as the "opposite transition", i.e. by the frequency of transitions from LOL states to healthy states.

$$\mathrm{LOLF}=\sum_{i\in S}\left(F_i - f_i\right) \tag{2.7}$$

In the above expression, F_i denotes the frequency of departures from any of the LOL states and f_i denotes the frequency of transitions where both the departure state and the arriving state are LOL states. Thus, only the transitions crossing the boundary between the two sets, divided into healthy states and LOL states, are counted. This thesis uses a suitable expression for the LOLF index as calculated from the MCS samples, as shown below.

$$\mathrm{LOLF}=\frac{\sum_{i=1}^{N} z_i(x_i, x_{i-1})}{N},\ z_i=\begin{cases} 1 \text{ if } (x_i=1)\cap(x_{i-1}=0) \\ 0 \text{ if } (x_i=1)\cap(x_{i-1}=1) \\ 0 \text{ if } (x_i=0)\cap(x_{i-1}=1) \\ 0 \text{ if } (x_i=0)\cap(x_{i-1}=0) \end{cases} \tag{2.8}$$

If a new system failure has occurred, the value of z_1 is set to one and zero otherwise. As defined in (2.8), the system failure is only counted whenever two conditions apply: when the system state of the time increment has LOL and the previous time increment has no LOL state.

2.3 Random Variables

An important element in the MCS methodology is the sampling of random numbers from various distributions. Due to the deterministic feature of computers, they are only able to provide pseudo random numbers, normally sampled from the uniform distribution with a range of [0, 1]. The simulations performed in this master thesis use the "rand" function of MATLAB. According to the documentation [18], MATLAB uses algorithms that ensure that the generated random numbers pass various statistical tests of randomness and independence. However, all random number generators will eventually fail a statistical test for randomness if the test is sufficiently specific, as they are based on deterministic algorithms. The effect, however, is unlikely to be larger than the sampling error of a MCS [18]. This thesis has used the Mersenne Twister generator for obtaining random numbers when a non-parallel MCS is performed [18], and the Combined Multiple Recursive generator when a parallel MCS scheme is applied [19]. Both are default generators of the "rand" function in MATLAB.

2.3.1 The Uniform Distribution

The uniform distribution is an essential element in the MCS methodology. It can be used to sample system states directly or as a starting point when random variates are sampled from other distributions. An illustration of a uniform distribution with range [0,1], is shown in Figure 2.5, where all intervals of equal lengths on the distribution's support have identical probabilities of occurrence.

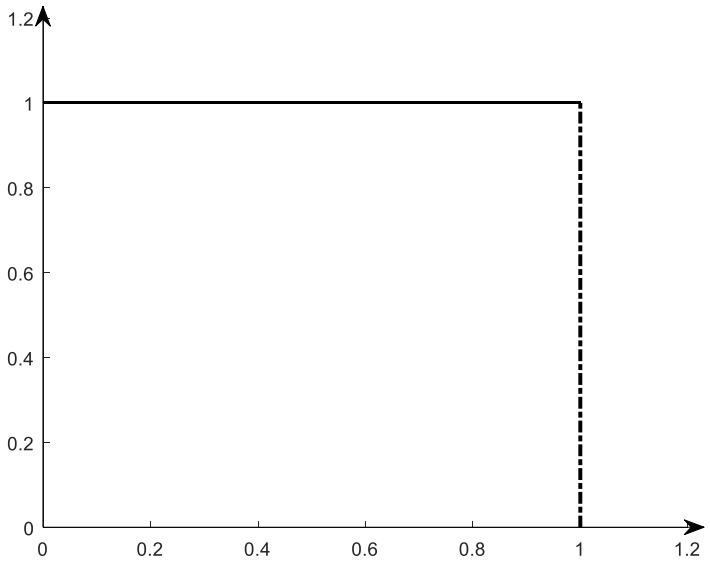

Figure 2.5: Uniform distribution.

2.3.2 The Exponential Distribution

Another probability distribution that is commonly used in reliability studies is the exponential distribution. The transition times, both time to failure (TTF) and time to repair (TTR), are often assumed to follow this distribution. A general expression for the distribution is given in (2.9), where the shape of the distribution depends on the rate parameter λ.

$$f(x) = \lambda \cdot e^{-\lambda \cdot x} \tag{2.9}$$

When a random variate is to be obtained from an exponential distribution, it is useful to obtain the distribution's cumulative distribution function (CDF). An important characteristic of the CDF is that the function value is monotonically increasing from zero to one. The CDF of the exponential function is obtained by integrating the function from zero to x.

$$F(X) = \int_0^x \lambda \cdot e^{-\lambda \cdot v} dv = 1 - e^{-\lambda \cdot x} \tag{2.10}$$

Setting (2.10) equal to U before it is solved for X, gives the inverse transform of the exponential CDF function.

$$X = F^{-1}(U) = -\frac{1}{\lambda} \cdot \ln(1 - U) = -\frac{1}{\lambda} \cdot \ln U \tag{2.11}$$

The distributions of U and (1-U) are equal when U is limited to a range from zero to one [7].

2.3.3 Inverse Transform Method

A random variate that follows another distribution than the uniform, cannot be obtained directly by a random number generator. Thus, there is a need for a method to generate it. An approach is to use the inverse transform method, which takes advantage of an important characteristic of CDFs. Since a CDF's value is monotonically increasing, it ensures that for each function value there exists only one variable value. The inverse transform method is illustrated graphically for an exponential distribution in Figure 2.6, and a stepwise presentation is made in the following.

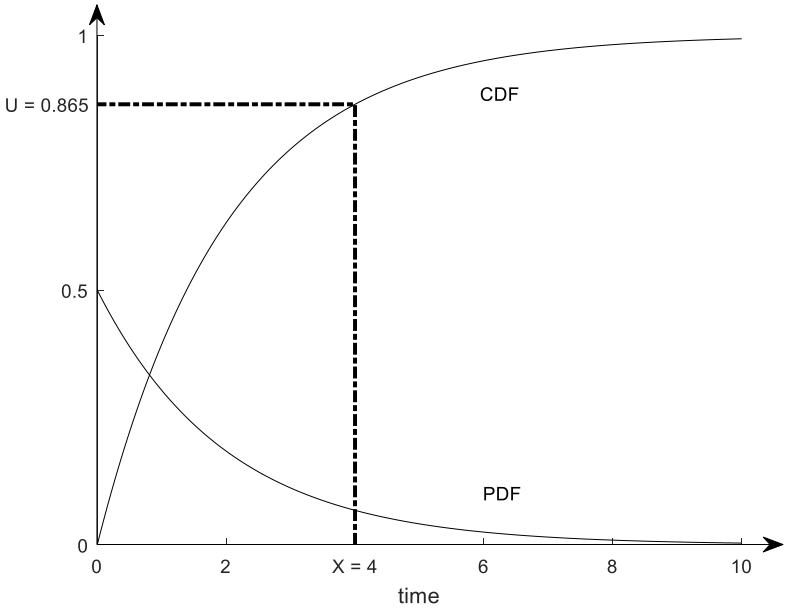

Figure 2.6: The inverse transform method.

The first step is to generate a random number, U, from a uniform distribution with range [0,1]. This value is then used to calculate a random variate, X, by (2.11). Graphically, the second step is equal to finding the value of U on the y-axis, then drawing a horizontal line from the point until the line intersects the CDF. A vertical line can then be drawn from the intersection until the line crosses the x-axis. The value of the x-axis at this point of crossing gives the value of the random variate X. In the example of Figure 2.6, a random number of 0.865 is generated and a corresponding random variate of 4 is obtained.

2.4 Monte Carlo Simulation Basics

In this master thesis, MCS is used as the tool for sampling the system states. There exist various MCS methods, which can be classified as non-sequential methods or sequential methods. Whereas a non-sequential MCS method samples a set of system states randomly, a sequential MCS method obtains a sequence of system states where each system state depends on the

previous system state. A system state is given by the combination of the individual components' states. Thus, a system state can be expressed as a state vector **S**, where the m state variables give the individual component's states.

$$\mathbf{S} = \{S_1 \quad S_2 \quad \ldots \quad S_m\} \tag{2.12}$$

A brief introduction to the three MCS methods used in this master thesis is provided in the following. The presentations of the methods are based on the approach of [7].

2.4.1 State Sampling

The state sampling method is non-sequential, which means that a sample is independent from both the preceding and the following samples. Each component that is a part of the system, has probabilities of being available or on outage, where the latter probability is denoted forced outage rate (FOR). The method obtains a system state sample by generating a random number [0,1] per component of the system. For each component, a comparison of the generated random number against the FOR is performed. If the random number is larger than or equal to the FOR value, the component is deemed available. Otherwise it is on outage, as shown in Table 2.1. The method can easily be extended to incorporate de-rated states, by splitting the range [0,1] into additional sub-intervals, as illustrated in Table 2.2.

Table 2.1: Component state probability, two states.

Unit State	Probability Table
Up	$U \geq FOR$
Down	$U < FOR$

Table 2.2: Component state probability, additional de-rated state.

Unit State	Probability Table
Up	$U \geq FOR_2$
50%	$FOR_1 \leq U < FOR_2$
Down	$U < FOR_1$

2.4.1.1 Illustrative Example

To illustrate how the system state samples are obtained by the method, an illustrative example is provided. The system of the example consists of three 100 MW generators that have equal FOR values of 0.5, as shown in Table 2.3.

Table 2.3: 100MW generators with FOR of 0.5.

Unit State	Probability Table
Up	$U \geq 0.5$
Down	$U < 0.5$

A limited set of six samples was obtained. Each system state was obtained by generating three random numbers that were compared against the FOR values of the generators. The resulting system states and the generating capacities of the samples are presented in Table 2.4.

Table 2.4: State sampling example.

Trial	Random Numbers $\{U_1\ U_2\ U_3\}$	System State $\{S_1\ S_2\ S_3\}$	Generating Capacity [MW]
1	{0.6 0.9 0.7}	{0 0 0}	300
2	{0.5 0.1 0.2}	{0 1 1}	100
3	{0.4 0.9 0.7}	{1 0 0}	200
4	{0.5 0.8 0.4}	{0 0 1}	200
5	{0.3 0.7 0.2}	{1 0 1}	100
6	{0.1 0.1 0.2}	{1 1 1}	0

2.4.2 State Duration Method

The state duration method is a sequential method, which creates chronological state histories for each of the system's components individually. A state history of a component is created by drawing random variates from the TTF distribution and the TTR distribution in sequence, whenever a failure or a repair of the component happens. A complete system state history is obtained by combining the individual state histories together. It is common to assume that the TTFs and TTRs are exponentially distributed, although other distributions are equally applicable. As an initial starting point, all components are assumed to be available. If the simulation is performed for a short time span, the assumption may lead to an overestimation of the system's reliability. However, as the reliability indices, which are calculated from a

sequential simulation, often require a large quantity of samples to converge, the effect is often negligible.

An example, illustrating how the state histories of two components evolve, are shown in Figure 2.7. The underlying drawing order of TTFs and TTRs, which is used to create the state duration curve of the first component, is provided in Table 2.5. When the state duration curves of the two components are combined, the system state curve of Figure 2.8 is obtained.

Table 2.5: TTF and TTR sequence for component 1.

Time	State	TTF [hours]	TTR [hours]
0	0	2	-
2	1	-	1
3	0	5	-
8	1	0	1
9	0	6	-

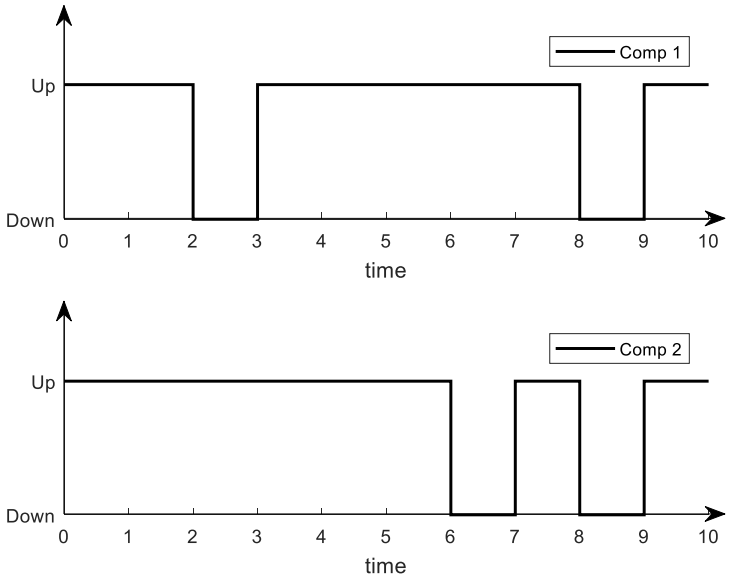

Figure 2.7: State duration curves of two components.

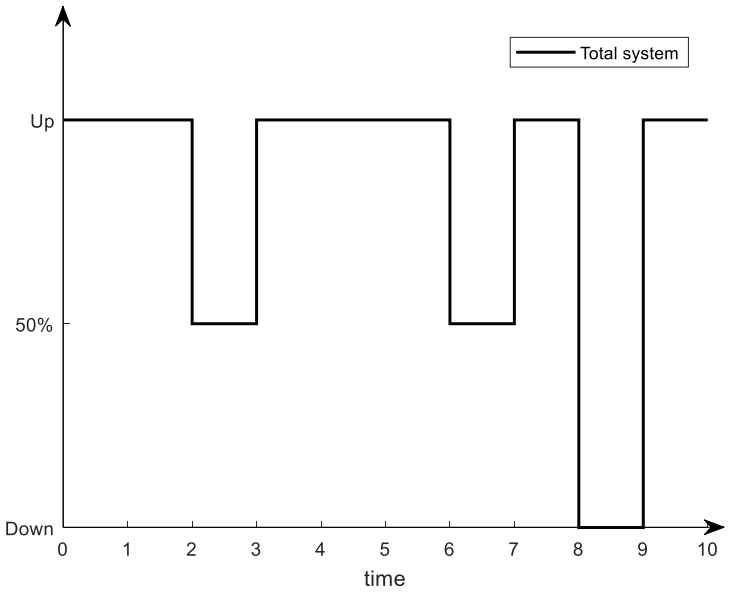

Figure 2.8: System state curve.

The state duration method is also applicable when components have additional de-rated states [13]. An approach is to represent a component with de-rated states by its transition rate matrix (TRM) (2.13), where the transition rates to and from the de-rated states are included [8].

$$\mathbf{TRM} = \begin{bmatrix} -(\lambda_{12}+\lambda_{13}) & \lambda_{12} & \lambda_{13} \\ \mu_{21} & -(\mu_{21}+\lambda_{23}) & \lambda_{23} \\ \mu_{31} & \mu_{32} & -(\mu_{31}+\mu_{32}) \end{bmatrix} \tag{2.13}$$

A transition rate is considered as failure rate, λ_{ij}, if it leads to a poorer state of a component and a repair rate if it leads to an improved state of a component. Each system state has a corresponding row and column in the TRM. For example, the transition from state 1 to state 2 is given by the element in row 1 and column 2.

The process of obtaining a state duration curve for a component is slightly modified when a component has additional de-rated states. In the following n denotes the possible states of a component. Instead of generating only a single random number that is used to calculate the random variate by (2.11), n-1 random numbers are generated to calculate n-1 random variates. The transition, which corresponds to the smallest variate is selected, and consequently gives the time to the next event and the next state.

2.4.2.1 Illustrative Example

The system of the illustrative example contains two generators, each with a capacity of 100 MW. In Figure 2.7, the state duration curves for the two generators are shown, while the total system's state duration curve is shown in Figure 2.8. The resulting states and the associated generation capacities of the hourly time increments are presented in Table 2.6.

Table 2.6: State duration example.

Time [hour]	System State $\{S_1\ S_2\}$	Generating Capacity [MW]
0	{0 0}	200
1	{0 0}	200
2	{0 1}	100
3	{0 0}	200
4	{0 0}	200
5	{0 0}	200
6	{0 1}	100
7	{0 0}	200
8	{1 1}	0
9	{0 0}	200

2.4.3 State Transition Method

The method focuses on the state transitions of the whole system instead of the transitions at component level. An understanding of the method was gained from [20]; the reader is referred to it for mathematical proof of the method. The method is only applicable if the components' times to transition, both TTF and TTR, are exponentially distributed. If this is the case, the total transition rate out of the current system state is given as the sum of transition rates out of it (2.14). An analogy can be made to the series structure representation used in reliability studies, where the next system state is given by the first component to depart from its present state [8]. Thus, the time to transition of system state is given by an exponential distribution, where the total transition rate is used as the shape parameter.

$$\lambda = \sum_{i=1}^{n} \lambda_i \tag{2.14}$$

The duration of the current system state could therefore be expressed with a random variate T, which follows an exponential distribution with shape parameter λ. Another expression for T is given as the minimum of the n individual components' times to state transition.

$$T = \min\{T_1 \quad T_2 \quad \dots \quad T_n\} \tag{2.15}$$

The probability that the next system state is a specific state when it is known that the transition happens at time instant t_0, can be given by the conditional probability of (2.16).

$$P_j = \left(T_j = t_0 \mid T = t_0\right) = \frac{P\left(T_j = t_0 \cap T = t_0\right)}{P\left(T = t_0\right)} \tag{2.16}$$

Since the involved times to transition follow exponential distributions, (2.17) can be derived from (2.16) as performed in [20]. Hence, the probability that state j is the next system state, can be expressed in terms of the transition rate from the present state to state j, divided by the total transition rate from (2.14).

$$P_j = \frac{\lambda_j}{\sum_{i=1}^{n} \lambda_i} \tag{2.17}$$

A system must eventually make a transition to another state; thus, the sum of system state probabilities must equal one (2.18).

$$\sum_{j=1}^{n} P_j = 1 \tag{2.18}$$

Thus, it is only necessary to generate a uniform random number in the range [0,1], to decide the next system state. A generation of an additional uniform random number is necessary to calculate the time to the next transition by (2.11). It is important to note that the total transition rate from (2.14) must be used when the time to transition is calculated. The principle of the method can be illustrated graphically by dividing a line segment of range [0,1] into sub-intervals, where each sub-interval corresponds to the probability of a specific system state becoming the next system state, as shown in Figure 2.9.

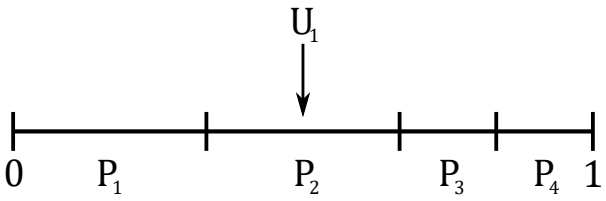

Figure 2.9: Decision of the next system state.

2.4.3.1 Illustrative Example

The system of the illustrative example consists of 4 components, including a pair of similar generators and a pair of similar lines. All components are assumed to be available in the initial state, thus giving the list of the possible transitions out of the initial state in Table 2.7.

Table 2.7: State probabilities.

Component	Transition rate [#/year]	Probability of state	Upper limit of interval
Generator 1	4.0	0.333	0.333
Generator 2	4.0	0.333	0.666
Line 1	2.0	0.167	0.833
Line 2	2.0	0.167	1.000
Total	12.0	1.000	1.000

A starting point is to generate a uniform random number, U, which is compared against the elements of the upper limits in the last column of Table 2.7. The sub-interval that U belongs to, gives the transition to the next system state. An example is that a random number of value 0.6, will give the next system state with generator 2 on outage, **S** = {0, 1, 0, 0}. The time until next transition is calculated by generating a second uniform random number. This number is used to calculate the transition time by (2.11), with the total transition rate out of the present state as parameter. When the next step of the cycle is to be determined, the failure rate of generator 2 is replaced with the repair rate of the generator before the procedure is repeated over again.

2.5 Coefficient of Variation

The statistical foundation of MCS lies in the central limit theorem and the law of large numbers [21]. A description of the central limit theorem can be found in most statistics textbooks, such as [22], while the law of large numbers is described further in [21]. A MCS is a converging process, which not necessarily provides a more precise estimate of a reliability index by adding

an additional observation value to a sample. However, as the size of a sample increases, the variance of an index's estimated mean distribution decreases, i.e. the precision of the estimate increases. Thus, it can be assumed that the expected estimate of an index converges towards a value equal to the true mean of the index's distribution. To understand the properties of MCS fully, it may be necessary to look at some fundamentals from statistics.

In this thesis, a reliability index value of a simulation year can be looked at as an observation value X_i. The totality of values that can be observed for such an index constitute a population. A MCS obtains a sample, which is a subset of this population, consisting of a set of observations equal to the N simulated years. The distribution of the population may be unknown, but it is assumed in the following to have a true mean, μ_X, and a finite variance σ_X^2. An infinite set of samples, of size N, can be obtained from this population by performing new MCSs. From these samples, estimates, $\overline{X}$, of the population mean can be calculated by (2.19), and the variance of such samples can be calculated from (2.20). The totality of estimates constitutes a new population, which has a true mean equal to the mean of the original population and a variance of $\sigma_{\overline{X}}^2$. An estimate of the variance of the sampling distribution can be calculated by (2.21), which is common to use [7]. It is worth noting that the use of (2.20) and (2.21) assumes independence between observation values.

$$E(X) = \overline{X} = \frac{1}{N}\sum_{i=1}^{N} X_i \tag{2.19}$$

$$s^2(X) = \frac{1}{N-1}\sum_{i=1}^{N}\left(X_i - \overline{X}\right)^2 \tag{2.20}$$

$$Var\left(\overline{X}\right) = \frac{1}{N}Var(X) = \frac{1}{N}\left(\frac{1}{N-1}\sum_{i=1}^{N}\left(X_i - \overline{X}\right)^2\right) \tag{2.21}$$

The law of large numbers states that a MCS estimate of the sample mean and sample variance tends towards the population mean and population variance when the sample size increases towards infinity as expressed in (2.22). The central limit theorem, however, states that the sample distribution of the estimated mean can be approximated by a normal distribution, with mean μ_X and a variance σ_X^2/N, provided N is sufficiently large. If N is sufficiently large, the true variance of the sample distribution can be approximated by (2.21).

$$\lim_{N\to\infty} \bar{X} = \mu_X \tag{2.22}$$

In MCS, it is common to use a unitless coefficient to measure the convergence of a simulation. The coefficient of variation (CV) provides the ratio of the sample's standard deviation (SD) to the sample's mean as a unitless quantity. It can be calculated from (2.23), where the SD of a sample is given by s(X).

$$\beta = \frac{s(X)}{\sqrt{N}\cdot E(X)} \tag{2.23}$$

2.6 Accuracy and Precision

It is important to clarify the difference between two terms that are used to describe an estimate obtained by MCS, namely accuracy and precision. Accuracy denotes how close the expectation value of an estimator is to the true value of a distribution, thus representing the systematical error. Precision, on the other hand, is related to the variance of the sampling distribution and represents the random error of a MCS [23]. A MCS with better accuracy has a higher probability of providing an estimate close to the true mean of the distribution. Low accuracy can be the result of various errors, for instance coding error or error in input data. Another potential source of error can be application of a poor system model to a system. To verify the accuracy level of a MCS, it is necessary to compare the obtained results against results from other studies or other independent calculations [21]. It is also desirable to have a high level of precision for a MCS, because a higher precision yields a higher probability of obtaining an estimate that is close to the expectation value of the estimator. A higher precision can be achieved by reducing the variance of the sampling distribution. From (2.21), it can be observed that the precision of a MCS is proportional to the number of simulation years. To highlight the properties of a MCS estimate, an illustrative example is provided in the following.

The system of the example consists of two identical generators, both having a rated capacity of 100MW and FOR of 0.2 as can be seen in Table 2.8. A CYPL of 100 MW is assumed throughout the year for simplicity. Four different sampling distributions are obtained of the LOLE index, a distribution with high accuracy and high precision, a distribution with high accuracy and low precision, a distribution with low accuracy and high precision, and a distribution with low accuracy and low precision, cf. Figure 2.10. Each sampling distribution is obtained by performing 1000 MCS simulations where each simulation provides an estimate of the LOLE index. The low accuracy distributions are obtained by introducing a systematical

error into the MCS, which is due to using an erroneous FOR value in the input data of generator 1. A difference in the precision is achieved by using 400 000 simulation years in each simulation of the high precision MCS and 200 000 simulation years in each simulation of the low precision MCS.

Table 2.8: The generators of the accuracy vs. precision example.

Component	Capacity [MW]	True FOR	Error FOR
G1	100	0.20	0.21
G2	100	020	-

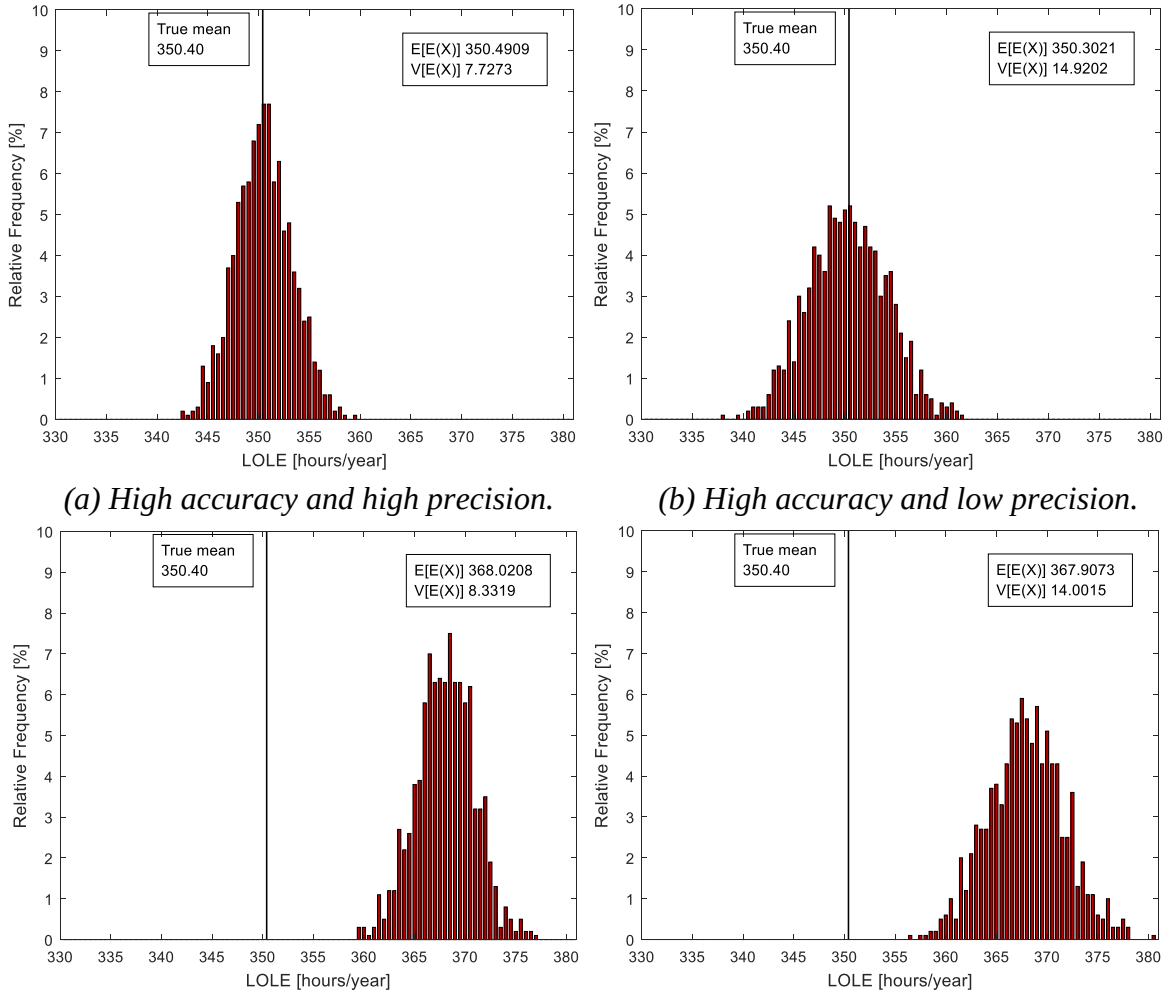

(a) High accuracy and high precision.

(b) High accuracy and low precision.

(c) Low accuracy and high precision.

(d) Low accuracy and low precision.

Figure 2.10: Illustration of accuracy and precision.

2.7 Approximate Confidence Intervals

Confidence intervals can be established to provide an indication of the precision level of MCS. A confidence interval (CI) that is created by using the critical values of the t-distribution, relies on the assumption of an underlying normal distribution for the random variables X_i. If the random variables follow a normal distribution, a test statistic, t_n, can be established as shown in [24], which follows the t-distribution with n-1 degrees of freedom:

$$t_n = t_n\left(X_1, X_2 \ldots X_N\right) = \frac{\sqrt{N}\cdot\left(\bar{X}-\mu_x\right)}{s(X)} = \frac{\sqrt{N}\cdot\left(\bar{X}-\mu_x\right)}{\sigma_x}\cdot\frac{\sigma_x}{s(X)} \tag{2.24}$$

The assumption of normality does not hold if the random variables follow another distribution. However, according to [24], the test statistic, t_n, has a limit distribution that is standard normal, Z(0,1), by application of the central limit theorem and Slutsky's theorem, regardless of the underlying distribution's shape. This holds as long as the underlying distribution has a mean and a finite variance. Thus, when the size of a sample is large, as is common in MCS, approximate CIs can be created by (2.25), with critical values from the t-distribution. The critical values of the t-distribution approach the critical values of the normal distribution, due to the large sample size. Critical values of the t-distribution are provided in Table 2.9 for two-sided CIs.

$$\bar{X} \pm t_{1-\alpha,N-1}\cdot\frac{s(x)}{\sqrt{N}} \tag{2.25}$$

Table 2.9: Critical values for two-sided CIs.

Confidence level	Critical Value t
95%	1.96
99%	2.576

It is worth mentioning that the information provided by a CI is limited. The confidence level gives simply a percentage expectation of how often a CI created from a sample is expected to contain the mean of the sampling distribution.

3 Methodological Approach

The thesis work developed methodological approaches on how adequacy assessment on HLI and HLII can be performed. Assessments at both levels rely on models for the system's load and generation. There is an additional need for a model representing the network topology at HLII. When it comes to the choice of load model, various representations of the system's load exist. This thesis uses the same load model for both assessment levels, while the generation models are obtained by MCS sampling. The approach of obtaining a generation model is presented in the generation adequacy section. A similar approach is used in the composite system assessment for obtaining of generation and load models. The only difference is the allocation of generation capacities and loads among the buses of the system. In the following sections, the load model representation is first described, thereafter the approaches for the assessment on HLI and HLII are presented.

3.1 Load Model

There exist various load model representations of a system, all being forecasts on future system load based on historical data. Common for the representations are the description of the system's load for a defined period, usually a year, from which the adequacy metrics are calculated. The period is further divided into time increments of equal sizes, where each time increment is characterized by its duration and load level. Depending on the duration of the increments, the obtained adequacy metrics will have different interpretations as mentioned in chapter 2. It is common to choose an increment size of either an hour, a day or a year. Here, it is worth noting that the simplest model obtained by choosing an increment sizing of a year, e.g. a CYPL curve of one increment at the system's yearly peak load, will give a more pessimistic result than if load models with more increments are used. More pessimistic results are also experienced when a DPL is used instead of an HPL [17].

The load model representation can either be a sorted representation, where the load levels are sorted from the largest to the smallest load, or a chronological representation. If the chosen representation is the former, the curve is called a load duration curve (LDC). The reason behind a more pessimistic adequacy metric as the number of chosen increments decrease, becomes visible when the hourly, daily and yearly load models are sorted as LDCs and plotted against each other in Figure 3.1. It is worth noting that a LDC is only applicable when a non-sequential

MCS method is chosen. Hence, when the simulation method is sequential, a chronological curve must be used, like the one illustrated in Figure 3.2.

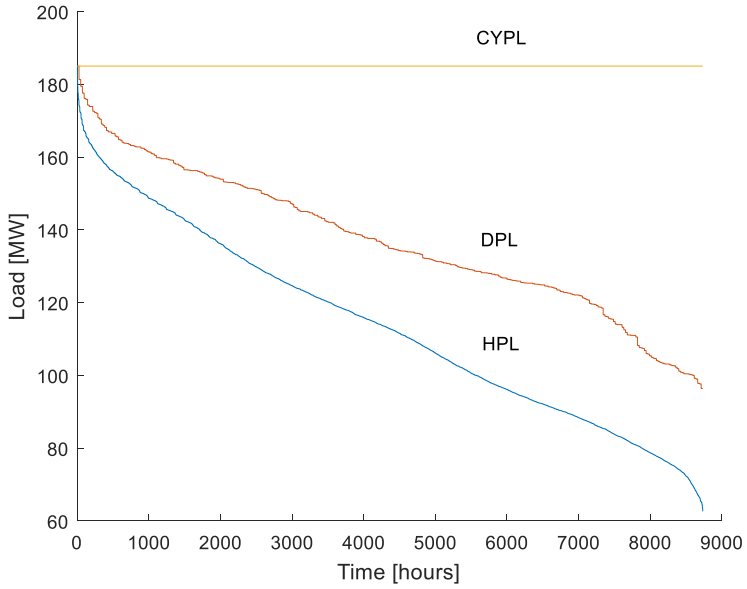

Figure 3.1: Various LDCs of the RBTS for a one-year period.

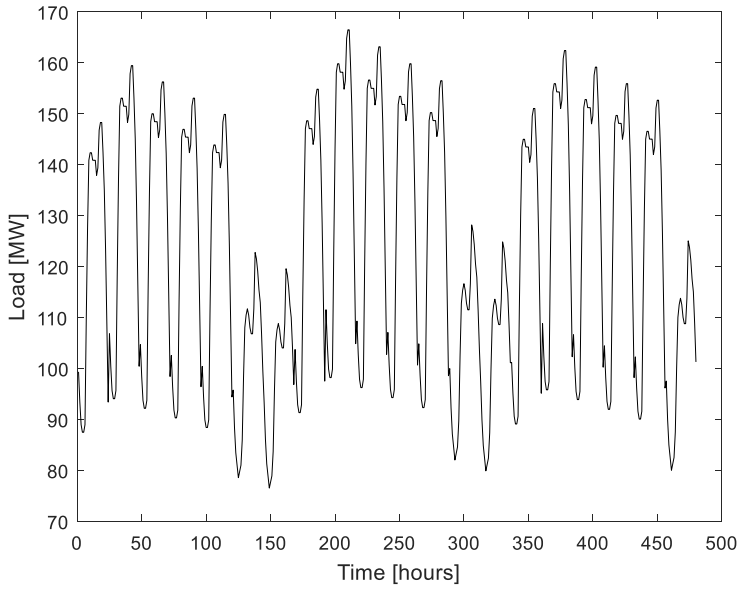

Figure 3.2: The first 20 days of the RBTS chronological HPL curve.

3.2 Generation Adequacy

Generation system adequacy is in simple terms performed by evaluation of the generation model against the load model of the system. In this thesis, the load model is represented by the chronological HPL model described in the previous section. The generation models of this thesis are obtained by the three MCS methods that are described briefly in chapter 2. In each time increment, a system state is obtained by combining the states of the individual generators. This system state gives the available generation capacity, which is evaluated against the load requirement of the system according to (3.1). If the inequality does not hold, the state is recorded as a failure and the corresponding severity of the failure is calculated by (3.2). In the following sections, the procedures used to obtain the generation models used in HLI evaluation are described in detail.

$$\sum_{i=1}^{n} P_{cap,i} \geq \sum_{j=1}^{k} P_{load,j} \tag{3.1}$$

$$ENS = \left(\sum_{j=1}^{k} P_{load,j} - \sum_{i=1}^{n} P_{cap,i} \right) \cdot \Delta t \tag{3.2}$$

3.2.1 Generation Model Input

Common to the state sampling method, the state duration method and the state transition method, is that they need a complete list of the generators in the system as input. For the state sampling method, the list must contain the capacity of each generator in MW and the FOR value of each generator as shown in Table 3.1.

Table 3.1: Generator input for the state sampling method.

Generator	Capacity [MW]	FOR
1	$P_{cap,1}$	FOR_1
2	$P_{cap,2}$	FOR_2
n	$P_{cap,n}$	FOR_n

A slight adjustment must be made to the generator list for the sequential MCS methods, where the FOR column must be replaced by two columns, which contain the respective failure and repair rates of the generators as illustrated in Table 3.2.

Table 3.2: Generator input for the sequential methods.

Generator	Capacity [MW]	Failure rate λ [#/hour]	Repair rate μ [#/hour]
1	$P_{cap,1}$	λ_1	μ_1
2	$P_{cap,2}$	λ_2	μ_2
n	$P_{cap,n}$	λ_n	μ_n

There are situations where it is of interest to represent some of the generators with multiple states, i.e. include de-rated states. A variation of the state duration method was created, during the thesis work, to handle these generators. In this case there needs to be some modifications to the generator input data. The generator list of Table 3.1 is modified by replacing the FOR column with a column with the number of possible generator states. Based on the generator list, a three-dimensional matrix is created. Each row element along the first dimension corresponds to one generator. By using a 3D-matrix instead of a struct, the script takes advantage of the matrix computational strength of MATLAB. Each row element of the 3D-matrix is loaded with the generator's TRM and an additional column with the capacities associated with each generator state. An example showing a certain generator input, is illustrated in Table 3.3, where a red rectangle marks the input format. The transition rates are the respective annualized failure and repair rates in accordance with [13]. Inside the red rectangle, the element of row 1 and column 2 (1,2) represents the transition rate from state 1 to state 2, i.e. a failure rate.

Table 3.3: Multi-state representation of the RTS 400MW generator.

State	1	2	3	[MW]
1	-8	4	4	400
2	44	-44	0	200
3	44	0	-44	0

3.2.2 Step by Step Guide

In this section, the algorithmic approaches for the three MCS methods are described in a step by step manner. The presented MCS methods use a similar chronological HPL curve, of 8736 hours, when the indices are evaluated. It could be argued that the state sampling method could sample random load levels from a HPL LDC curve instead of sampling chronologically from a chronological load curve, as performed in [7] due to the time independence of the method. The

sequential methods, on the other hand, rely on the use of chronological curves due to the history dependence of the methods. A basis for the MCS methodology presented here has its foundation in the basic principles of the three MCS methods presented in chapter 2 of this thesis in addition to the presentation of the methods in [7]. The three MCS methods are implemented using MATLAB scripts, which are further tested in chapter 4.

3.2.2.1 State Sampling Method

The input to the script is a list of the format presented in Table 3.1. First, a record matrix, with the number of columns equal to the number of simulation years is created. For each of the simulated years, the reliability indices of interest are calculated and stored in the column corresponding to a specific year. For the state sampling method, this thesis uses the LOLE and EENS indices. In addition, the LOLP index is "re-engineered" from the LOLE index. The proposed procedure to obtain the yearly indices are presented in the following steps.

Step 1: Loop through each of the hours in a year [1,8736].

a) Loop through the generators of the system [1, n].
    i) Generate a random number, U, by drawing from the uniform distribution [0,1].
    ii) If U is larger than or equal to the corresponding FOR value of the generator, the generator is available and contributing to the generating capacity at the hourly time increment.
b) Add the total generation capacity being available at the hourly time increment.
c) Compare the available generation capacity against the load requirement of the time increment according to (3.1). If the capacity is insufficient, count the "failure" (1 hour) and the energy deficit (MWh) according to (3.2).

Step 2: At the end of each simulation year, obtain the LOLE and EENS indices of the year by adding the counted failures and energy deficits of the year.

The above steps are repeated until the last simulation year is finished. After finishing the simulation process, the estimates of the indices are calculated as their long-term average values together with the indices' CVs. The latter is calculated to verify that the values of the indices have converged.

3.2.2.2 State Duration Method

The input data to the script are presented in the preceding section, where the generators of the system are represented by one common three-dimensional matrix. On a yearly basis, the method creates chronological up, de-rated and down cycles for the system's generators. The cycles are recorded in a matrix where the generators have their own rows and each column corresponds to an hour of a yearly cycle. In addition, one "remaining time" matrix is created to keep track of the time to next event, current state and next state for each generator at the end of a year. A record matrix is created to keep track of the reliability indices per simulation year, as previously described in the state sampling procedure. Due to the sequential nature of the method, a frequency index, LOLF, can easily be included in the assessment. The proposed methodology is presented in the following steps. Initially, for the first simulation year, it is assumed that all the generators are functioning.

Step 1: Loop through the generators of the system [1, n].

a) Check the number of possible states for the generator, denoted v in the following.
b) Loop through the hours of a year [1, 8736].
    i) Check the state of the generator at the hourly time increment (Up = 1, De-rated 1 = 2, De-rated 2 = 3 … Down = v).
    ii) Generate v-1 random numbers from the uniform distribution.
    iii) Calculate the (v-1) possible transition times (TTF or TTR) out of the current state by (2.11) with one random number for each possible state.
    iv) Select the smallest of the calculated transition times, denoted t, and find the state corresponding to the selected transition time, which is the next state.
    v) Update the elements of the generator row in the status matrix from the current time increment k, to k + (t - 1) with the current state at time increment k. Set the element of column k + t equal to the value corresponding to the next state.
    vi) Increment the time of the year with the transition time k + t.
c) When the value of the time increment k exceeds the number of hours in a year, subtract the hours in a year from the time increment k, which gives the remaining time to the next event.
d) The remaining time to the next event, the current generator state and the arriving state of the generator are stored in the generator's row in the remaining time matrix.

Step 2: Use the status matrix to obtain the available generation capacity for each of the time increments. First, loop through the hours of a year [1, 8736].

a) For each time increment, loop through the generators of the system [1, n].
   i) Add the available capacity of each generator to the total capacity of the time increment, given by the generator state.
   ii) Compare the available generation capacity against the load requirement of the time increment according to (3.1). If the capacity is insufficient, count the "failure" (1 hour) and the energy deficit (MWh) according to (3.2). The frequency counter is only updated if the previous time increment was recorded as a success.

Step 3: At the end of each simulation year, obtain the LOLE, EENS and LOLF indices of the year by using the respective counters.

Step 4: The following year, start with a continuation of the previous year. This is accomplished by setting the initial states of the generators according to the "remaining time" matrix created at the end of the previous year.

The procedure is repeated until the final simulation year. Then the estimates of the indices are obtained by their long-term average values as described in the state sampling procedure.

3.2.2.3 State Transition Method

The input data to the script is a list of the generators with a format presented in Table 3.2. First, two additional columns are added to the generator list, to keep track of the current- and arriving-state of each generator. As in the other two approaches, a record matrix is created to store the yearly reliability indices of the assessment. A frequency index, LOLF, is also included as in the state duration method. The proposed procedure of the method is described in the following steps. One aspect that is worth noting is that there is a large probability for one or more events happening inside one single time increment, one hour, due to the relatively short mean time to repair (MTTR) of the generators.

Step 1: Loop through the hours of a year [1,8736].

a) The current time increment is denoted k.

b) A *while* loop is executed as long as the time to next event, t, is too small to increment the time to the next hour of the year. (The *while* loop is necessary due to the possibility of two events occurring inside a single time increment).
    i) In the generator list: Update the current state column with the elements of the next state column.
    ii) Create a vector with the transition rates out of the current state as elements.
    iii) Calculate the sum of the transition rates according to (2.14).
    iv) Create a vector with the probabilities of each possible new system state according to (2.17).
    v) Construct a cumulative probability vector of the probabilities by adding the next state probability to the sum of the preceding entries. The concept is illustrated in Figure 2.9.
    vi) Generate a random number, U, from the uniform distribution.
    vii) Find the interval that U falls into in the cumulative vector. This corresponds to the next state.
    viii) Update the entry of the next state column of the generator list with the new system state.
    ix) Generate a new uniformly distributed number between [0,1] and use the inverse transform method of (2.11) with the sum of the transition rates as the shape parameter to obtain the time to next event.
    x) Update the time of occurrence of the next event to k + t
c) Sum the available generation capacity at time increment k, in accordance with the current state column of the generator list.
d) Compare the available generation capacity against the load requirement of the time increment according to (3.1). If the capacity is insufficient, count the "failure" (1 hour) and the energy deficit (MWh) according to (3.2). The frequency counter is only updated if the previous time increment is recorded as a success.

Step 2: Subtract the number of hours in a year from the time of occurrence of the next event at the end of a simulation year.

Step 3: At the end of each simulation year, obtain the LOLE, EENS and LOLF indices of the year by using the respective counters.

Step 4: Repeat the procedure for the rest of the simulation years.

After the simulation process is finished, the long-term averages of the reliability indices are obtained in a similar manner as the description in the state sampling approach.

3.2.3 Illustrative Generation Adequacy Example

The following example is presented to illustrate the main features of generation adequacy evaluation. It is a system composed of three generators with equal capacities of 100MW. The load requirement of the system is assumed to be constant, e.g. a CYPL of 150MW. Since the example is for illustrative purpose only, the sample size, N, is limited to 10 years, where the system state samples are obtained by using the state sampling approach presented earlier. The reliability indices used are the LOLE, LOLP' and EENS. Resulting states and their contributions to the adequacy metrics are presented in Table 3.4. The contributions to the indices are evaluated from (3.1) and (3.2).

Table 3.4: Expectation and variance example.

Year	System State	Generating Capacity [MW]	LOL [years]	ENS [MWh/year]
1	0,0,0	300	0	0
2	0,1,1	100	1	438000
3	1,0,0	200	0	0
4	0,0,1	200	0	0
5	1,0,1	100	1	438000
6	1,1,1	0	1	1314000
7	0,0,0	300	0	0
8	0,0,0	300	0	0
9	1,0,0	200	0	0
10	1,1,0	100	1	438000

Using (2.2) for obtaining the LOLE index yields a LOLE index of 0.4 years/year, meaning that 4 out of 10 years are expected to experience a LOL situation. The special case of using a CYPL gives a LOLP equal to LOLE.

$$\text{LOLE} = \frac{0+1+0+0+1+1+0+0+0+1}{10} = 0.4 \text{ years/year} \tag{3.3}$$

The SD of the LOLE index with respect to the yearly samples of the index is 0.5164, giving a CV using (2.23) of 40.8%.

$$\beta = \frac{0.5164}{\sqrt{10} \cdot 0.4} = 0.4083 \tag{3.4}$$

The EENS index is calculated by using (2.6) as 262800 MWh/year.

$$\begin{aligned} \text{EENS} &= \frac{0 + 438000 + 0 + 0 + 438000 + 1314000 + 0 + 0 + 0 + 438000}{10} \\ &= 262800 \text{ MWh/year} \end{aligned} \tag{3.5}$$

For the EENS index, the SD of the yearly ENS samples is 423150. Using (2.23) yields the index' coefficient of variance of 50.9%.

$$\beta = \frac{423150}{\sqrt{10} \cdot 262800} = 0.5092 \tag{3.6}$$

3.3 Composite System Adequacy

In composite system adequacy assessment, there is a need for a model representing the network topology in addition to the load and generation models described in the previous sections. The proposed methodologies of system state sampling in generation adequacy assessment are also applicable, with some minor adjustments, when the system states are obtained in composite system analysis. In short, the main difference lies in the evaluation of system states, while the process of sampling system states is similar in principle, only including the additional sampling of the lines' statuses. The evaluation at HLI is limited to a comparison of the generation capacity against the load requirement, while the composite system assessment depends on a load flow based analysis. Therefore, a choice should be made regarding the desired accuracy of the load flow analysis. A simplified approach is to use a DC-based load flow analysis, but if more accurate results are desired, a full AC-based load flow analysis should be used. Whichever the analysis of choice, additional network data[1] must be supplied as input to both the MCS sampling process and the evaluation step. More specific generation and load data are also needed where allocation of generation capacity and load requirement among the buses is specified.

For the composite system assessment part of this thesis, the MCS methods used for sampling of system states are limited to the state sampling and state transition methods, so as to cover one time independent and one sequential approach. As stated earlier, the system states are

[1] Network topology, impedances and current limits of the lines.

evaluated by use of two different “contingency solvers”, one based on DC-load flow analysis and another based on AC-load flow analysis, all implemented in MATLAB during the thesis work. The proposed methodology of the solvers is presented in the following sections, with one section describing the general parts that are similar for the DC- and AC-solvers. Thereafter, both contingency solvers are presented in detail.

3.3.1 General Elements

There are some general elements common for the two contingency solver approaches, AC and DC, proposed in this thesis. Both methods depend on input data in a specific format. Through MCS sampling, the system state of a given time increment is obtained and handed to the contingency solver for further evaluation. Thus, a specific format of input data to solver, e. g. the system state is needed.

3.3.1.1 Input Data

A representation of the network data format used by the MCS state sampling method for full AC analysis is shown in Table 3.5. If the load flow analysis is based on DC, the columns of the resistances and shunt susceptances are left out. The MCS state transition method uses a similar format except that the FOR column is replaced by two columns, one for the failure rates and one for the repair rates.

Table 3.5: Line input data, State Sampling AC-solver.

Line	Bus	Bus	FOR	Resistance [p.u.]	Reactance [p.u.]	Half of Shunt Susceptance [p.u.]	Current Limit [p.u.]
1	1	2	FOR_1	R_{12}	X_{12}	y_{10}	$Ilim_1$
2	2	3	FOR_2	R_{23}	X_{23}	y_{20}	$Ilim_2$
n	5	6	FOR_n	R_{56}	X_{56}	y_{50}	$Ilim_n$

For the AC based analysis to be conducted, reactive power capabilities of the generators must be added to the generator input data. Thus, the specified format used by the MCS state sampling method is presented in Table 3.6, where the minimum and maximum reactive power capability of each generator are specified. If the MCS state transition method is used, the FOR column is replaced by two transition rate columns. The DC based analysis uses similar input, without the columns of reactive power capabilities.

Table 3.6: Generator input data, State Sampling AC-solver.

Generator	Capacity [MW]	Bus #	Min Reactive [MVAr]	Max Reactive [MVAr]	FOR
1	$P_{cap,1}$	N_1	$Qmin_1$	$Qmax_1$	FOR_1
2	$P_{cap,2}$	N_2	$Qmin_2$	$Qmax_2$	FOR_2
n	$P_{cap,n}$	N_n	$Qmin_n$	$Qmax_n$	FOR_n

An additional table specifying the specific bus data of the system is also included as input. Both the AC and the DC solvers need one column specifying the allocation of loads in the system and one column where the cost of load curtailments at each bus are specified. For the AC-analysis, the minimum and maximum voltage limits of the buses are included as well. The format used by the AC solver is presented in Table 3.7.

Table 3.7: Bus specification, AC-solver.

Bus	Share of load	Vmin [pu]	Vmax [pu]	IEAR [$/kWh]
1	$Load_1$	$Vmin_1$	$Vmax_1$	$Cost_1$
2	$Load_2$	$Vmin_2$	$Vmax_2$	$Cost_2$
n	$Load_n$	$Vmin_n$	$Vmax_n$	$Cost_n$

3.3.1.2 System State

A system state of a time increment is sampled through MCS sampling, giving the states of the generators and lines as two vectors. Each component state is given by a binary value [0, 1], termed X_i, where a zero denotes an available component and a value of one denotes that the component is down. Thus, the vectors giving the states of the n generators and the m lines are of formats presented in the following.

$$P_g = \begin{bmatrix} X_1 & X_2 & \dots & X_n \end{bmatrix}^T \tag{3.7}$$

$$L = \begin{bmatrix} X_1 & X_2 & \dots & X_m \end{bmatrix}^T \tag{3.8}$$

Due to the allocation of generators at different buses of the system, the generator capacities at each of the k buses can be combined, according to their state given from (3.7) and their rated capacity, to give the bus generation capacities. Thus, the system's generation capacity can be represented by a generation capacity vector with k elements for the DC approach.

$$P_{g,lim} = \begin{bmatrix} P_{cap,1} & P_{cap,2} & \dots & P_{cap,k} \end{bmatrix}^T \tag{3.9}$$

For the AC approach, the generation capacity vector is extended to a matrix with three columns, which give the respective active power, minimum reactive power and maximum reactive power capabilities of the buses.

$$G_{lim} = \begin{bmatrix} P_{cap,1} & Q_{min,1} & Q_{max,1} \\ P_{cap,2} & Q_{min,2} & Q_{max,2} \\ \vdots & \vdots & \vdots \\ P_{cap,k} & Q_{min,k} & Q_{max,k} \end{bmatrix} \tag{3.10}$$

In addition, the load requirement allocation among the k buses of a system is needed. Hence, the active power load requirement is represented by a load vector of k elements for the DC approach.

$$P_{load} = \begin{bmatrix} P_{load,1} & P_{load,2} & \dots & P_{load,k} \end{bmatrix}^T \tag{3.11}$$

For the AC approach, the load requirement vector is extended with an additional column giving the reactive power requirement of the loads at the buses.

$$P_{load} = \begin{bmatrix} P_{load,1} & P_{load,2} & \cdots & P_{load,k} \\ Q_{load,1} & Q_{load,2} & \cdots & Q_{load,k} \end{bmatrix}^T \tag{3.12}$$

3.3.1.3 Isolated Buses

A possible challenge that might occur during the simulation process of system state sampling, is the occurrence of multiple lines on outage at the same time. This might lead to isolation of one or more buses or parts of the system being islanded, depending on the number of outages and where they occur. If the developed load flow analysis tools lack a part that detects and handles the isolation of buses properly, the load flow problem becomes infeasible, due to the inclusion of isolated buses in the matrix representing the system, i.e. Ybus. Among the problems is the nonexistence of an inverse admittance matrix. The task is to make a general approach that works correctly for all possible cases, i.e. to create an algorithm that only captures the buses that are isolated. A point worth noting regarding the development of such an algorithm, is that a system of small size does not necessarily reveal the limitations of a proposed algorithm, which might become evident only when the approach is applied to a test system of larger size. The

decision strategy on how to handle possible isolation of buses used by the "contingency solvers" presented in the thesis, is presented in the following:

Step 1: When the state of a line is sampled as a failure, i.e. outage, the admittance of the line is set to zero.

Step 2: When an isolated bus is identified, the elements corresponding to the bus are removed from the matrices and vectors representing the system. This step ensures that the OPF problem remains solvable.

Step 3: After the identification of isolated buses and the subsequent matrix modifications, the load curtailments due to the isolation of buses are given according to the following criteria:

a) The slack bus of the system, i.e. bus 1[1] is the only bus able to operate in islanded mode.
   i) If the slack bus is isolated from the rest of the system, all loads are shed in the system except from the loads at the slack bus.
   ii) The generators at an isolated bus are not able to provide the load requirement at the bus.

3.3.1.4 Identification of Isolated Buses

The RBTS system, presented in Appendix I, is used as a simple example to show how isolated buses and possible islands can be identified through inspection of either the conductance or susceptance matrix. A case of islanding, i.e. isolation of bus 2 and bus 4 from the rest of the system, occurs if lines L3, L4 and L8 of the RBTS are on outage. The isolation can be identified by looking at the system's susceptance matrix presented in Table 3.8.

Table 3.8: The susceptance matrix of the RBTS.

11	0	-11	0	0	0
0	3	0	-3	0	0
-11	0	19	0	-8	0
0	-3	0	3	0	0
0	0	-8	0	17	-8
0	0	0	0	-8	8

[1] The slack bus of the system must always be bus number 1 for the approach to be valid. If the slack bus of the system has a different original number, the buses of the system must be given new numbers.

When investigating row two of the susceptance matrix, it can be identified that bus 2 has no connection to bus 1, but only a connection to bus 4. Further investigation of row 4 in the matrix reveals that bus 4 has a connection to bus 2 only. The other four buses of the system are interconnected. Based on the above discovery, a simple approach is presented:

Step 1: Check for left-connectivity, i.e. examine whether the bus under consideration is connected to a bus with a lower number.

a) Iterate from bus number 2 to the last bus [2, k].
    i) For each bus under consideration, examine whether it is connected to a bus with a lower number.
        - If no, flag the bus under consideration as ‘isolated’.
        - If yes, also check if the bus to which the bus under consideration is connected has already been marked as ‘isolated’.
            - If yes, flag the bus under consideration as ‘isolated’.

Step 2: Check the right-connectivity, i.e. examine whether the bus under consideration is connected to a bus with a higher number.

a) Iterate from the last bus to bus number 2 [k, 2].
    i) For each bus under consideration flagged as isolated from step 1, examine whether it is connected to a bus with a higher number that is not flagged as isolated. If yes, the ‘isolated’ flag is removed for the bus under consideration. If no, the ‘isolated’ flag is retained.

However, the approach is found to be insufficient for more complicated system configurations, thus representing a possible pitfall. Even for the RBTS system, a system of relatively small size, an error occurs if the approach is applied to the system configuration of Figure 3.3, where lines L1, L6 and L8 are on outage.

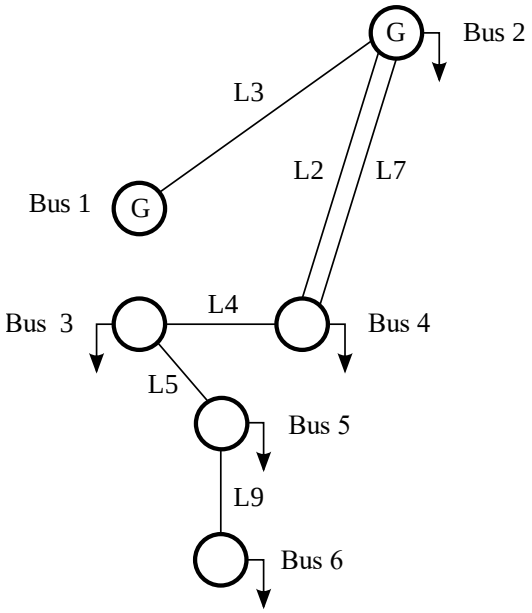

Figure 3.3: The RBTS special case with outages.

If a thorough inspection of the algorithm's steps applied to the case of Figure 3.3 is performed, it becomes clear that the algorithm marks buses 5 and 6 incorrectly as isolated. The intermediate results obtained by applying the algorithm step by step are presented in Table 3.9, where a one denotes an isolation flag.

Table 3.9: Intermediate flags, RBTS case.

Bus	Flag after Step 1	Flag after Step 2	Result
1	0	0	Not isolated
2	0	0	Not isolated
3	1	0	Not isolated
4	0	0	Not isolated
5	1	1	Isolated
6	1	1	Isolated

When lines L1, L6 and L8 are on outage, a visual inspection of Figure 3.3 shows that none of the buses is isolated. However, the algorithm has resulted in the incorrect isolation of buses 5 and 6. Thus, a limitation of the above presented bus isolation algorithm is revealed. Such a limitation is encountered when the outages of lines lead to the creation of new radials containing buses numbered in no particular sequence. An illustration of such a configuration where the bus isolation algorithm might encounter difficulties, is presented in Figure 3.4.

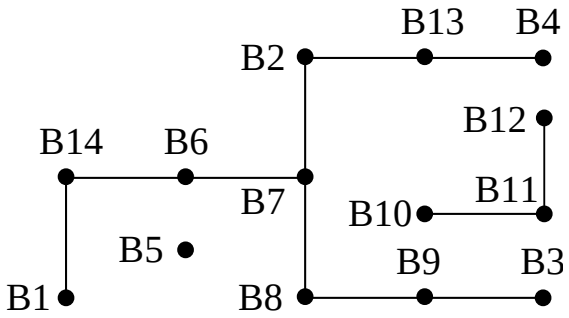

Figure 3.4: Radial Example.

Based on the special configuration of the RBTS and the radial example of Figure 3.4, a new more detailed algorithmic approach is proposed, with basis in the first suggested algorithm:

Step 1: Check the left-connectivity, i.e. examine whether the bus under consideration is connected to a bus with a lower number.

a) Iterate from bus number 2 to the last bus [2, k].
    i) For each bus under consideration, examine whether it is connected to a bus with a lower number.
        - If no, flag the bus under consideration as ‘isolated’.
        - If yes, also check if the bus to which the bus under consideration is connected has already been marked as ‘isolated’.
            - If yes, flag the bus under consideration as ‘isolated’.
            - If no, check whether the bus under consideration is directly connected to any of the other buses with lower numbers that have already been flagged as isolated.
                - If yes, clear the flags of all the buses that are directly connected to the bus under consideration.

Step 2: Examine whether the bus under consideration is connected to any other another bus. To ensure that none of the buses are incorrectly marked as isolated after finalization of step 2, the step is started over again if a special combination occurs; the bus is cleared from its isolation flag and leads to the clearing of additional buses’ flags.

a) Iterate from the last bus to bus number 2 [k, 2], iterator m.
    i) For each bus under consideration flagged as isolated from step 1, examine whether it is connected to a bus that is not flagged as isolated.
        1) If yes, remove the flag of bus m.

i. Iterate from bus number 2 to bus k [2, k], iterator n.
   - If bus n is flagged as isolated and a connection to bus m exists, remove the flag of bus n.

ii. If one or more flags are removed during the loop by iterator n, step 2 is restarted from the beginning with iterator m starting from the last bus.

The importance of including a restarting of the algorithm's step 2 becomes clear by applying the new suggested algorithm step by step on the radial example of Figure 3.4. In Table 3.10, the obtained intermediate results are presented. The parentheses surrounding some of the numbers, indicates a clearing of a flag in the inner loop of the algorithm, i.e. point a.i).1).

Table 3.10: Radial example.

Bus	Step 1	Step 2 #1	Step 2 #2	Step 2 #3	Step 3 #4
1	0				0
2	1	(0)			0
3	1			(0)	0
4	1		(0)		0
5	1				1
6	1 (0)				0
7	1	0			0
8	1	1 (0)			0
9	1	1		0	0
10	1	1		1	1
11	1	1		1	1
12	1	1		1	1
13	1	1	0	0	0
14	0	0	0	0	0

3.3.2 DC – Contingency Solver

The considerations of the DC "contingency solver" are presented in this section. First, an introduction to the approximations and equations used to represent the system is made, before the OPF problem is formulated. The solver is then tested on a selection of system states, before a final example illustrating the details is given.

3.3.2.1 Network Model

In the DC based approach, the network is represented by the DC power flow formulations and approximations found in most available power system analysis text books, for example [25]. By using the assumptions of DC-power flow, it is possible to formulate the power flows through the lines as linear functions of the net power injections at the buses [26]. The assumptions of the DC-power flow formulations are listed in the following:

i) The resistance of a line is much smaller than its reactance ($r_{ij} << x_{ij}$).
ii) The difference in voltage phasor angle between two interconnected buses is small. Thus, two reasonable approximations are to set the *sin* of the difference in phasor angle equal to the difference and the *cos* of the same difference equal to one[1] ($\sin \delta_{ij} = \delta_{ij}$ and $\cos \delta_{ij} = 1$).
iii) The lines' susceptances to earth are neglected ($b_{i0} = 0$ and $b_{j0} = 0$).
iv) The voltages are fixed at a magnitude of one p.u., ($V_i = 1$).

By using the stated assumptions, the power flow equations are simplified to expressions in terms of the lines' susceptances and the differences in voltage phasor angles between the buses.

$$P_i = \sum_{j=1}^{k} B_{ij}\delta_{ij} \text{ where } \delta_{ij} = \delta_i - \delta_j \tag{3.13}$$

Where the susceptance elements, B_{ij} and $B_{ii,}$ are defined according to (3.14).

$$B_{ij} = b_{ij} = -\frac{1}{X_{ij}} \text{ and } B_{ii} = -\sum_{j=1, j\neq i}^{k} b_{ij} \tag{3.14}$$

The formulation of (3.13) is rewritten to matrix notation in (3.15), where the net power injection vector is expressed in terms of the susceptance matrix and the column vector of voltage phasor angles δ.

$$[P] = [B] \cdot [\delta] \tag{3.15}$$

A general view of the elements in the susceptance matric, B, is given in (3.16).

[1] The angles must be expressed in radians.

$$B = \begin{bmatrix} B_{11} & B_{12} & \cdot & B_{1k} \\ B_{21} & B_{22} & \cdot & B_{2k} \\ \cdot & \cdot & \cdot & \cdot \\ B_{k1} & B_{k2} & \cdot & B_{kk} \end{bmatrix} \tag{3.16}$$

The set of linear equations is singular, since one of the rows could be expressed as the linear combination of the other rows. To overcome the problem, the concept of a slack bus is introduced. The implication is that the row and vector elements corresponding to the slack bus, are removed from the susceptance matrix, giving a sub matrix **B'**. If the first bus is chosen as the slack bus, the corresponding sub matrix is defined by (3.17).

$$B' = \begin{bmatrix} B_{22} & \cdot & B_{2k} \\ \cdot & \cdot & \cdot \\ B_{k2} & \cdot & B_{kk} \end{bmatrix} \tag{3.17}$$

Since the net power injection of the slack bus could be expressed as the linear combination of power injections at the other buses of the system, a new set of equations becomes:

$$[P] = [B'] \cdot [\delta] \tag{3.18}$$

$$P_{slack} = \sum_{j=1, j \neq slack}^{k} P_j \tag{3.19}$$

The implication is that the slack bus compensates the surplus or deficit of generation in the system. A further development of (3.18) give the voltage phasor angles expressed in terms of the inverse of the sub matrix **B'** and the net power injections. To include the slack bus into the expression again, the row and the column of the slack bus are reintroduced in the inverse sub matrix B' with values of zero, naming the new matrix **Z**.

$$[\delta] = \begin{bmatrix} 0 & 0 & \cdots & 0 \\ 0 & & & \\ \vdots & & [B']^{-1} & \\ 0 & & & \end{bmatrix} \cdot [P] = [Z] \cdot [P] \tag{3.20}$$

The active power flow through a line between bus i and j is further given as the difference in voltage phasor angles, between the two connected buses, divided by the reactance of the line.

$$P_{ij} = \frac{\delta_i - \delta_j}{X_{ij}} \tag{3.21}$$

If the above notations of (3.20) are used, each voltage phasor angle of (3.21) could be expressed as a row of the **Z** matrix times the net power injection vector. Thus, the power flow through the line between bus i and j in (3.21) could be reformulated:

$$P_{ij} = \frac{z_{i1} - z_{j1}}{X_{ij}} P_1 + \frac{z_{i2} - z_{j2}}{X_{ij}} P_2 + ... + \frac{z_{ik} - z_{jk}}{X_{ij}} P_k \tag{3.22}$$

Rewriting the expression of (3.22) to an expression in terms of the power distribution factors, denoted $a_{ij,k}$, gives the simplified format of the line flow:

$$P_{ij} = a_{ij,1} P_1 + a_{ij,2} P_2 + ... + a_{ij,k} P_k \tag{3.23}$$

When the rest of the system's line flow equations are developed similarly, the line flows are expressed in terms of the sensitivity matrix, **A**, times the net bus injection vector, **P**.

$$\left[T_p\right] = \left[A\right] \cdot \left[P\right] \tag{3.24}$$

The net injection vector, **P**, is defined in terms of the vector of load requirements subtracted from the vector of generation. The load requirements are considered as constants in the analysis. If the loads need to be reduced to maintain the power balance, it is done by curtailing loads at the load buses. Thus, an additional load curtailment vector, C_p, is introduced into the net injection vector of (3.25).

$$\left[P\right] = \left[P_g\right] + \left[C_P\right] - \left[P_{load}\right] \tag{3.25}$$

3.3.2.2 Contingency Solver Description

The network model of the system by a DC power flow representation, simplifies the constraints of the load flow problem. In DC power flow, only the active power is accounted for while the losses are ignored. Hence, the list of the constraints that are considered by the contingency solver, is presented in the following:

i) The system's generation capacity must be larger than or equal to the load requirement.
ii) The power flow through the lines are limited by their power ratings.
iii) The load curtailment at a bus cannot exceed the load requirement of the bus.

iv) The actual generation at a bus cannot exceed the generation capacity of the bus.

v) The load curtailment at a bus cannot be negative.

vi) The actual generation at a bus cannot be negative.

When a system state is handed to the "contingency solver", the solver tries to find a feasible operating state without violating any of the above listed constraints. If a violation of a constraint is present, a measure or a combination of measures is taken to restore the system back into a feasible operating point. First, the solver tries to reschedule the generation, but if the action is insufficient in removing the violation, it will be necessary to try load curtailments at one or more buses. The order of the possible actions is controlled by introducing an objective function with differing costs of rescheduling of generation and load curtailments. If the costs of load curtailments are set higher than the costs of rescheduling of generation, the solver will ensure that rescheduling of generation is tried before load curtailments are considered. By differing the costs of load curtailments at the buses, it is possible to make a prioritized list of the loads, where the loads at the bus with the lowest cost of curtailment are curtailed first [27]. Hence, the costs of the possible actions can be expressed by a row vector of 2 times k elements, where k is given as the number of buses in the system.

$$W = \begin{bmatrix} w_1 & w_2 & \dots & w_{2k} \end{bmatrix} \tag{3.26}$$

The first k elements of the cost vector correspond to the cost of rescheduling of generation, while the next k elements correspond to the cost of load curtailments. In this thesis, the costs of rescheduling of generation are set equal to zero, while the costs of load curtailments are set according to the specification in the input data. Each cost element has a corresponding decision variable, that is optimized with the goal of minimizing the overall cost. The set of decision variables are represented by a column vector, where the first k elements give the generation, P_{gi}, at the buses, while the next k elements give the load curtailments, C_i, at the buses.

$$X = \begin{bmatrix} P_{g1} & \dots & P_{gk} & C_1 & \dots & C_k \end{bmatrix}^T \tag{3.27}$$

3.3.2.3 Optimal Power Flow Formulation

After representing the system by matrices and vectors, the final step is to formulate the problem as an OPF problem. A general representation of such an OPF problem is given below in accordance with the formulation presented by Billinton and Li [7], where the objective is to minimize the load curtailments.

$$\text{Min } f = \sum_{i=1}^{k} C_i \tag{3.28}$$

$$\sum_{i=1}^{k} P_{gi} + \sum_{i=1}^{k} C_i = \sum_{i=1}^{k} P_{load,i} \tag{3.29}$$

$$\left|[A]\cdot[P]\right| \le [T_{Lim}] \tag{3.30}$$

$$0 \le P_{gi} \le P_{cap,i} \tag{3.31}$$

$$0 \le C_i \le P_{load,i} \tag{3.32}$$

The formulation needs some minor modifications to be in a format suited for solving with the dual simplex method of the built-in "linprog" function of MATLAB. Using the above presented vector notations, the objective function of (3.28) is as the cost vector times the vector of decision variables.

$$\text{Min } f = [W]\cdot[X] \tag{3.33}$$

The equality constraint of (3.29), which stipulates that the sum of the system's power generation and load curtailment must equal the load requirement, is modified to (3.34). In the equation, K is a row vector of 2 times k elements with values of one. Thus, an expression in terms of the decision variables is obtained.

$$[K]\cdot[X] = \sum_{i=1}^{k} P_{load,i} \tag{3.34}$$

The inequality constraint of (3.30), limiting the power flows through the lines, must be converted to two inequality constraints to remove the absolute value sign from the equation. The absolute value sign in the equation is needed, because the multiplication of A and P can give negative values. When using the fact that the load requirements are constant, the sensitivity matrix times the load requirement vector could be moved over to the constant side of the inequality. Thus the new inequalities are given in terms of the decision variables in (3.35) and (3.36).

$$\begin{bmatrix} A & A \end{bmatrix} \cdot [X] \leq [T_{lim}] + [A] \cdot [P_{load}] = [T_{lim1}] \tag{3.35}$$

$$-\begin{bmatrix} A & A \end{bmatrix} \cdot [X] \leq [T_{lim}] - [A] \cdot [P_{load}] = [T_{lim2}] \tag{3.36}$$

3.3.2.4 Contingency Solver Verification

A few selected system states, using the RBTS system at peak load of 185 MW, were tested in the contingency solver, to verify that the proposed OPF methodology of the DC-contingency solver gives valid results. The load requirement of the system is the same and divided according to Table 3.11 in all the test cases.

Table 3.11: The RBTS load distribution at a peak load of 185 MW.

Bus	Load demand [MW]
1	0
2	20
3	85
4	40
5	20
6	20
Sum:	185

3.3.2.4.1 Case 1

The first test is performed to check that there are no erroneous load curtailments when there are no outages of the components. When this is the case, the generation capacity of bus one and two are given by their installed capacity, cf. Table 3.12. As can be seen in Table 3.13, the contingency solver returns no erroneous load curtailments.

Table 3.12: The installed generation capacity of the RBTS.

Bus	Active Power [MW]
1	110
2	130

Table 3.13: The results of case 1.

Bus	Generation [MW]	Curtailment [MW]
1	55.00	0.00
2	130.00	0.00
3	0.00	0.00
4	0.00	0.00
5	0.00	0.00
6	0.00	0.00
Sum:	185.00	0.00

3.3.2.4.2 Case 2

The solver is also tested to check whether the load curtailments are correct when the generation capacity of the system is insufficient. A specification of the generation capacity is presented in Table 3.14. All the lines were available during the test. In Table 3.15 a total load curtailment of 35 MW is the result, making up for the deficit of generation capacity.

Table 3.14: The generation capacity of case 2.

Bus	Active Power [MW]
1	100
2	50

Table 3.15: The results of case 2.

Bus	Generation [MW]	Curtailment [MW]
1	100.00	0.00
2	50.00	0.00
3	0.00	35.00
4	0.00	0.00
5	0.00	0.00
6	0.00	0.00
Sum:	150.00	35.00

3.3.2.4.3 Case 3

The generation capacity of the system is equal to the installed capacity, specified in Table 3.12. Bus 2 and 4 are isolated from the rest of the system, due to outages of line L3, L4 and L8. The stated assumption that only the slack bus can operate in islanded mode, give load curtailments equal to the load requirements at buses 2 and 4. In addition, the generation capacity at bus 1 is insufficient to meet the total load requirement of buses 3, 5 and 6. The complete load curtailments are presented in Table 3.16.

Table 3.16: The results of case 3.

Bus	Generation [MW]	Curtailment [MW]
1	110.00	0.00
2	0.00	20.00
3	0.00	15.00
4	0.00	40.00
5	0.00	0.00
6	0.00	0.00
Sum:	110.00	75.00

3.3.2.4.4 Case 4

The generation capacity of the system is still equal to the installed capacity, given in Table 3.12, but this time there are outages of lines L5 and L8, leading to the islanding of buses 5 and 6. The load curtailments of this case are presented in Table 3.17, and are found to be equal to the load requirements at the isolated buses.

Table 3.17: The results of case 4.

Bus	Generation [MW]	Curtailment [MW]
1	15.00	0.00
2	130.00	0.00
3	0.00	0.00
4	0.00	0.00
5	0.00	20.00
6	0.00	20.00
Sum:	145.00	40.00

3.3.2.4.5 Case 5

In this case, a combination of generator and line outages occurs at the same time. The generation capacity is reduced according to the specification in Table 3.18, while line L2 and L7 are on outage. Here, the power transfer limit through line L3 is the constraint that limits the active power generation at bus 2. The resulting load curtailments of 74 MW are given in Table 3.19. It can be observed that the generation of bus 2 is limited to 91 MW for this case, which shows that the line flow constraint of L3 is binding.

Table 3.18: The generation capacity of case 5.

Bus	Active Power [MW]
1	20
2	130

Table 3.19: The results of case 5.

Bus	Generation [MW]	Curtailment [MW]
1	20.00	0.00
2	91.00	0.00
3	0.00	34.00
4	0.00	0.00
5	0.00	20.00
6	0.00	20.00
Sum:	111.00	74.00

3.3.2.5 Illustrative Example

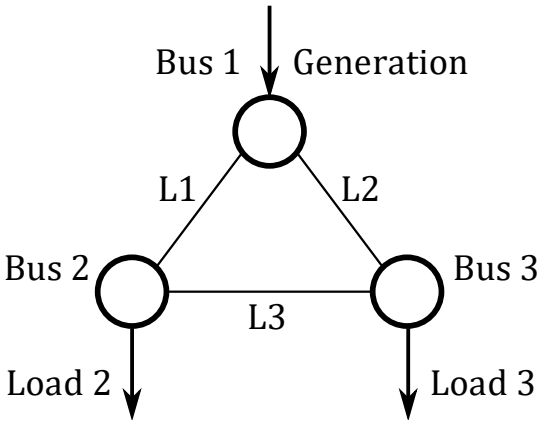

Figure 3.5: The 3-bus test system.

The following example, is presented to illustrate the basic principles of the composite system assessment methodology in a pedagogical way, where the step by step numerical calculations are included. The test system of the example is shown in Figure 3.5. It consists of 3 buses, where bus 1 is a generator bus with two connected generators, and buses 2 and 3 are load buses with constant load requirements. A network of three lines, all with equal transfer limits but different reactances, interconnect the buses. The system data is summarized in Table 3.20 - Table 3.22.

Table 3.20: The generator data of the 3-bus test system.

Generator	Bus	Capacity [MW]	FOR
G1	1	50	0.01
G2	1	50	0

Table 3.21: The loads of the 3-bus test system.

Bus	Load [MW]	Cost of load curtailment [$/kWh]
1	0	-
2	30	1
3	40	1

Table 3.22: The network data of the 3-bus test system.

Line	Reactance [pu]	Transfer limit [MW]	FOR
L1	0.1	50	0.01
L2	0.2	50	0
L3	0.2	50	0

The system is configured to have a limited number of possible contingencies, to have an example of limited size. It is accomplished by having only two components, a generator and a line, with FOR values larger than zero. Thus, the other components are assumed to be available 100 percent of the time. The power base of the system is 100MVA.

3.3.2.5.1 Step by Step Calculations

The step by step numerical calculations performed when the equations are set up according to the presented methodology, are shown for two system states. In this section, the base case where all the components are available, is shown. An additional numerical example on how to construct the problem with line L1 on outage, is provided in Appendix V.

Step 1: Obtain the elements of the sub matrix, **B'**, of the susceptance matrix using (3.14).

a) Calculate the susceptance of the three lines:

$$\begin{aligned} b_{12} = b_{21} &= -\frac{1}{0.1} = -10 \\ b_{13} = b_{31} &= -\frac{1}{0.2} = -5 \\ b_{23} = b_{32} &= -\frac{1}{0.2} = -5 \end{aligned} \tag{3.37}$$

b) Calculate the elements of the **B** matrix:

$$\begin{aligned} B_{11} &= -\left(b_{12} + b_{13}\right) = 10 + 5 = 15 \\ B_{12} &= B_{21} = b_{12} = -10 \\ B_{13} &= B_{31} = b_{13} = -5 \\ B_{22} &= -\left(b_{21} + b_{23}\right) = 10 + 5 = 15 \\ B_{23} &= B_{32} = b_{23} = -5 \\ B_{33} &= -\left(b_{31} + b_{32}\right) = 5 + 5 = 10 \end{aligned} \tag{3.38}$$

c) Create the **B** matrix:

$$B = \begin{bmatrix} 15 & -10 & -5 \\ -10 & 15 & -5 \\ -5 & -5 & 10 \end{bmatrix} \tag{3.39}$$

d) Bus 1 is chosen as the slack bus, giving the sub matrix **B'**:

$$B' = \begin{bmatrix} 15 & -5 \\ -5 & 10 \end{bmatrix} \tag{3.40}$$

Step 2: When the sub matrix **B'** is established, the next step is to obtain the **Z** matrix of (3.20).

a) Calculate the inverse of the **B'** matrix

$$[B']^{-1} = \begin{bmatrix} 0.08 & 0.04 \\ 0.04 & 0.12 \end{bmatrix} \tag{3.41}$$

b) Use the notation of (3.20) to obtain **Z** with 3x3 elements:

$$Z = \begin{bmatrix} 0 & 0 & 0 \\ 0 & 0.08 & 0.04 \\ 0 & 0.04 & 0.12 \end{bmatrix} \tag{3.42}$$

Step 3: Establish the power transfer distribution factor matrix, **A**, of (3.24).

a) The factors are obtained for each line by use of (3.22).

i) First, the factors of L1 are calculated:

$$\begin{aligned} P_{12} &= \frac{z_{11} - z_{21}}{X_{12}} \cdot P_1 + \frac{z_{12} - z_{22}}{X_{12}} \cdot P_2 + \frac{z_{13} - z_{23}}{X_{12}} \cdot P_3 \\ &= \frac{0-0}{0.1} \cdot P_1 + \frac{0-0.08}{0.1} \cdot P_2 + \frac{0-0.04}{0.1} \cdot P_3 \\ &= 0 \cdot P_1 - 0.8 \cdot P_2 - 0.4 \cdot P_3 \end{aligned} \tag{3.43}$$

ii) Similarly, the factors of L2 are calculated:

$$\begin{aligned} P_{13} &= \frac{z_{11}-z_{31}}{X_{13}}\cdot P_1 + \frac{z_{12}-z_{32}}{X_{13}}\cdot P_2 + \frac{z_{13}-z_{33}}{X_{13}}\cdot P_3 \\ &= \frac{0-0}{0.2}\cdot P_1 + \frac{0-0.04}{0.2}\cdot P_2 + \frac{0-0.12}{0.2}\cdot P_3 \\ &= 0\cdot P_1 - 0.2\cdot P_2 - 0.6\cdot P_3 \end{aligned} \tag{3.44}$$

iii) Finally, the factors of L3 are calculated:

$$\begin{aligned} P_{23} &= \frac{z_{21}-z_{31}}{X_{23}}\cdot P_1 + \frac{z_{22}-z_{32}}{X_{23}}\cdot P_2 + \frac{z_{23}-z_{33}}{X_{23}}\cdot P_3 \\ &= \frac{0-0}{0.2}\cdot P_1 + \frac{0.08-0.04}{0.2}\cdot P_2 + \frac{0.04-0.12}{0.2}\cdot P_3 \\ &= 0\cdot P_1 + 0.2\cdot P_2 - 0.4\cdot P_3 \end{aligned} \tag{3.45}$$

b) Then, the sensitivity matrix is built with the power transfer distribution factors:

$$A = \begin{bmatrix} 0 & -0.8 & -0.4 \\ 0 & -0.2 & -0.6 \\ 0 & 0.2 & -04 \end{bmatrix} \tag{3.46}$$

Step 4: Modify the line's power flow limits according to (3.35) and (3.36), by using the load data in Table 3.21 and the line limits in Table 3.22.

a) Obtain the elements of the $\mathbf{T_{lim1}}$ vector:

$$\begin{aligned} T_{Line1} &= T_{lim} + 0\cdot P_{L1} - 0.8\cdot P_{L2} - 0.4\cdot P_{L3} \\ &= 0.5 + 0\cdot 0 - 0.8\cdot 0.3 - 0.4\cdot 0.4 = 0.1 \\ T_{Line2} &= T_{lim} + 0\cdot P_{L1} - 0.2\cdot P_{L2} - 0.6\cdot P_{L3} \\ &= 0.5 + 0\cdot 0 - 0.2\cdot 0.3 - 0.6\cdot 0.4 = 0.2 \\ T_{Line3} &= T_{lim} + 0\cdot P_{L1} + 0.2\cdot P_{L2} - 0.4\cdot P_{L3} \\ &= 0.5 + 0\cdot 0 + 0.2\cdot 0.3 - 0.4\cdot 0.4 = 0.4 \end{aligned} \tag{3.47}$$

b) Obtain the elements of the $\mathbf{T_{lim2}}$ vector:

$$\begin{aligned} T_{Line1} &= T_{lim} - 0\cdot P_{L1} + 0.8\cdot P_{L2} + 0.4\cdot P_{L3} \\ &= 0.5 - 0\cdot 0 + 0.8\cdot 0.3 + 0.4\cdot 0.4 = 0.9 \\ T_{Line2} &= T_{lim} - 0\cdot P_{L1} + 0.2\cdot P_{L2} + 0.6\cdot P_{L3} \\ &= 0.5 - 0\cdot 0 + 0.2\cdot 0.3 + 0.6\cdot 0.4 = 0.8 \\ T_{Line3} &= T_{lim} - 0\cdot P_{L1} - 0.2\cdot P_{L2} + 0.4\cdot P_{L3} \\ &= 0.5 - 0\cdot 0 - 0.2\cdot 0.3 + 0.4\cdot 0.4 = 0.6 \end{aligned} \tag{3.48}$$

c) The new limits in vector form are given by:

$$T_{lim,1} = \begin{bmatrix} 0.1 \\ 0.2 \\ 0.4 \end{bmatrix} \text{ and } T_{lim,2} = \begin{bmatrix} 0.9 \\ 0.8 \\ 0.6 \end{bmatrix} \tag{3.49}$$

Step 5: The final formulation of the OPF problem is formulated by reducing the number of decision variables from 6 to 3, recognizing the non-existence of generation at buses 2 and 3 and load requirement at bus 1. Thus, the final OPF formulation becomes:

$$\text{Min } f = 0 \cdot P_{g1} + 1 \cdot C_2 + 1 \cdot C_3 \tag{3.50}$$

$$1 \cdot P_{g1} + 1 \cdot C_2 + 1 \cdot C_3 = 0.7 \tag{3.51}$$

$$\begin{aligned} 0 \cdot P_{g1} - 0.8 \cdot C_2 - 0.4 \cdot C_3 &\le 0.1 \\ 0 \cdot P_{g1} - 0.2 \cdot C_2 - 0.6 \cdot C_3 &\le 0.2 \\ 0 \cdot P_{g1} + 0.2 \cdot C_2 - 0.4 \cdot C_3 &\le 0.4 \end{aligned} \tag{3.52}$$

$$\begin{aligned} 0 \cdot P_{g1} + 0.8 \cdot C_2 + 0.4 \cdot C_3 &\le 0.9 \\ 0 \cdot P_{g1} + 0.2 \cdot C_2 + 0.6 \cdot C_3 &\le 0.8 \\ 0 \cdot P_{g1} - 0.2 \cdot C_2 + 0.4 \cdot C_3 &\le 0.6 \end{aligned} \tag{3.53}$$

$$\begin{aligned} P_{g1} &\le 1.0 \\ C_2 &\le 0.3 \\ C_2 &\le 0.4 \end{aligned} \tag{3.54}$$

$$P_{g1}, C_2, C_3 \ge 0 \tag{3.55}$$

3.3.2.5.2 Composite System Adequacy Assessment

The possible system states of the 3-bus example are presented in Table 3.23. Since only two of the system's five components have FORs larger than zero, the possible system states are given by combining the possible states of the two components with non-zero FOR. An underline of a component denotes a component on outage. The load curtailments are obtained by solving the OPF problem corresponding to each system state.

Table 3.23: The system states with probability and severity.

Event	State of the Components	Probability	Load curtailment [MW]
P(N)	G1, L1	0.9801	0
P(A)	G1, L1	0.0099	20
P(B)	G1, L1	0.0099	20
P(C)	G1, L1	0.0001	20

The probability of each system state, is calculated in (3.56) by multiplication of the state probabilities of G1 and L1, using the component data of Table 3.20 and Table 3.22.

$$\begin{aligned} P(N) &= 0.99 \cdot 0.99 = 0.9801 \\ P(A) &= 0.01 \cdot 0.99 = 0.0099 \\ P(B) &= 0.99 \cdot 0.01 = 0.0099 \\ P(C) &= 0.01 \cdot 0.01 = 0.0001 \end{aligned} \tag{3.56}$$

The four system states and the resulting power flows are illustrated in Figure 3.6 - Figure 3.8.

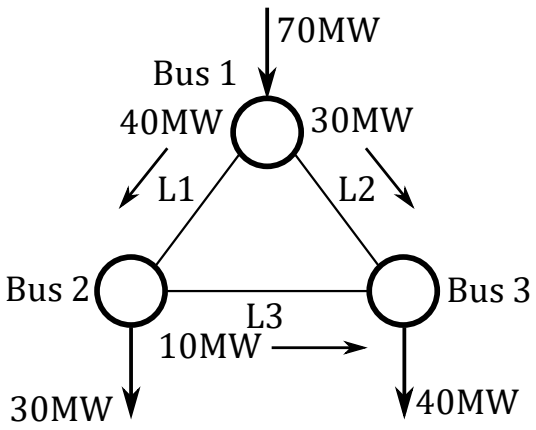

Figure 3.6: Event P(N).

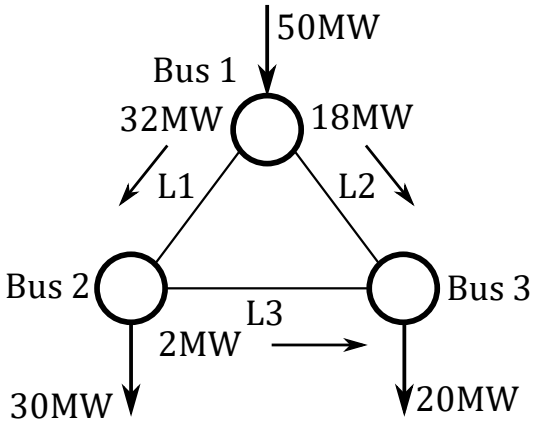

Figure 3.7: Event P(A).

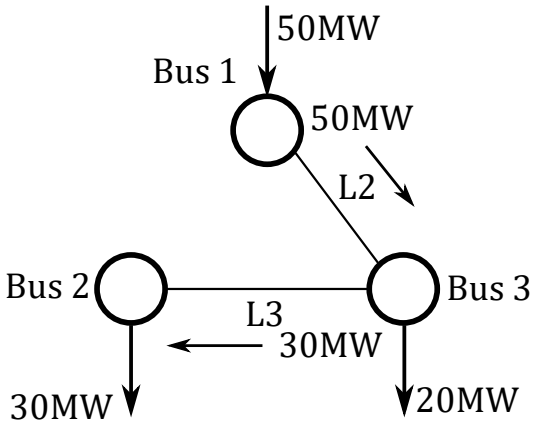

Figure 3.8: Event P(B) and P(C).

3.3.2.5.3 Calculation of the Reliability Indices

The reliability indices used in the assessment are the LOLE and EENS indices. Both are obtained by using (2.1) and (2.5) respectively. Hence, a LOLE of 0.0199 years in one year and an EENS of 3486 MWh in one year are obtained, when assuming a CYPL. The numerical calculations are shown below:

$$\begin{aligned} \mathrm{LOLE} &= X_N \cdot P(N) + X_A \cdot P(A) + X_B \cdot P(B) + X_C \cdot P(C) \\ &= 0 \cdot 0.9801 + 1 \cdot 0.0099 + 1 \cdot 0.0099 + 1 \cdot 0.0001 \\ &= 0.0199 \text{ years/year} \end{aligned} \tag{3.57}$$

$$\begin{aligned} \mathrm{EENS} &= \left[C(N) \cdot P(N) + C(A) \cdot P(A) + C(B) \cdot P(B) + C(C) \cdot P(C)\right] \cdot T \\ &= \left(0 \cdot 0.9801 + 20 \cdot 0.0099 + 20 \cdot 0.0099 + 20 \cdot 0.0001\right) \cdot 8760 \\ &= 3486.48 \text{ MWh/year} \end{aligned} \tag{3.58}$$

3.3.3 AC – Contingency Solver

The considerations of the AC contingency solver are presented in this section. First, an introduction to the equations and assumptions that are used is made, before the general form of the AC OPF problem is formulated. Then tests of the solver are performed on the same selection of system states as that of the DC contingency solver. A final illustrative example is given, to highlight the intermediate steps of the presented methodology.

3.3.3.1 Network Model

A choice must be made regarding how the network model is represented in the OPF problem of the AC contingency solver. There exist two network models that are common to use, namely the bus injection model and the branch flow model [28]. The bus injection model represents a compact form of the AC power flow equations, where the system is represented in terms of nodal variables at each system bus, i.e. active and reactive power injections, voltage phasors and current injections. It has been the most widely used network model in OPF problems since the first presented papers on OPF [28]. The branch flow model represents the system in terms of power flows and currents through each branch instead. In later years, the branch flow model has received an increased interest due to its advantages regarding convex relaxation of OPF problems [29] and [30]. This thesis uses the AC power flow equations derived from the bus injection model to represent the network. Derivations of the AC power flow equations can be found in most power system analysis textbooks, such as [25].

An important part of the AC power flow equations is how the various branch elements of the network are represented. Most of these, including transmission lines, cables and nominal transformers, can simply be represented by their π-equivalent model, cf. Figure 3.9.

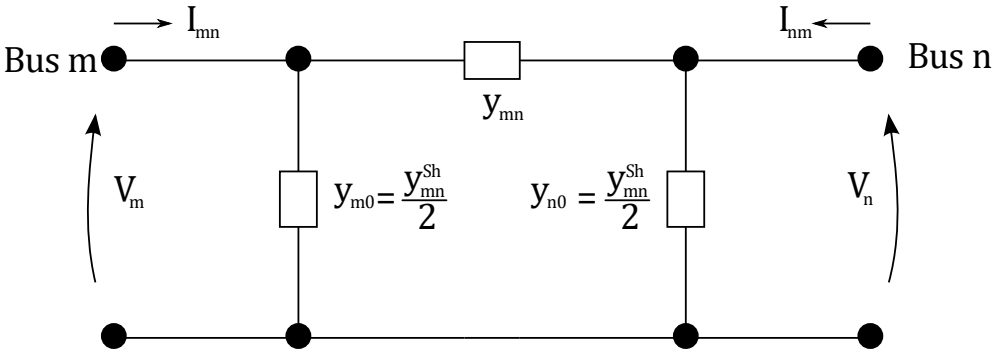

Figure 3.9: π-equivalent model.

For transmission lines and cables, the branch characteristics are normally specified in terms of a series impedance and a shunt susceptance; it is common to neglect the shunt susceptance for

transformers. As shown in Figure 3.9, the shunt susceptance is equally divided between the two buses at each end of the branch, while the series admittance of the figure, y_{mn}, is calculated from the series impedance as follows.

$$y_{mn} = \frac{1}{r_{mn} + jx_{mn}} = \frac{r_{mn}}{r_{mn}^{\ 2} + x_{mn}^{\ 2}} - j \cdot \frac{x_{mn}}{r_{mn}^{\ 2} + x_{mn}^{\ 2}} = g_{mn} + jb_{mn} \tag{3.59}$$

The net injections of currents at the two buses of Figure 3.9, can be expressed in terms of the system's admittances and voltages. Derivation from Kirchhoff's Current Law, expressing that the sum of currents flowing into a node must equal the sum of currents flowing out of the node, gives the net injection of current at each bus expressed in terms of a bus admittance matrix, Y_{bus}, times the nodal voltages [25].

$$\begin{bmatrix} I_m \\ I_n \end{bmatrix} = \begin{bmatrix} Y_{mm} & Y_{mn} \\ Y_{nm} & Y_{nn} \end{bmatrix} \cdot \begin{bmatrix} V_m \\ V_n \end{bmatrix} \tag{3.60}$$

The elements of the Y_{bus} matrix are mounted according to the following scheme. Each row and column corresponds to a bus, e.g. the elements of row 2 and column 2 correspond to bus 2. The diagonal elements of the matrix are mounted by summing the following for each of the lines that are connected to the bus: the series admittance and half of the shunt susceptance. Off-diagonal elements are set to zero if there are no branch elements between the corresponding buses, otherwise the elements are mounted by adding the negative of the branch element's series admittance. If two or more lines are connected in parallel between the two buses, the negatives of the series admittances are added together. Thus, the Y_{bus} of the two-bus system in Figure 3.9 is given by:

$$Y_{bus} = \begin{bmatrix} y_{mn} + y_{m0} & -y_{mn} \\ -y_{nm} & y_{nm} + y_{n0} \end{bmatrix} \tag{3.61}$$

If the transformer is off-nominal, a more complex branch model must be used by introducing additional variables into the equations. A tap changing transformer has a real turns ratio, a:1, while a phase shifting transformer has a complex turns ratio. This turns ratio can be represented in polar coordinates with magnitude T_{mn} and phase shift φ_{mn}. If the turns ratio is real, the phase shift is set to zero.

$$a_{mn} = T_{mn} \cdot e^{j\varphi_{mn}} \tag{3.62}$$

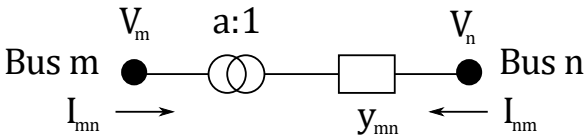

Figure 3.10: Off-nominal transformer.

A single line representation of an off-nominal transformer is shown in Figure 3.10. As previously stated it is common to neglect the shunt susceptance of transformers. Thus, the Y_{bus} elements of an off-nominal transformer branch are given in (3.63). An inspection of the matrix elements shows that the two off-diagonal elements, Y_{mn} and Y_{nm}, differ by opposite signs of the phase shift variables, giving an unsymmetrical Y_{bus}.

$$Y_{bus} = \begin{bmatrix} \frac{y_{mn}}{T_{mn}^2} & -\frac{y_{mn}}{T_{mn} \cdot e^{-j\varphi_{mn}}} \\ -\frac{y_{mn}}{T_{mn} \cdot e^{j\varphi_{mn}}} & y_{mn} \end{bmatrix} \tag{3.63}$$

The system's bus admittance matrix can be mounted by adding the elements of each branch together. It is worth noting that the Y_{bus} of a large system would be sparse, consisting of mostly zeros in the off-diagonal elements, due to each bus being directly connected to only one or a few other buses.

$$Y_{bus} = \begin{bmatrix} Y_{11} & Y_{12} & \cdots & Y_{1k} \\ Y_{21} & Y_{22} & \cdots & Y_{2k} \\ \vdots & \vdots & \ddots & \vdots \\ Y_{k1} & Y_{k2} & \cdots & Y_{kk} \end{bmatrix} \tag{3.64}$$

This thesis uses a separation of the Y_{bus} matrix into its real and imaginary parts, namely a separation into a conductance and a susceptance matrix, to avoid having complex numbers in the AC power flow equations.

$$[Y_{bus}] = [G_{bus}] + j \cdot [B_{bus}] \tag{3.65}$$

It is common to separate the AC power flow equations into active and reactive power injections at each bus. Thus, the equations where the voltages are expressed in polar coordinates and the

bus admittance matrix elements are expressed in rectangular coordinates, are given by (3.66) and (3.67) for each bus:

$$P_i(V,\delta) = V_i \cdot \sum_{j=1}^{k} V_j \left[G_{ij} \cdot \cos(\delta_i - \delta_j) + B_{ij} \cdot \sin(\delta_i - \delta_j) \right] \tag{3.66}$$

$$Q_i(V,\delta) = V_i \cdot \sum_{j=1}^{k} V_j \left[G_{ij} \cdot \sin(\delta_i - \delta_j) - B_{ij} \cdot \cos(\delta_i - \delta_j) \right] \tag{3.67}$$

The vectors giving the net injection of powers at each bus, both active and reactive, are defined similarly as in the DC approach. Thus, (3.25) gives the net injection of active power vector, while (3.68) gives the net injection of reactive power vector. Both give the net injections as the load requirements subtracted from the sum of actual power generations and load curtailments. It is worth noting that the load requirements at each bus are treated as a constant in the OPF problem, while a vector of load curtailments are introduced to have the option of reducing the loads to reach a feasible solution to the OPF problem.

$$[Q] = [Q_g] + [C_Q] - [Q_{load}] \tag{3.68}$$

Another important part of the network model are the constraints limiting the flow of current through the branches. The magnitude of the current flowing through a branch is given by the magnitude of the voltage drop over the branch, times the magnitude of the series admittance:

$$|I_{mn}| = |V_m - V_n| \cdot |y_{mn}| \leq I_{mn}^{max} \tag{3.69}$$

3.3.3.2 Contingency Solver Description

A representation of the system by the AC power equations leads to a larger of number of considered constraints in the OPF problem than for the DC based approach. The list of constraints that are considered by the AC contingency solver is presented in the following:

a) The system's generation capacity must be larger than or equal to the sum of the system's load requirements and losses, where both active and reactive power are considered.
b) The power flow through the lines are limited by the maximum current rating of the lines.
c) The load curtailment at a bus cannot exceed the load requirement of the bus, where both active and reactive power are considered.

d) The actual generation at a bus cannot exceed the generation capacity of the bus, where both active and reactive power are considered.
e) The actual active power generation at a bus cannot be negative.
f) The actual reactive power generation at a bus cannot be lower than the minimum reactive power capability of the bus.
g) The load curtailment at a bus cannot be negative, when both active and reactive power are considered[1].
h) The voltage magnitude at each bus must be inside the specified limits.

The possible actions of the AC contingency solver are similar to the ones of the DC based solver, e.g. rescheduling of generation and load curtailment. When a system state is handed to the AC contingency solver, the solver tries to find a feasible operating point that is not violating any of the above listed constraints. Rescheduling of generation is tried first, before load curtailments are considered. Due to the inclusion of reactive power considerations in the analysis, there is an increased number of system states that require actions compared to when the DC approximations are applied. An example of such a situation is when the voltage at one or more buses drops below the specified voltage limit, due to voltage drops in the transmission lines in spite of sufficient generation capacity in the system. In a similar fashion as for the DC based approach, the control actions are controlled by the objective function of the OPF problem. The objective function consists of a vector of decision variables that is multiplied by a cost vector. Each element of the cost vector corresponds to the cost of increasing a decision variable. In the approach suggested in this thesis, there are only costs associated with load curtailments. The cost of load curtailments at each bus are specified according to the input data of the test system.

$$W = \begin{bmatrix} w_1 & w_2 & \cdots & w_{6k} \end{bmatrix}^T \tag{3.70}$$

Compared to the OPF problem of the DC contingency solver, the number of decision variables is increased. It is common to partition the decision variables into two sets [28], [31]: a set of control variables and a set of state variables. Control variables are the independent variables that are controllable, typically active and reactive power generation at each bus. The voltage magnitudes and voltage angles at the buses form the set of state variables that are dependent.

[1] The reactive power part of the load requirement is limited to positive values. A negative load requirement value is defined as a generation capacity instead.

Load requirements at the buses are fixed parameters for each system state. If it is necessary to reduce the load of the system to overcome a constraint violation, it is handled by introducing load curtailment variables at each bus to the set of control variables. Thus, the decision variables used in this thesis are:

$$X = \left[P_{g1} \quad \cdots \quad Q_{g1} \quad \cdots \quad C_P \quad \cdots \quad C_Q \quad \cdots \quad V_1 \quad \cdots \quad \delta_1 \quad \cdots \right] \tag{3.71}$$

The vector of decision variables consists of 6k elements, where k elements[1] of each decision variable type are ordered in sequence: active power generation, reactive power generation, active power load curtailment, reactive power load curtailment, voltage magnitude and voltage angle. It is also possible to include additional control variables in the set of decision variables. Among them are more advanced controls, such as tap changing and phase shifting of off-nominal transformers, thus increasing the number of variables considerably and complicating the problem [28]. If more control variables are added to the set of decision variables, the vectors of (3.70) and (3.71) must be updated accordingly.

3.3.3.3 Optimal Power Flow Formulation

The OPF problem formulation used in this thesis has its basis in the classic formulation presented in [28]. It is a variant based on the classic form presented in [31], which has the typical objective of reducing the total cost of generation. For the considered OPF problems of this thesis, the desired objective is to minimize the total cost of load curtailments. In the following, the general OPF problem is formulated using the notations and matrices of the previous sections. It is important to note that all quantities must be in per unit notation, and angles must be expressed in radians, for the equations to be applicable.

$$\min f = [X] \cdot [W] \tag{3.72}$$

$$P_{gi} + C_{Pi} - P_{load,i} - P_i(V, \delta) = 0 \tag{3.73}$$

$$Q_{gi} + C_{Qi} - Q_{load,i} - Q_i(V, \delta) = 0 \tag{3.74}$$

$$I_{mn} \leq I_{mn}^{max} \tag{3.75}$$

[1] Each element corresponds to one of the system's k buses.

$$H_{Load,i} \cdot C_{Pi} - C_{Qi} = 0 \tag{3.76}$$

$$0 \le P_{gi} \le P_{gi}^{max} \tag{3.77}$$

$$Q_{gi}^{min} \le Q_{gi} \le Q_{gi}^{max} \tag{3.78}$$

$$0 \le C_{Pi} \le P_{load,i} \tag{3.79}$$

$$0 \le C_{Qi} \le Q_{load,i} \tag{3.80}$$

$$V_i^{min} \le V_i \le V_i^{max} \tag{3.81}$$

$$-\pi \le \delta_i \le \pi \tag{3.82}$$

In the approach used in this thesis, bus number 1 of the system is selected as the slack bus. Thus, the constraint of (3.82) for this bus is limited to a fixed angle of 0 radians. Equations (3.73) and (3.74) are extended to complete form by rewriting them in terms of the decision variables by use of (3.66) and (3.67). The inequalities in the form of (3.75) must also be rewritten in a format suitable for the nonlinear solver. A suitable form is given in (3.83) by rewriting (3.69) in terms of the decision variables, where the current limit is moved to the left side of the inequality.

$$\left(V_m \cdot \cos\delta_m - V_n \cdot \cos\delta_n\right)^2 + \left(V_m \cdot \sin\delta_m - V_n \cdot \sin\delta_n\right)^2 - \left(\frac{I_{mn}^{max}}{y_{mn}}\right)^2 \le 0 \tag{3.83}$$

An equation set in the form of (3.76) is needed to keep the power factors of the loads fixed, when loads are curtailed. $H_{load,i}$ gives the specified relation between active and reactive power load requirement at each bus, thus ensuring a constant power factor. The equation set represents a set of linear equality constraints, which could be expressed by an **A** matrix times the vector of decision variables in (3.84), where the **A** matrix is filled to comply with (3.76).

$$[A] \cdot [X] = \begin{bmatrix} 0 \\ \vdots \\ 0 \end{bmatrix} \tag{3.84}$$

If additional control variables, such as tap changing and phase shifting, are included in the set of decision variables, additional constraints that limit the range of these controls must be added to the problem.

$$T_{mn}^{min} \leq T_{mn} \leq T_{mn}^{max} \tag{3.85}$$

$$\varphi_{mn}^{min} \leq \varphi_{mn} \leq \varphi_{mn}^{max} \tag{3.86}$$

3.3.3.4 Initial Starting Point

In nonlinear optimization, the choice of starting point is important for the solution of the OPF problem, i.e. the initialization of the system. Two common approaches are typical: either use a "flat start" where voltage magnitudes are set to 1.0 p.u. and voltage angles to zero, or a "warm start" where the voltage magnitudes and voltage angles are initialized according to a pre-solved load flow [28]. The convergence of the OPF problem's power flow equations rely on the choice of starting point.

During the thesis work, different choices of starting points were tested to ensure that the contingency solver returned valid solutions for all possible system states. The nonlinear solver used in this thesis, is the *fmincon* solver of MATLAB with the interior point algorithm [32]. An inbuilt feature of the solver is that an exitflag can be returned along with the OPF solution. The exitflag provides additional information regarding the solution according to the following:

a) Exitflag +2: Might be an optimal solution, but the solution should be tested further. The solver ends, because the change in the solution is smaller than the step tolerance of 1E-10, i.e. the solver tries to take a step that is smaller than this value.
b) Exitflag +1: A local optimum is found.
c) Exitflag 0: The solver returns a solution due to reaching the maximum number of iterations or function evaluations. The standard settings of the *fmincon* solver, interior point algorithm, are 3 000 for the MaxFunctionEvalutaions and 10 000 for the MaxIterations settings.
d) Exitflag -1: The solver is interrupted and ended by an output or plot function.
e) Exitflag -2: No feasible solution is found.

Thus, a solution should only be accepted if an exitflag of +1 is returned along with the solution. By practical experience during the thesis work, it was discovered that it was advantageous to increase the number of maximum function evaluations according to Table 3.24.

Table 3.24: Tuning of the fmincon solver.

Test System Setting	Maximum Function Evaluations
Standard	3 000
Specific for RBTS	50 000
Specific for RTS	70 000

It was also discovered through testing on the test systems, that different starting points gave correct solutions for some system states, but failed to deliver correct solutions for other system states. When such is the case, the solver also returns an exitflag different from +1. Thus, a scheme that is presented below was created by taking advantage of the returned exitflags. Common for the tries of starting points presented in the following are that all use a "flat start" for the state variables, i.e. voltage magnitudes of 1.0 p.u. and angles set to zero. Load curtailments, both active and reactive, are also initialized to zero.

Try 1: The starting point, x0, is initialized with active power generation set equal to the available capacity at each bus, while the reactive power generation at each bus is set to zero.

a) If the solver returns an exitflag of +2 or 0, the solver is run again with the new solution as starting point.
    i) If an exitflag of +1 is returned, the solution is accepted.
    ii) Any other exitflag, leads to try number 2.
b) If an exitflag of +1 is returned, the solution is accepted.
c) Any other exitflag, leads to try number 2.

Try 2: The starting point, x0, is initialized with both active and reactive power generation set equal to the available capacity at each bus.

a) If the solver returns an exitflag of +2 or 0, the solver is run again with the new solution as starting point.
    i) If an exitflag of +1 is returned, the solution is accepted.
    ii) Any other exitflag, leads to try number 3.

b) If an exitflag of +1 is returned, the solution is accepted.
c) Any other exitflag, leads to try number 3.

Try 3: The starting point, x0, is initialized with both active and reactive power generation set to zero.

a) If the solver returns an exitflag of +2 or 0, the solver is run again with the new solution as starting point.
    i) If an exitflag of +1 is returned, the solution is accepted.
b) If an exitflag of +1 is returned, the solution is accepted.

To capture cases where the final solution was received with an exitflag different from +1, an error script was written, which writes a text file with system details for system states that were solved by more than one tries of initial starting points.

3.3.3.5 Contingency Solver Verification

The contingency solver was tested to verify the suggested OPF methodology on a similar selection of system states to the ones used for the DC contingency solver, i.e. on the RBTS test system at peak load of 185 MW with various configurations. In Table 3.25, the load requirements at each bus are specified.

Table 3.25: The RBTS load distribution at a peak load of 185 MW.

Bus	Active Load Demand [MW]	Reactive Load Demand [MVAr]
1	0	0
2	20	4
3	85	17
4	40	8
5	20	4
6	20	4
Sum:	185	37

3.3.3.5.1 Case 1

In the first test, all components are assumed to be working. Thus, the generation capacities at buses 1 and 2 are equal to the installed capacities, cf. Table 3.26. The test is performed to verify that no loads are curtailed erroneously.

Table 3.26: The installed generation capacity of the RBTS.

Bus	Active Power [MW]	Min Reactive Power [MVAr]	Max Reactive Power [MVAr]
1	110	-37	53
2	130	-43	75

Table 3.27: The results of case 1.

Bus	Generation [MW]	Generation [MVAr]	Curtailment [MW]	Voltage [p.u.]
1	94.00	31.30	0.00	1.04
2	95.50	-1.30	0.00	1.04
3	0.00	0.00	0.00	1.00
4	0.00	0.00	0.00	1.00
5	0.00	0.00	0.00	0.99
6	0.00	0.00	0.00	0.98
Sum:	189.50	-	0.00	-

3.3.3.5.2 Case 2

Another test is performed to verify that the contingency solver curtails loads when the system's generation capacity is insufficient. During the test, all lines of the system were available. The generation capacity of the case is specified in Table 3.28, with generators 7, 8 and 11 on outage. A total load curtailment of 37.5 MW can be seen in Table 3.29, which is 2.5 MW higher than the result obtained by the DC contingency solver in Table 3.15. The higher load curtailment is reasonable, because the losses of the lines are included in the AC solution.

Table 3.28: The generation capacity of case 2.

Bus	Active Power [MW]	Min Reactive Power [MVAr]	Max Reactive Power [MVAr]
1	100	-37	46
2	50	-14	34

Table 3.29: The results of case 2.

Bus	Generation [MW]	Generation [MVAr]	Curtailment [MW]	Voltage [p.u.]
1	100.00	12.30	0.00	1.05
2	50.00	-1.20	0.00	1.05
3	0.00	0.00	37.40	1.02
4	0.00	0.00	0.00	1.02
5	0.00	0.00	0.00	1.01
6	0.00	0.00	0.10	1.00
Sum:	150.00	-	37.50	-

3.3.3.5.3 Case 3

Another test is performed to verify that the contingency solver handles the isolation of buses properly. The system's generation capacity is equal to the installed capacity, cf. Table 3.26. Lines L3, L4 and L8 are on outage, leading to the islanding of buses 2 and 4. A total load curtailment of 77.5 MW is observed in Table 3.30, where the loads at the isolated buses are curtailed correctly although the isolated part of the system has connected generators. There are also load curtailments at buses 3 and 6, due to bus 1 being unable to supply the total load demand of the connected part. It can be observed that the AC based solver returns a higher load curtailment than the DC based solver does for the same case, as it takes the transfer losses into account.

Table 3.30: The results of case 3.

Bus	Generation [MW]	Generation [MVAr]	Curtailment [MW]	Voltage [p.u.]
1	110.00	27.30	0.00	1.05
2	0.00	0.00	20.00	0.00
3	0.00	0.00	17.40	1.01
4	0.00	0.00	40.00	0.00
5	0.00	0.00	0.00	0.99
6	0.00	0.00	0.10	0.98
Sum:	110.00	-	77.50	-

3.3.3.5.4 Case 4

The system's generation capacity is still equal to the installed capacity, cf. Table 3.26. Lines L5 and L8 are on outage, leading to the islanding of buses 5 and 6. A total load curtailment of 40 MW can be seen in Table 3.31, where the loads at the isolated buses are curtailed correctly. For this case, the generation capacity is sufficient to handle the sum of load demands and losses in the connected part, and thus the AC contingency solver gives an equal load curtailment as the DC contingency solver does for this case.

Table 3.31: The results of case 4.

Bus	Generation [MW]	Generation [MVAr]	Curtailment [MW]	Voltage [p.u.]
1	71.00	18.50	0.00	1.02
2	76.40	-3.00	0.00	1.03
3	0.00	0.00	0.00	1.00
4	0.00	0.00	0.00	1.00
5	0.00	0.00	20.00	0.00
6	0.00	0.00	20.00	0.00
Sum:	147.40	-	40.00	-

3.3.3.5.5 Case 5

Another test is performed on a case where both generators and lines are on outage. The generation capacity is specified in Table 3.32, where generators 1, 3 and 4 are on outage. Lines L2 and L7 are on outage, and thus the transfer of power that is generated at bus 2, is limited to line L3. A total load curtailment of 100.1 MW can be seen in Table 3.33. The higher load curtailment, 26.1 MW, than the one of the DC contingency solver in Table 3.19, is due the large voltage drop associated with power transfers trough the remaining lines. For the DC case, the current rating of line L3 was the binding constraint, but for the AC case the voltage limit at bus 6 is the binding constraint.

Table 3.32: The generation capacity of case 5.

Bus	Active Power [MW]	Min Reactive Power [MVAr]	Max Reactive Power [MVAr]
1	20	-7	12
2	130	-43	75

Table 3.33: The results of case 5.

Bus	Generation [MW]	Generation [MVAr]	Curtailment [MW]	Voltage [p.u.]
1	20.00	12.00	0.00	1.01
2	68.10	6.40	0.00	1.05
3	0.00	0.00	84.80	0.98
4	0.00	0.00	0.00	0.97
5	0.00	0.00	0.00	0.97
6	0.00	0.00	15.30	0.97
Sum:	88.10		100.10	

3.3.3.6 Illustrative Example

A small example is presented to illustrate the basic principles of the AC based composite system assessment methodology in a pedagogical way. Numerical calculations that are performed when the OPF problem is formulated, are included. The test system is the same 3-bus test system that was presented in the DC contingency solver section 3.3.2.5. An illustration of the system can be seen in Figure 3.5. Additional system details are included in Table 3.34 through Table 3.36, due to the need to consider reactive power and voltages. The system power base is 100 MVA. Voltages at the buses are limited to a range from 0.95 to 1.05 p.u. The power factors of the loads are fixed at 0.98, implying that a curtailment of 1 p.u. active load must be met by a curtailment of 0.2 p.u. reactive load to maintain a constant power factor.

Table 3.34: The generator data of the 3-bus test system.

Generator	Bus	Active Power [MW]	Min Reactive Power [MVAr]	Max Reactive Power [MVAr]	FOR
G1	1	50	-10	20	0.01
G2	1	50	-10	20	0

Table 3.35: The loads of the 3-bus test system.

Bus	Active Load [MW]	Reactive Load [MVAr]	Cost of load curtailment [$/kWh]
1	0	0	-
2	30	6	1
3	40	8	1

Table 3.36: The network data of the 3-bus test system.

Line	From	To	Resistance [p.u.]	Reactance [p.u.]	Half of Shunt Susceptance [p.u.]	Transfer limit [p.u]	FOR
L1	1	2	0.02	0.1	0.01	0.5	0.01
L2	1	3	0.04	0.2	0.02	0.5	0
L3	2	3	0.04	0.2	0.02	0.5	0

The number of possible contingencies for the system are limited, due to only considering the outages of G1 and L1 as possible. FOR values of the components are similar to that of the DC based example, yielding equal system states and corresponding possibilities.

3.3.3.6.1 Step by Step Calculations

A step by step approach with numerical details, where the OPF problem is formulated according to the suggested methodology, is presented in this section. The base case is presented here, while an additional example with line L1 on outage is provided in Appendix VI.

Step 1: Obtain the conductance and susceptance matrices of (3.65):

a) Calculate the series admittance of the lines by (3.59):

$$\begin{aligned} y_{12} &= \frac{1}{0.02+j0.1} = \frac{0.02}{0.02^2+0.1^2} - j\frac{0.1}{0.02^2+0.1^2} = 1.9231 - j9.6154 \\ y_{13} &= \frac{1}{0.04+j0.2} = \frac{0.04}{0.04^2+0.2^2} - j\frac{0.2}{0.04^2+0.2^2} = 0.9615 - j4.8077 \\ y_{23} &= y_{13} \end{aligned} \tag{3.87}$$

b) Calculate the elements of the conductance matrix, $\mathbf{G_{bus}}$:

$$\begin{aligned} G_{11} &= g_{12} + g_{13} = 1.9231 + 0.9615 = 2.8846 \\ G_{22} &= g_{12} + g_{23} = 1.9231 + 0.9615 = 2.8846 \\ G_{33} &= g_{13} + g_{23} = 0.9615 + 0.9615 = 1.9231 \\ G_{12} &= G_{21} = -g_{12} = -1.9231 \\ G_{13} &= G_{31} = -g_{13} = -0.9615 \\ G_{23} &= G_{32} = -g_{23} = -0.9615 \end{aligned} \tag{3.88}$$

c) Calculate the elements of the susceptance matrix, $\mathbf{B_{bus}}$:

$$
\begin{aligned}
B_{11} &= b_{12} + b_{13} + b_{10}^{L1} + b_{10}^{L2} = -9.6154 - 4.8077 + 0.01 + 0.02 = -14.3931 \\
B_{22} &= b_{12} + b_{23} + b_{20}^{L1} + b_{20}^{L3} = -9.6154 - 4.8077 + 0.01 + 0.02 = -14.3931 \\
B_{33} &= b_{13} + b_{23} + b_{30}^{L2} + b_{30}^{L3} = -4.8077 - 4.8077 + 0.02 + 0.02 = -9.5754 \\
B_{12} &= B_{21} = -b_{12} = 9.6154 \\
B_{13} &= B_{31} = -b_{13} = 4.8077 \\
B_{23} &= B_{32} = -b_{23} = 4.8077
\end{aligned}
\tag{3.89}
$$

d) Create the conductance matrix, $\mathbf{G_{bus}}$:

$$
G_{bus} = \begin{bmatrix} 2.88 & -1.92 & -0.96 \\ -1.92 & 2.88 & -0.96 \\ -0.96 & -0.96 & 1.92 \end{bmatrix} \tag{3.90}
$$

e) Create the susceptance matrix**,** $\mathbf{B_{bus}}$:

$$
B_{bus} = \begin{bmatrix} -14.39 & 9.62 & 4.81 \\ 9.62 & -14.39 & 4.81 \\ 4.81 & 4.81 & -9.58 \end{bmatrix} \tag{3.91}
$$

Step 2: Set up the AC power flow equations (3.66) and (3.67) for each of the three buses:

a) Active power:

$$
\begin{aligned}
P_1(V,\delta) &= V_1V_1\left[G_{11}\cos(\delta_1-\delta_1)+B_{11}\sin(\delta_1-\delta_1)\right] \\
&\quad + V_1V_2\left[G_{12}\cos(\delta_1-\delta_2)+B_{12}\sin(\delta_1-\delta_2)\right] \\
&\quad + V_1V_3\left[G_{13}\cos(\delta_1-\delta_3)+B_{13}\sin(\delta_1-\delta_3)\right] \\
&= 2.88\cdot V_1^2 - 1.92\cdot V_1V_2\cos(\delta_1-\delta_2) + 9.62\cdot V_1V_2\sin(\delta_1-\delta_2) \\
&\quad -0.96\cdot V_1V_3\cos(\delta_1-\delta_3) + 4.81\cdot V_1V_3\sin(\delta_1-\delta_3)
\end{aligned}
\tag{3.92}
$$

$$
\begin{aligned}
P_2(V,\delta) &= V_2V_1\left[G_{21}\cos(\delta_2-\delta_1)+B_{21}\sin(\delta_2-\delta_1)\right] \\
&\quad + V_2V_2\left[G_{22}\cos(\delta_2-\delta_2)+B_{22}\sin(\delta_2-\delta_2)\right] \\
&\quad + V_2V_3\left[G_{23}\cos(\delta_2-\delta_3)+B_{23}\sin(\delta_2-\delta_3)\right] \\
&= -1.92\cdot V_2V_1\cos(\delta_2-\delta_1) + 9.62\cdot V_2V_1\sin(\delta_2-\delta_1) + 2.88\cdot V_2^2 \\
&\quad -0.96\cdot V_2V_3\cos(\delta_2-\delta_3) + 4.81\cdot V_2V_3\sin(\delta_2-\delta_3)
\end{aligned}
\tag{3.93}
$$

$$\begin{aligned}P_3(V,\delta) &= V_3V_1\left[G_{31}\cos(\delta_3-\delta_1)+B_{31}\sin(\delta_3-\delta_1)\right]\\ &+V_3V_2\left[G_{32}\cos(\delta_3-\delta_2)+B_{32}\sin(\delta_3-\delta_2)\right]\\ &+V_3V_3\left[G_{33}\cos(\delta_3-\delta_3)+B_{33}\sin(\delta_3-\delta_3)\right]\\ &=-0.96\cdot V_3V_1\cos(\delta_3-\delta_1)+4.81\cdot V_3V_1\sin(\delta_3-\delta_1)\\ &-0.96\cdot V_3V_2\cos(\delta_3-\delta_2)+4.81\cdot V_3V_2\sin(\delta_3-\delta_2)+1.92\cdot V_3^2\end{aligned} \tag{3.94}$$

b) Reactive Power:

$$\begin{aligned}Q_1(V,\delta) &= V_1V_1\left[G_{11}\sin(\delta_1-\delta_1)-B_{11}\cos(\delta_1-\delta_1)\right]\\ &+V_1V_2\left[G_{12}\sin(\delta_1-\delta_2)-B_{12}\cos(\delta_1-\delta_2)\right]\\ &+V_1V_3\left[G_{13}\sin(\delta_1-\delta_3)-B_{13}\cos(\delta_1-\delta_3)\right]\\ &=14.39\cdot V_1^2-1.92\cdot V_1V_2\sin(\delta_1-\delta_2)-9.62\cdot V_1V_2\cos(\delta_1-\delta_2)\\ &-0.96\cdot V_1V_3\sin(\delta_1-\delta_3)-4.81\cdot V_1V_3\cos(\delta_1-\delta_3)\end{aligned} \tag{3.95}$$

$$\begin{aligned}Q_2(V,\delta) &= V_2V_1\left[G_{21}\sin(\delta_2-\delta_1)-B_{21}\cos(\delta_2-\delta_1)\right]\\ &+V_2V_2\left[G_{22}\sin(\delta_2-\delta_2)-B_{22}\cos(\delta_2-\delta_2)\right]\\ &+V_2V_3\left[G_{23}\sin(\delta_2-\delta_3)-B_{23}\cos(\delta_2-\delta_3)\right]\\ &=-1.92\cdot V_2V_1\sin(\delta_2-\delta_1)-9.62\cdot V_2V_1\cos(\delta_2-\delta_1)+14.39\cdot V_2^2\\ &-0.96\cdot V_2V_3\sin(\delta_2-\delta_3)-4.81\cdot V_2V_3\cos(\delta_2-\delta_3)\end{aligned} \tag{3.96}$$

$$\begin{aligned}Q_3(V,\delta) &= V_3V_1\left[G_{31}\sin(\delta_3-\delta_1)-B_{31}\cos(\delta_3-\delta_1)\right]\\ &+V_3V_2\left[G_{32}\sin(\delta_3-\delta_2)-B_{32}\cos(\delta_3-\delta_2)\right]\\ &+V_3V_3\left[G_{33}\sin(\delta_3-\delta_3)-B_{33}\cos(\delta_3-\delta_3)\right]\\ &=-0.96\cdot V_3V_1\sin(\delta_3-\delta_1)-4.81\cdot V_3V_1\cos(\delta_3-\delta_1)\\ &-0.96\cdot V_3V_2\sin(\delta_3-\delta_2)-4.81\cdot V_3V_2\cos(\delta_3-\delta_2)+9.58\cdot V_3^2\end{aligned} \tag{3.97}$$

Step 3: Set up the power balance equations for each bus, by using the AC power flow equations from step 2 and the net injection equations of (3.25) and (3.68), and the nonlinear line current constraints for each line using (3.83):

a) The power balance at each bus:

$$\begin{aligned}
&P_{g1}+C_{P1}-P_{load,1}-P_1(V,\delta)=P_{g1}+C_{P1}-P_1(V,\delta)=0\\
&P_{g2}+C_{P2}-P_{load,2}-P_2(V,\delta)=P_{g2}+C_{P2}-P_2(V,\delta)-0.3=0\\
&P_{g3}+C_{P3}-P_{load,3}-P_3(V,\delta)=P_{g3}+C_{P3}-P_3(V,\delta)-0.4=0\\
&Q_{g1}+C_{Q1}-Q_{load,1}-Q_1(V,\delta)=Q_{g1}+C_{Q1}-Q_1(V,\delta)=0\\
&Q_{g2}+C_{Q2}-Q_{load,2}-Q_2(V,\delta)=Q_{g2}+C_{Q2}-Q_2(V,\delta)-0.06=0\\
&Q_{g3}+C_{Q3}-Q_{load,3}-Q_3(V,\delta)=Q_{g3}+C_{Q3}-Q_3(V,\delta)-0.08=0
\end{aligned} \tag{3.98}$$

b) The current constraints for the three lines:

i) Line L1:

$$\begin{aligned}
&(V_1\cos\delta_1-V_2\cos\delta_2)^2+(V_1\sin\delta_1-V_2\sin\delta_2)^2-\left(\frac{I_{12}^{max}}{\sqrt{g_{12}^2+b_{12}^2}}\right)^2\le 0\\
&(V_1\cos\delta_1-V_2\cos\delta_2)^2+(V_1\sin\delta_1-V_2\sin\delta_2)^2-\frac{0.5^2}{1.92^2+9.62^2}\le 0\\
&(V_1\cos\delta_1-V_2\cos\delta_2)^2+(V_1\sin\delta_1-V_2\sin\delta_2)^2-0.002598\le 0
\end{aligned} \tag{3.99}$$

ii) Line L2:

$$\begin{aligned}
&(V_1\cos\delta_1-V_3\cos\delta_3)^2+(V_1\sin\delta_1-V_3\sin\delta_3)^2-\left(\frac{I_{13}^{max}}{\sqrt{g_{13}^2+b_{13}^2}}\right)^2\le 0\\
&(V_1\cos\delta_1-V_3\cos\delta_3)^2+(V_1\sin\delta_1-V_3\sin\delta_3)^2-\frac{0.5^2}{0.96^2+4.81^2}\le 0\\
&(V_1\cos\delta_1-V_3\cos\delta_3)^2+(V_1\sin\delta_1-V_3\sin\delta_3)^2-0.010392\le 0
\end{aligned} \tag{3.100}$$

iii) Line L3:

$$\begin{aligned}
&(V_2\cos\delta_2-V_3\cos\delta_3)^2+(V_2\sin\delta_2-V_3\sin\delta_3)^2-\left(\frac{I_{23}^{max}}{\sqrt{g_{23}^2+b_{23}^2}}\right)^2\le 0\\
&(V_2\cos\delta_2-V_3\cos\delta_3)^2+(V_2\sin\delta_2-V_3\sin\delta_3)^2-\frac{0.5^2}{0.96^2+4.81^2}\le 0\\
&(V_2\cos\delta_2-V_3\cos\delta_3)^2+(V_2\sin\delta_2-V_3\sin\delta_3)^2-0.010392\le 0
\end{aligned} \tag{3.101}$$

Step 4: Set up the equations that maintain the power factor of the loads at each load bus:

$$\begin{aligned} 0.2 \cdot C_{P2} - C_{Q2} = 0 \\ 0.2 \cdot C_{P3} - C_{Q3} = 0 \end{aligned} \tag{3.102}$$

Step 5: Set up the final OPF problem, recognizing that bus 1 is a generator bus without connected loads and that buses 2 and 3 have no connected generators. Thus, the number of decision variables could be reduced. The angle of the slack bus is the reference angle of the system, and it is fixed at zero radians.

$$\begin{aligned} \text{Min } f = 0 \cdot P_{g1} + 0 \cdot Q_{g1} + 1 \cdot C_{P2} + 1 \cdot C_{P3} + 1 \cdot C_{Q2} + 1 \cdot C_{Q3} \\ +0 \cdot V_1 + 0 \cdot V_2 + 0 \cdot V_3 + 0 \cdot \delta_1 + 0 \cdot \delta_2 + 0 \cdot \delta_3 \end{aligned} \tag{3.103}$$

$$\begin{aligned} P_{g1} - 2.88 \cdot V_1^2 + 1.92 \cdot V_1 V_2 \cos(\delta_1 - \delta_2) - 9.62 \cdot V_1 V_2 \sin(\delta_1 - \delta_2) \\ +0.96 \cdot V_1 V_3 \cos(\delta_1 - \delta_3) - 4.81 \cdot V_1 V_3 \sin(\delta_1 - \delta_3) = 0 \end{aligned} \tag{3.104}$$

$$\begin{aligned} C_{P2} + 1.92 \cdot V_2 V_1 \cos(\delta_2 - \delta_1) - 9.62 \cdot V_2 V_1 \sin(\delta_2 - \delta_1) - 2.88 \cdot V_2^2 \\ +0.96 \cdot V_2 V_3 \cos(\delta_2 - \delta_3) - 4.81 \cdot V_2 V_3 \sin(\delta_2 - \delta_3) - 0.3 = 0 \end{aligned} \tag{3.105}$$

$$\begin{aligned} C_{P3} + 0.96 \cdot V_3 V_1 \cos(\delta_3 - \delta_1) - 4.81 \cdot V_3 V_1 \sin(\delta_3 - \delta_1) \\ +0.96 \cdot V_3 V_2 \cos(\delta_3 - \delta_2) - 4.81 \cdot V_3 V_2 \sin(\delta_3 - \delta_2) - 1.92 \cdot V_3^2 - 0.4 = 0 \end{aligned} \tag{3.106}$$

$$\begin{aligned} Q_{g1} - 14.39 \cdot V_1^2 + 1.92 \cdot V_1 V_2 \sin(\delta_1 - \delta_2) + 9.62 \cdot V_1 V_2 \cos(\delta_1 - \delta_2) \\ +0.96 \cdot V_1 V_3 \sin(\delta_1 - \delta_3) + 4.81 \cdot V_1 V_3 \cos(\delta_1 - \delta_3) = 0 \end{aligned} \tag{3.107}$$

$$\begin{aligned} C_{Q2} + 1.92 \cdot V_2 V_1 \sin(\delta_2 - \delta_1) + 9.62 \cdot V_2 V_1 \cos(\delta_2 - \delta_1) - 14.39 \cdot V_2^2 \\ +0.96 \cdot V_2 V_3 \sin(\delta_2 - \delta_3) + 4.81 \cdot V_2 V_3 \cos(\delta_2 - \delta_3) - 0.06 = 0 \end{aligned} \tag{3.108}$$

$$\begin{aligned} C_{Q3} + 0.96 \cdot V_3 V_1 \sin(\delta_3 - \delta_1) + 4.81 \cdot V_3 V_1 \cos(\delta_3 - \delta_1) \\ +0.96 \cdot V_3 V_2 \sin(\delta_3 - \delta_2) + 4.81 \cdot V_3 V_2 \cos(\delta_3 - \delta_2) - 9.58 \cdot V_3^2 - 0.08 = 0 \end{aligned} \tag{3.109}$$

$$\begin{aligned} (V_1 \cos\delta_1 - V_2 \cos\delta_2)^2 + (V_1 \sin\delta_1 - V_2 \sin\delta_2)^2 - 0.002598 \le 0 \\ (V_1 \cos\delta_1 - V_3 \cos\delta_3)^2 + (V_1 \sin\delta_1 - V_3 \sin\delta_3)^2 - 0.010392 \le 0 \\ (V_2 \cos\delta_2 - V_3 \cos\delta_3)^2 + (V_2 \sin\delta_2 - V_3 \sin\delta_3)^2 - 0.010392 \le 0 \end{aligned} \tag{3.110}$$

$$\begin{aligned} 0.2 \cdot C_{P2} - C_{Q2} = 0 \\ 0.2 \cdot C_{P3} - C_{Q3} = 0 \end{aligned} \tag{3.111}$$

$$
\begin{aligned}
0 \le P_{g1} \le 1.0 \\
-0.2 \le Q_{g1} \le 0.4 \\
0 \le C_{P2} \le 0.3 \\
0 \le C_{P3} \le 0.4 \\
0 \le C_{Q2} \le 0.06 \\
0 \le C_{Q3} \le 0.08
\end{aligned}
\tag{3.112}
$$

$$
\begin{aligned}
0.95 \le V_1 \le 1.05 \\
0.95 \le V_2 \le 1.05 \\
0.95 \le V_3 \le 1.05 \\
0 \le \delta_1 \le 0 \\
-\pi \le \delta_2 \le \pi \\
-\pi \le \delta_3 \le \pi
\end{aligned}
\tag{3.113}
$$

3.3.3.6.2 Composite System Adequacy Assessment

The system states and their probability of occurrence are presented in Table 3.37. State probabilities are equal to the ones of the DC based example, which were calculated in (3.56). The severity of each state, i.e. the active power load curtailment of each system state, is calculated by solving the corresponding OPF problem.

Table 3.37: The system states with probability and severity.

Event	State of the Components	Probability	Load curtailment [MW]
P(N)	G1, L1	0.9801	0
P(A)	G1, L1	0.0099	20.3
P(B)	G1, L1	0.0099	19.3
P(C)	G1, L1	0.0001	21.0

The following illustrations, Figure 3.11-Figure 3.14, show the system states where the flow of currents are included along with some additional details.

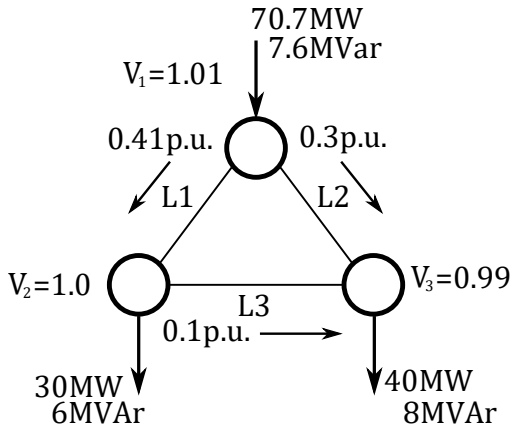

Figure 3.11: Event P(N).

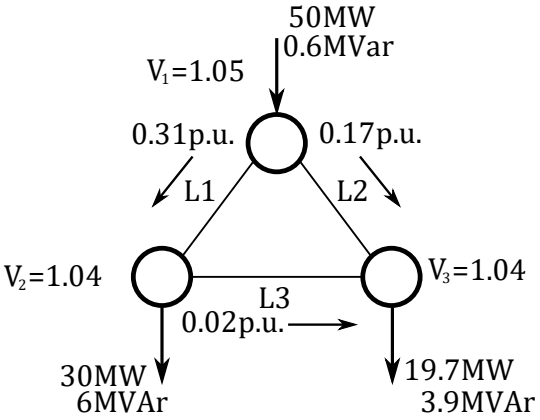

Figure 3.12: Event P(A).

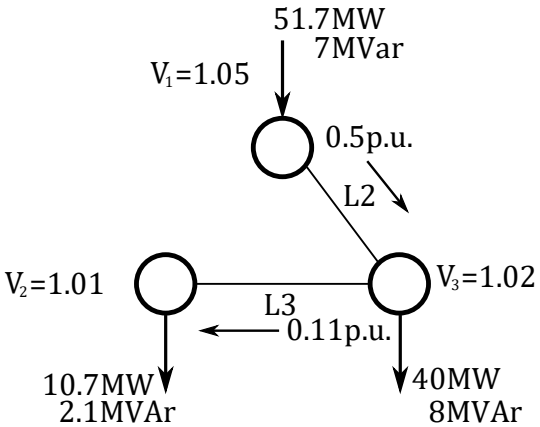

Figure 3.13:Event P(B).

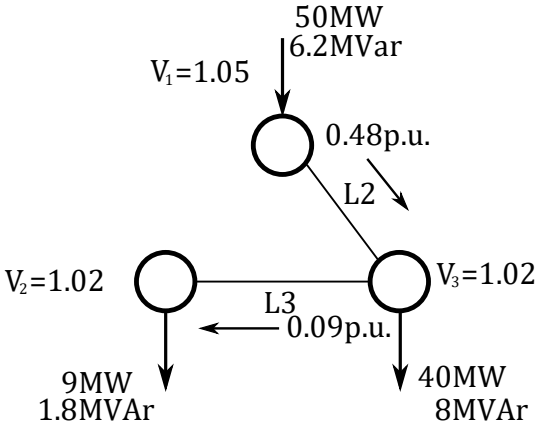

Figure 3.14: Event P(C).

The reliability indices used in the assessment are the LOLE and EENS indices. A LOLE of 0.0199 years in one year, same as the LOLE of the DC based example, is obtained, since load curtailments occur for the same system states. However, the calculation for the EENS index yields a different result of 3452 MWh in one year, which is slightly lower than the DC based result. The higher EENS result of the DC based solution is due to the approximation of voltages at 1.0 p.u., not accounting for the increased power transfer capability of a transmission line when the voltages are increased.

$$\begin{aligned} EENS &= \left[C(N)\cdot P(N) + C(A)\cdot P(A) + C(B)\cdot P(B) + C(C)\cdot P(C)\right]\cdot T \\ &= \left(0\cdot 0.9801 + 20.3\cdot 0.0099 + 19.3\cdot 0.0099 + 21\cdot 0.0001\right)\cdot 8760 \\ &= 3452.67\,\text{MWh/year} \end{aligned} \tag{3.114}$$

To highlight the impact of reducing the maximum voltage limit, the severities of each system state when the maximum voltage limit is changed to 1 p.u., are provided in Table 3.38.

Table 3.38: Additional example.

Event	State of the Components	Probability	Load curtailment [MW]
P(N)	G1, L1	0.9801	0
P(A)	G1, L1	0.0099	20.3
P(B)	G1, L1	0.0099	21.9
P(C)	G1, L1	0.0001	21.9

The new severities give an expected EENS of 3679 MWh per year as shown below, which is higher than the expected EENS of the DC based approach.

$$\begin{aligned} EENS &= \left[C(N)\cdot P(N) + C(A)\cdot P(A) + C(B)\cdot P(B) + C(C)\cdot P(C)\right]\cdot T \\ &= \left(0\cdot 0.9801 + 20.3\cdot 0.0099 + 21.9\cdot 0.0099 + 21.9\cdot 0.0001\right)\cdot 8760 \\ &= 3678.94 \text{MWh/year} \end{aligned} \quad (3.115)$$

3.3.4 Reducing the Computation Time of HLII Assessment

The computation time associated with HLII evaluation of system states is increased compared to the time spent on evaluation of system states at HLI, because the evaluation involves solving OPF problems instead of simple algebraic equations. When the OPF problems are based on an AC representation of the network, the computation time increases even more. Thus, it was discovered that some measures had to be taken to reduce the computation time spent on the evaluation of system states. In the following three sections, details on the measures taken, are given. The first section gives details on how criteria were established, which separate the system states into states that need to be solved by a contingency solver and states that are certain to have no load curtailments, by performing some simple algebraic calculations. Thus, a reduction in the number of system states that need to be run through a contingency solver is achieved. Another measure was taken to improve the speed of the simulations by implementing a parallel simulation scheme. The final section gives a description of how the number of system states that need to be evaluated by a contingency solver could be further reduced for the state transition method; this is done by recognizing features of the method's sequential nature.

3.3.4.1 Contingency Pre-Screening

A lot of the sampled system states are certain to have no associated load curtailments. The simplest case is when none of the components are on outage. Other system states can be cleared by performing some simple algebraic calculations instead of executing the OPF step of evaluation. Thus, the number of system states tested by a contingency solver can be reduced considerably [7]. The test systems used for testing the scripts, have buses (load points) with identical load curves, giving perfect correlation between the loads at the buses. This makes it possible to limit the number of system states that need to be evaluated by OPF considerably. If the load curves of the buses were different, a larger number of system states would need to be evaluated by OPF. It is worth noting that different load curves of the buses would be closer to the behavior of a real power system, and as such the effectiveness of establishing the mentioned criteria would not be as beneficial as for the specific test systems considered in this thesis.

When criteria are to be set, there are three aspects that have great influence on the system's reliability; the load level, outages of lines and outages of generators. The criteria used in this

thesis are based on these aspects. Tests were performed to find the effect of applying a criterion to the system states that are evaluated through OPF. Other tests were performed to make sure that the criteria were reliable, i.e. that the system states that contribute to the reliability indices are evaluated correctly. The criteria were adjusted throughout the process with the primary goal of finding reliable criteria, thus there are other efficient criteria that could be applied. The various tests employed are presented as follows.

The criteria presented in Table 3.39 were established through testing of the scripts. The first criterion (3.116) is related to the load level of the system, which ensures that the system states are evaluated by a contingency solver whenever the total active generation is lower than a specified multiple of the total active load. A lower load level requires less generation capacity than a higher load level. However, such a criterion alone does not account for the possibility that multiple outages of generators can happen at the same vicinity of a power system. Reduced generation capacity in one part of the power system might lead to the system being unable to serve the required load without violating any transfer limit, and/or any voltage limit if AC power flow is considered. Thus, a criterion should be included, where the maximum number of generators on outage are specified before the system state is analyzed by a contingency solver. It was found that it simplified the pre-analysis, if all system states with lines on outage are evaluated by a contingency solver. The strict criterion increases the number of system states that needs to be evaluated by a contingency solver only slightly, because the test systems used in this thesis have reliable transmission systems compared to the generation systems.

$$\sum_{i=1}^{k} P_{gi} < H \cdot \sum_{i=1}^{k} P_{load,i} \tag{3.116}$$

Table 3.39: Criteria for running contingency solvers.

Test system	Generation capacity to load	Max # lines on outage	Max # generators on outage	Extra Criteria
DC RBTS	1.00 x Total load	0	-	-
AC RBTS	1.04 x Total load	0	2	-
DC RTS	1.01 x Total load	0	5	-
AC RTS	1.10 x Total load	0	5	x

A testing scheme was created to test the “worst-case” load level of contingencies that are not evaluated by a contingency solver because of applying the criteria. Through the testing scheme,

it was found that an additional criterion must be added to the criteria, when simulations are performed on the RTS with AC considerations. If the three generators connected to bus 7 are on outage at the same time, the system state should be evaluated by OPF. The testing scheme is given below, where line contingencies are neglected as all system states with any line on outage will be captured by the line on outage criterion. If any generator contingency leads to the violation of (3.116) with the system's load at peak level, the system's load is reduced until the violation is removed. Thus, the new load level represents the worst-case load level that is to be evaluated by a contingency solver.

Test scheme for generator outages:

a) Normal system state, all generators available.
b) Set of contingencies with 1 generator on outage.
c) Set of contingencies with 2 generators on outage.
d) Set of contingencies with n generators on outage.

In theory, the testing could be performed until all possible generator outages are considered. However, such a pre-analysis is not practical to be conducted, unless the system is of limited size. For the RBTS system, tests were performed on all possible generator contingencies. However, for the RTS system the tests of generator contingencies were ended after analyzing the set of contingencies with 5 generators on outage; The number of system states to be analyzed by a contingency solver was reduced to a manageable amount.

The criteria were tested through Monte Carlo Sampling of 100 simulation years on both test systems, to get an estimate of the number of system states per year that need to be evaluated by the DC/AC contingency solvers. In Table 3.40, the obtained averages from the simulation are given for both DC and AC. The percentage is calculated by recognizing that a simulation year contains 8736 system states.

Table 3.40: The number of system states to analyze.

Test system	System states to analyze per year	Percentage of sampled system states
DC RBTS	207	2.37
AC RBTS	215	2.46
DC RTS	249	2.85
AC RBTS	290	3.32

3.3.4.2 Parallel Computation

The MATLAB programming language that is used for implementing the assessment methodology, has an inbuilt toolbox [19] that enables processing of loops in parallel by different *workers*. MATLAB handles the computation in parallel threads automatically when the standard "for" loop command is replaced with a "parfor" loop. The requirement that needs to be in place is the independence between iterations, i.e. an iteration cannot depend on the calculations performed in the previous iteration. When a "parfor" loop runs, the iterations are run in a random sequence that is different from the deterministic sequence when a "for" loop is executed. Each worker has its own unique random number stream, ensuring that the streams are independent.

The advantage of using parallel processing increases with the number of available CPU cores, where parallel processing in two cores can reduce the computation time by half if effective parallelization of the code into threads is achieved. A further reduction in computation time can be achieved if more CPU cores are available, but it can be limited by overhead from communication between the threads.

For the State Sampling method, where each simulation year is independent from the other simulation years, the simulation years can be run in parallel by simply replacing the "for" loop with a "parfor" loop, with the methodology used as described in section 3.2.2.1 of this thesis. After a simulation year is finalized and the reliability indices of the year are calculated, they are added to the record matrix.

For the State Transition method, which is a sequential method, the simulation years are dependent on the computations performed in the previous simulation year. Thus, it is not possible to run the simulation years in parallel. When a MCS is used on a reliable test system, it is necessary to use a large quantity of simulation years if the reliability indices are to converge.

Thus, a possible approach can be to run sequences of simulation years in parallel, from which the yearly indices are aggregated before the final reliability indices are calculated. A possible error that could be introduced by this approach is due to initialization of the system with all components being available at the start of each sequence. If the individual sequences are of limited size, because of the usage of too few simulation years divided between too many parallel threads, the system result can be too optimistic. However, if the number of simulation years are of a certain size, the "initialization" effect will be negligible. A similar approach is suggested in [33], although the approach of this thesis is slightly different, where a finite number of simulation years has been decided in advance.

3.3.4.3 State Transition Method Revised

Some simple modifications can be made to the proposed state transition methodology of section 3.2.2.3, to improve the speed of simulation. The system states of two successive time increments might be equal or differ by the state of a single component, since the method is sequential. By recognizing this, it is possible to reduce the number of system states that need to be evaluated by a contingency solver, thus improving the computation time of the method. Step 1 of the methodology must be modified slightly, while the other steps remain unchanged.

The goal of performing the modifications to the method is to limit the number of system states, that are evaluated by a contingency solver, for the cases listed below:

a) The system state of the previous time increment was a LOL state.
b) If a new failure of a component occurs in the time increment.
c) If the load level of the time increment is higher than the max load variable, which is reset to zero whenever a failure event occurs.

Thus, there is need for two additional variables to keep track of the above stated cases. One variable with a value of 1 in time increments where a failure of any component occurs and a value of zero if no failure occurs. The second variable is a variable keeping track of the maximum load level at the current system state or improved system states[1], without any associated load curtailments. This variable is reset to zero when the failure of a component occurs. The max load variable is only increased whenever a system state with higher load level

[1] A system state where one or more components are repaired, without the occurrence of any new failure of any other component during the repair process.

than the previous max load level, is evaluated by a contingency solver and the solver returns no load curtailments for the system state.

4 Case studies

4.1 Test Systems

There exist two well established test systems in the field of PSR: the RTS and the RBTS [7]. These are chosen as the test systems of this thesis. Both test systems use the same chronological load curve, which is specified in percent of system peak load for 8736 load points per year. The RBTS is a relatively small test system with its 11 generators, 9 lines and peak load of 185 MW, while the RTS is a larger system with its 32 generators, 38 lines and peak load of 2850 MW. Complete descriptions of the two test systems can be found in Appendix I and Appendix II, while load data are provided in Appendix III.

4.1.1 Load Model

The load data of the two test systems are supplied in three data tables, which give the weekly, daily and hourly load variations in percent of system peak load [34]. An additional table, giving the distribution of system load between the system's buses, is needed in HLII studies. It is also necessary to specify the reactive power load requirement of each bus in the AC based HLII studies. Each bus of the RBTS and RTS has a reactive power load requirement, specified as 20 % of its active power load requirement. The chronological load curve is obtained by multiplication of the percent values that correspond to a specific hour, day and week together with the yearly peak load (YPL) value of the system [35]. From (4.1) a HPL curve with 8736 load points (52weeks/year x 7 days/week x 24 hours/day) per year is obtained, which is a few hours less than the typical 8760 hours per year that are usually considered in reliability analysis [8].

$$\mathrm{HPL}_{h,d,w} = l_h \cdot l_d \cdot l_w \cdot \mathrm{YPL} \tag{4.1}$$

4.2 Generation Adequacy

The proposed methodology, presented in the preceding chapter, was used to develop MATLAB scripts for three MCS methods: state sampling, state duration and state transition. Tests were performed on the RTS and RBTS to verify the implementation of the methods. The results of the RTS system are verified against the results presented in [7] and [17], while the results of the RBTS system are only verified against [17]. An Intel Core i5-4210U processor was used to perform the simulations.

4.2.1 RBTS

The estimates of the RBTS indices were obtained by simulations of 30 000 years for each of the three MCS methods. A comparison of the results is made against the results of Billinton and Huang in [17], which are assumed to be benchmark results in this thesis. The benchmark results are obtained by a sequential MCS of 100 000 years, where the CV of the EENS index has reached a stated value below 1 %. Table 4.1 and Table 4.2 present the indices of the benchmark and the indices of this thesis. SDs of the LOL, ENS and LOLF samples are included in the tables to provide a measure of sample variance. An additional column, showing computation times of the methods, is included in Table 4.1 to provide an indication of the difference in computation time between the methods. It is worth noting that CPU time is dependent on the processor of the computer that is used. Hence, direct comparisons of CPU times between studies, cannot be made.

Table 4.1: The RBTS reliability indices 1.

Method	LOLE [hours/year]	LOL SD [hours/year]	LOLP'	CPU Time [s]
Benchmark [17]	1.0901	-	-	-
State Sampling	1.0899	1.0452	0.000125	113
State Duration	1.0986	4.2346	0.000126	83
State Transition	1.0846	4.1893	0.000124	37

Table 4.2: The RBTS reliability indices 2.

Method	EENS [MWh/year]	ENS SD [MWh /year]	LOLF [occ./year]	LOLF SD [occ./year]
Benchmark [17]	9.9268	-	0.2290	-
State Sampling	9.8260	13.1055	-	-
State Duration	10.0519	59.8684	0.2182	0.678
State Transition	9.7069	53.0442	0.2143	0.6704

The differences in percentage between the indices of this thesis and the indices of the benchmark study are presented in Table 4.3. The three MCS methods of this thesis provide estimates of the LOLE index that deviate less than 1 % from the benchmark estimate. Larger differences from the benchmark estimate can be observed for the EENS index, where the estimate of the state transition method deviates the most with 2.22 %. The two other methods

give estimates of the EENS index that deviate less than 1.3 % from the benchmark. The LOLF index is underestimated by the two sequential methods compared to the benchmark estimate, where the largest difference of 6.42 % can be observed for the state transition method. The large differences from the benchmark estimate may represent potential systematic errors in the sequential methods of this thesis. They should, however, be examined further by looking at the precision of the MCS estimates.

Table 4.3: The differences from the benchmark indices of the RBTS.

Method	LOLE [%]	EENS [%]	LOLF [%]
State Sampling	0.02	1.02	-
State Duration	0.78	1.26	4.72
State Transition	0.50	2.22	6.42

Table 4.4 presents the CVs of the estimated indices. The CVs of the EENS index have larger values than the CVs of the other indices. It can also be observed that the state sampling method gives estimates with a smaller CV than the two other methods, when equal sample sizes are used.

Table 4.4: The CVs of the RBTS indices.

Method	LOLE	EENS	LOLF
State Sampling	0.0055	0.0077	-
State Duration	0.0223	0.0344	0.0179
State Transition	0.0223	0.0315	0.0181

Table 4.5 - Table 4.7 present the 95 % and 99 % approximate CIs of the computed estimates. They are calculated by (2.25) and included to provide additional information regarding the uncertainty in the computed estimates. The LOLE and the EENS estimates have 95 % CIs that contain the benchmark estimate. If the widths of the CIs are compared, it can be observed that the two sequential methods have larger widths than the state sampling method for the same confidence level. The state sampling method provides estimates with higher precision than the two other methods. Since the state sampling method has a high precision, the estimate of the method provides a better indication on the methods' accuracy. The estimates of the two other methods have lower precisions. It is therefore more difficult to know how accurate the methods are, without repeating the MCSs multiple times.

Earlier, it was noted that methods of this thesis gave potential underestimations of the LOLF index. The LOLF estimates of the two sequential methods have 99 % CIs with upper bounds that are lower than the benchmark estimate. Since it is expected that 99 out of 100 samples will give estimates with 99 % CIs that contain the mean of the sampling distribution, it is likely that the two sequential methods of this thesis provide estimates from a sampling distribution with a lower mean than the one of the benchmark study. Thus, there may be systematical errors in the implementation of the two sequential methods of this thesis. Repeated simulations should however be performed. It is also important to note that the benchmark estimate is obtained by a simulation. Thus, there are also uncertainties in the estimates of the benchmark study.

Table 4.5: The approximate CIs of the RBTS LOLE.

Method	95% CI [hours/year]		99% CI [hours/year]	
	Lower	Upper	Lower	Upper
State Sampling	1.0781	1.1017	1.0744	1.1054
State Duration	1.0507	1.1465	1.0356	1.1616
State Transition	1.0372	1.1320	1.0223	1.1469

Table 4.6: The approximate CIs of the RBTS EENS.

Method	95% CI [MWh/year]		99% CI [MWh/year]	
	Lower	Upper	Lower	Upper
State Sampling	9.6777	9.9743	9.6311	10.0209
State Duration	9.3744	10.7294	9.1615	10.9423
State Transition	9.1066	10.3072	8.9180	10.4958

Table 4.7: The approximate CIs of the RBTS LOLF.

Method	95% CI [occ./year]		99% CI [occ./year]	
	Lower	Upper	Lower	Upper
State Duration	0.2105	0.2259	0.2081	0.2283
State Transition	0.2067	0.2219	0.2043	0.2243

The sequential MCS methods can provide the distributions of the indices in addition to the mean values. The distributions obtained by the state duration method are shown in Figure 4.1-Figure 4.3. Similar distributions of the state transition method are presented in Appendix VII. The distributions are given by the relative frequencies of observing various LOL, ENS or LOLF in the simulation years. The class interval widths of the LOLE index are 1.0 hours/year, where the first interval starts at -0.5 to center the class intervals at integer values. The last class interval contains the cumulative relative frequency of having a LOL of 14.5 hours/year or larger. From Figure 4.1, it can be observed that the relative frequency of having no LOL is 86.9 %, while the relative frequency of having a LOL of 14.5 hours/year or larger is 2.1 %. During the performed simulation, the largest observed LOL for a simulation year was 80 hours/year.

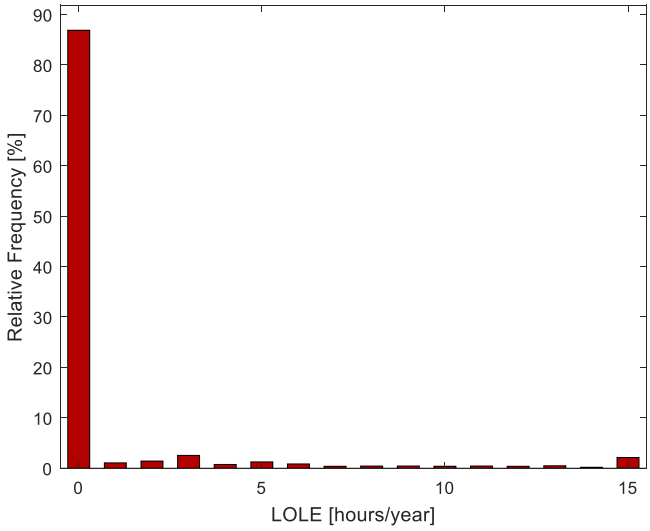

Figure 4.1: The LOLE distribution by the state duration method.

The class interval widths of the EENS index are 5 MWh/year, where the first class interval starts at -2.5 to center the intervals at multiples of 5. The last class interval contains the cumulative relative frequency of having an ENS larger than or equal to 62.5 MWh/year. From Figure 4.2, it can be observed that such an ENS has a relative frequency of 4.1 %. The largest record of ENS was 3197 MWh/year during the performed simulation.

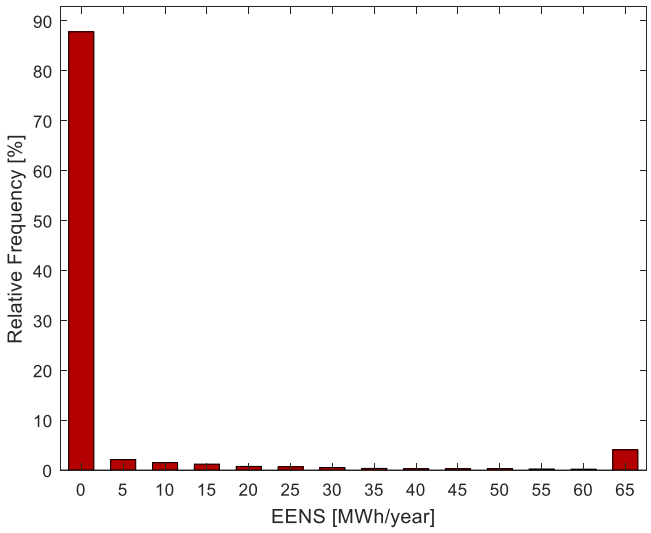

Figure 4.2: The EENS distribution by the state duration method.

The class interval widths of the LOLF index are 1 occurrence/year, where the first class interval starts at -0.5 to center the class intervals at integer values. The last class interval contains the cumulative relative frequency of observing more than 11 failures in a simulation year. The largest record of LOLF, however, was 9 occurrences/year during the performed simulation.

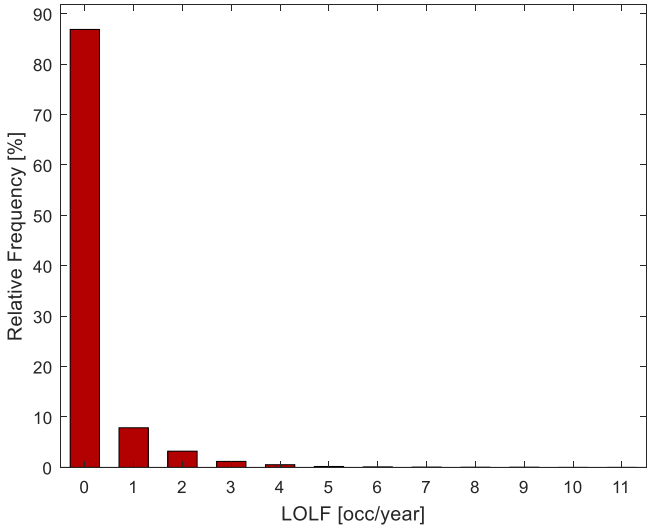

Figure 4.3: The LOLF distribution by the state duration method.

4.2.1.1 Convergence Process

Convergence plots were also created to illustrate the convergence process of the indices. Figure 4.4 presents the convergence process of the EENS index for a simulation of 10 000 years against the benchmark estimate. The estimates of indices in addition to the convergence plots of LOLE

and LOLF are provided in Appendix VII. In Figure 4.4, it can be observed that the estimated value of EENS varies considerably from the benchmark value in the beginning, before it converges closer to the benchmark estimate towards the end of the simulation process.

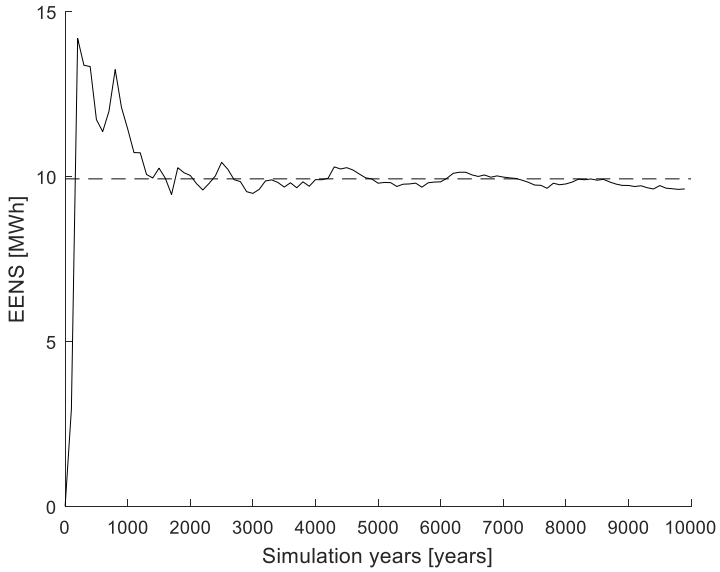

Figure 4.4: The Convergence process of the EENS index plotted together with the benchmark estimate of Billinton and Huang.

4.2.2 IEEE-RTS Results

Similar tests, to the ones performed on the RBTS, were performed on the RTS to test the scripts on a larger and different test system. The benchmark study of Billinton and Huang, presented in [17], used a sequential MCS of 20 000 simulation years. The CV of the EENS benchmark estimate has a stated CV below 1 %. The three MCS methods of this thesis were tested by performing simulations for 30 000 years. The estimates of the indices are provided together with benchmark estimates in Table 4.8 and Table 4.9. Sample SDs are included in the tables as the measures of sample variances.

The state transition method uses less than half the computing time of the two other methods to simulate an equal sample size. This can also be observed for the RBTS simulations. The three scripts provide estimates of LOLE and EENS that are close to the benchmark estimates. The estimates of the LOLF index are considerably lower than the benchmark estimate. This was also observed for the RBTS. Billinton and Li, however, presented an estimated LOLF of 1.9192 in [7], which is close to the estimates of this thesis. This estimate was obtained by a sequential simulation of 2500 simulation years, which is a relatively small sample size, which gives a large

CV of the index. Thus, estimates of a such simulation have low precision. Therefore, the presented results in [17] are assumed to provide a better basis for comparison.

Table 4.8: The RTS reliability indices 1.

Method	LOLE [hours/year]	LOL SD [hours/year]	LOLP'	CPU time [s]
Benchmark [17]	9.3868	16.4860	-	-
State Sampling	9.4108	3.0390	0.001077	301
State Duration	9.4449	16.1703	0.001081	288
State Transition	9.4590	16.4783	0.001083	116

Table 4.9: The RTS reliability indices 2.

Method	EENS [MWh/year]	ENS SD [MWh/year]	LOLF [occ./year]	LOLF SD [occ./year]
Benchmark [17]	1192.5072	3061.1416	2.0014	2.7907
State Sampling	1176.1327	520.0179	-	-
State Duration	1190.4824	2953.0423	1.9179	2.6425
State Transition	1198.7309	3047.5455	1.9038	2.6702

The differences in percentage between the estimates of this thesis and the benchmark estimates, are provided in Table 4.10. The estimates of the LOLE and the EENS are close to the benchmark estimates, where the state sampling EENS estimate has the largest difference of 1.37 %. The difference in percentage for the LOLF estimates, however, are between 4-5 % for the two sequential methods. The large differences may indicate possible systematical errors in the scripts, but other details from the MCSs should be examined further.

Table 4.10: The differences from the benchmark indices of the RTS.

Method	LOLE [%]	EENS [%]	LOLF [%]
State Sampling	0.26	1.37	-
State Duration	0.62	0.17	4.17
State Transition	0.77	0.52	4.88

Table 4.11 presents the CVs of the indices. The largest CVs are the ones of the EENS index, where the two sequential methods have CVs of ~1.5 %. The RTS has smaller CVs than the

RBTS, for equal sample sizes, since the precision of a MCS is dependent on the reliability of a system and not the system size [7].

Table 4.11: The CVs of the RTS indices.

Method	LOLE	EENS	LOLF
State Sampling	0.0019	0.0026	-
State Duration	0.0099	0.0143	0.0080
State Transition	0.0101	0.0147	0.0081

Table 4.12- Table 4.14 present the 95 % and the 99 % approximate CIs of the computed estimates. The CIs are calculated using (2.25). The three estimates of the LOLE index have 95 % CIs that contain the benchmark estimates. The state sampling estimate of the EENS index, however, has a 99 % CI with an upper bound that is lower than the benchmark estimate, while the two sequential estimates have 95 % CIs that contain the benchmark estimate. From this, one may assume that the state sampling method has a poorer accuracy than the two other methods. It is however worth noting that state sampling method has the highest precision of the three methods. Thus, the estimate of this method has a narrower CI than the two other methods. Therefore, one cannot make a such conclusion from a single MCS estimate.

The two sequential methods' estimates of the LOLF index are lower than the benchmark estimate. This was also observed for the RBTS. The two estimates have 99 % CIs with upper bounds which are lower than the benchmark estimate. When the observations of the RBTS and RTS are combined, it is likely that the scripts of this thesis systematically underestimate the LOLF index, if one assumes the benchmark estimate of the LOLF index to be close to the true value.

Table 4.12: The approximate CIs of the RTS LOLE.

Method	95% CI [hours/year]		99% CI [hours/year]	
	Lower	Upper	Lower	Upper
State Sampling	9.3764	9.4452	9.3656	9.4560
State Duration	9.2619	9.6279	9.2044	9.6854
State Transition	9.2725	9.6455	9.2139	9.7041

Table 4.13: The approximate CIs of the RTS EENS.

Method	95% CI [MWh/year]		99% CI [MWh/year]	
	Lower	Upper	Lower	Upper
State Sampling	1170.2481	1182.0173	1168.3987	1183.8667
State Duration	1157.0656	1223.8992	1146.5632	1234.4016
State Transition	1164.2447	1233.2171	1153.4061	1244.0557

Table 4.14: The approximate CIs of the RTS LOLF.

Method	95% CI [occ./year]		99% CI [occ./year]	
	Lower	Upper	Lower	Upper
State Duration	1.8880	1.9478	1.8786	1.9572
State Transition	1.8736	1.9340	1.8641	1.9435

Figure 4.5 - Figure 4.7 present the distributions of the reliability indices that are obtained by the state duration method. Similar distributions obtained by the two other MCS methods are provided in Appendix VIII. The figures show the relative frequencies of having various observations of LOL, ENS and LOLF during a simulation. The class interval widths of the LOLE index are 5 hours/year, where the first class interval starts at -2.5 to center the class intervals at multiples of 5. The last class interval contains the cumulative relative frequency of having a LOL of more than 102.5 hours/year. It was observed that the relative frequency of having a LOL with less than 2.5 hours/year was 49.9 %, while the relative frequency of a LOL higher than 102.5 hours/year was 0.25 %. A maximum LOL of 187 hours/year was recorded during the simulation.

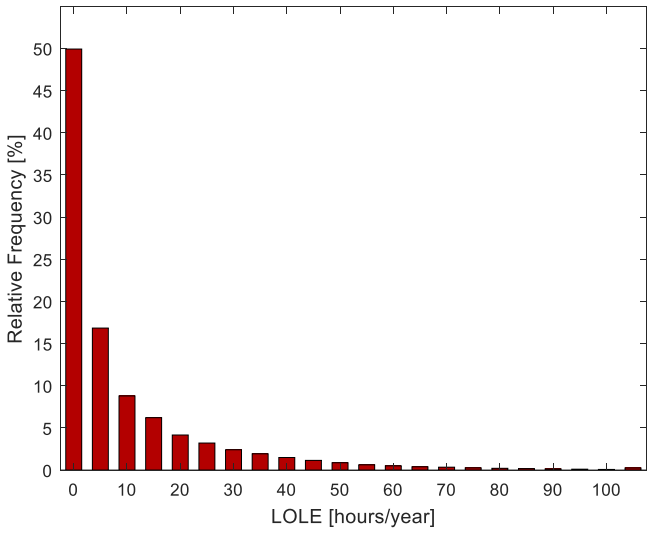

Figure 4.5: The LOLE distribution by the state duration method.

The class interval widths of the EENS index are 100 MWh/year, where the first class interval starts at -50 to center the class intervals around multiples of 100. The last class interval contains the cumulative relative frequency of having an ENS of more than 6250 MWh/year. Such an ENS has a relative frequency of 5 %. The largest observed ENS was 57 211 MWh in a year during the simulation.

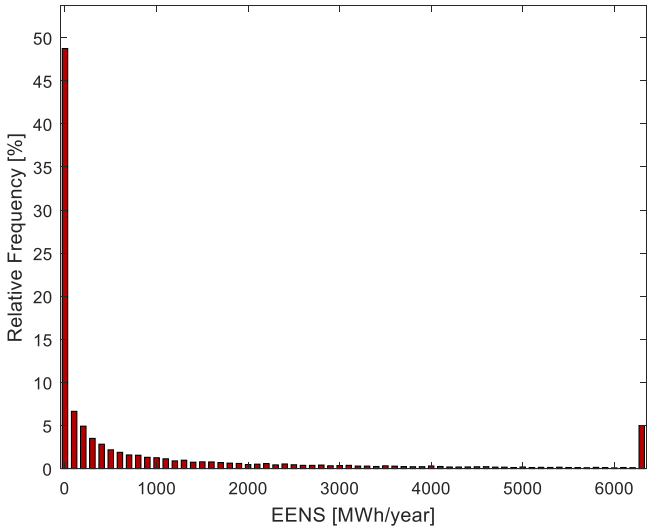

Figure 4.6: The EENS distribution by the state duration method.

The class interval widths of the LOLF index are 1 occurrence/year, where the first class interval starts at -0.5 to center the class intervals at integer values. Recordings that are higher than 14.5

occurrences/year are collected in the last class interval, which has a relative frequency of 0.29 %. The highest record of LOLF during the simulation was 23 occurrences/year.

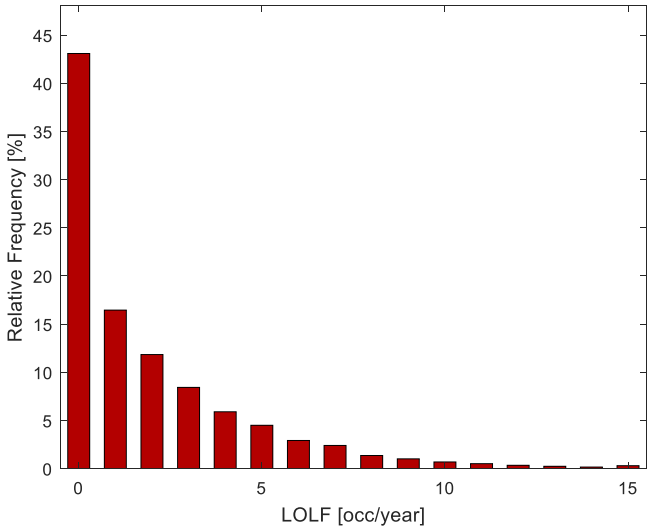

Figure 4.7: The LOLF distribution by the state duration method.

The distributions of the indices are obtained by the sequential methods and the state sampling method, have different shapes. It can be observed that the state sampling method gives distributions with normal distribution shapes, while the sequential methods give distributions with negative exponential shapes. Therefore, the state sampling method cannot be used to provide real distributions of the indices. If distributions of the indices are of interest, the MCS method of choice must be a sequential method as stated in [14] and [36].

4.2.2.1 Convergence Process

The convergence process of the EENS index against the benchmark estimate, is shown in Figure 4.8. It was obtained by a state transition simulation of 10 000 years. Additional figures, showing the convergence process of the LOLE and the LOLF indices, can be found in Appendix VIII. If the convergence process of Figure 4.8 is compared against the convergence process of Figure 4.4, it can be observed that the EENS index of the RTS converges faster than the EENS index of the RBTS. This is in accordance with the observation of smaller CVs of the RTS indices than of the RBTS indices, for equal sample sizes.

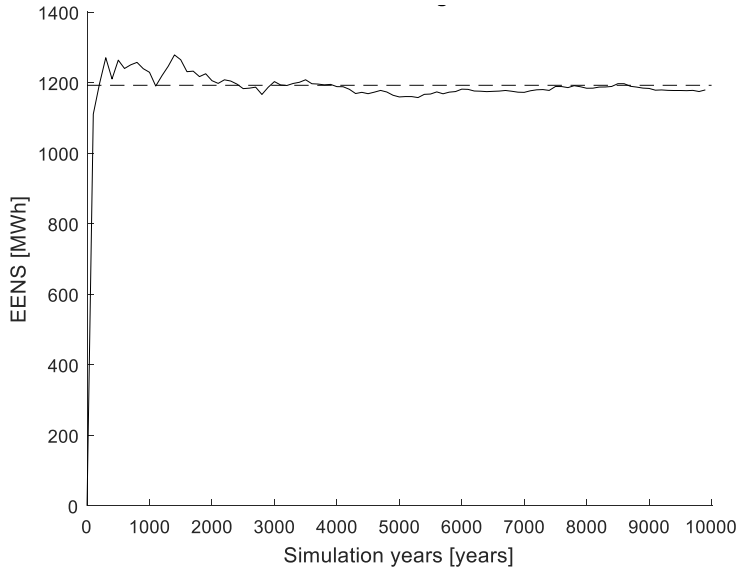

Figure 4.8: The convergence process of the EENS index plotted together with the benchmark result of Billinton and Huang.

4.2.2.2 De-Rated States

The results of the benchmark study of Billinton and Li [7] were obtained by a sequential MCS of 2500 years. The benchmark estimates of the indices have relatively large associated uncertainties because of the study's limited sample size. It is only included in this thesis to have a basis for comparison.

The state duration method of this thesis was developed to handle generator units with multiple de-rated states. Three of the generators in the RTS, the 350 MW and the two 400 MW generators, were modified by adding an additional generator state of half the capacity. A MCS of 30 000 years was performed to estimate the indices that are provided in Table 4.15 and Table 4.16. The distributions of the indices are provided in Appendix VIII.

The differences from the benchmark estimates are below 2 % for the LOLE and the LOLF indices, while it is 4.2 % for the EENS index. Since the benchmark study has used a small sample size, thus having a low precision, one cannot use the benchmark estimates to draw any conclusion regarding the accuracy level of the computed estimates.

The reliability of the RTS is increased when de-rated states are considered. It can be observed by comparing the estimates in Table 4.15 and Table 4.16 to the estimates of the RTS with standard configuration in Table 4.8 and Table 4.9. Another observation, that can be made from the figures of the LOLF distributions is that the relative frequency of having no LOL is increased to ~59% from ~43%.

Table 4.15: The reliability indices of the RTS with de-rated states 1.

Method	LOLE [hours/year]	LOL SD [hours/year]	LOLP'	CPU time [s]
Benchmark [7]	5.5404	-	-	-
De-rated	5.4356	11.9335	0.000622	289

Table 4.16: The reliability indices of the RTS with de-rated states 2.

Method	EENS [MWh/year]	ENS SD [MWh/year]	LOLF [occ./year]	LOLF SD [occ./year]
Benchmark [7]	642.0654	-	1.2140	-
De-rated	615.2101	1937.5085	1.1933	2.1105

Table 4.17: The differences from the benchmark results and the CVs of the RTS with de-rated states.

Type	LOLE	EENS	LOLF
Difference [%]	1.89	4.18	1.71
CV	0.0127	0.0182	0.0102

4.3 Composite System Adequacy

The proposed methodology of Chapter 3 was used to implement a DC based contingency solver and an AC based solver. Minor modifications were made to the state sampling and the state transition MCS scripts, to make the simulation tools applicable to composite system adequacy assessment. A priority order load curtailment philosophy was applied to the test systems to control the load curtailments. It was achieved by setting different costs for load curtailments at the buses according to the interrupted energy assessment rates (IEAR), which are specified in [27]. The measures that were described in section 3.3.4 were used to reduce the computation time of the simulations. It is important to note that in HLII studies compared to HLI studies, the results are more influenced by the choices that are made when the tools to evaluate system states are implemented, e.g. how system states with isolated buses are handled. Thus, it is possible that the estimates of various studies are different.

4.3.1 DC

This section presents estimates of the bus and system indices for the DC based approach. The bus indices of the buses without connected loads are omitted from the presented tables. Throughout this section, sample SD is used as the measure of variance in the underlying distributions of the indices. The CVs of the indices are provided in Appendix IX. Two load models were used when the RBTS and the RTS were tested: a CYPL and a HPL model. The state sampling method was tested with both load models, while the state transition method was only tested with the HPL model.

4.3.1.1 RBTS

The section starts with a presentation of the estimates of the bus and system indices, obtained from the three methods of MCS for the RBTS. Thereafter, a comparison of the estimates is made against the results of Geng, Zhao and Chen [37].

4.3.1.1.1 State Sampling

The state sampling MCS with a CYPL model was performed for 500 simulation years. The estimates of the bus and system indices are presented in Table 4.18. The CVs of the indices are provided in Appendix IX, where the CV of the system EENS index has a value of 0.63 %. The highest estimates of the LOLE and the EENS are observed for bus 3, as one would expect, because it has the lowest priority of the buses according to the IEAR. Another bus with high estimates of the LOLE and the EENS is bus 6. Bus 6 is connected to the rest of the system by a single line (line 9). Therefore, a failure of this line will always lead to load curtailment at bus 6. A comparison of the LOLP' of bus 6 against the FOR value of line 9 shows that the values are approximately equal. This indicates that the values of the LOLE and the EENS indices of bus 6, are mostly due to the outage of line 9. The load buses with the highest priority, buses 2 and 4, have no LOLE. In general, it can be perceived that buses with lower priority have higher expectations of the indices than buses with higher priority, if they have reliable connections to the rest of the system.

In Table 7.16 of Appendix IX, it can be observed that the EENS index of bus 3, which is the least reliable bus of the RBTS when a CYPL model is used, has a CV of 0.71 %. The EENS index of bus 5, which is the most reliable of the buses that experience LOL, has a CV of 44.5 %. A lower CV of an index indicates a higher precision of the estimate. Thus, the sample size should be increased, if more precise estimates of the reliable buses' indices are needed.

Table 4.18: The bus and system indices of the RBTS DC by state sampling with the CYPL model.

Bus	LOLE [hours/year]	LOL SD [hours/year]	LOLP'	EENS [MWh/year]	ENS SD [MWh/year]
2	0	0	0	0	0
3	74.7800	9.0194	0.008560	842.9332	133.8328
4	0	0	0	0	0
5	0.0100	0.0996	0.000001	0.2000	1.9918
6	9.9120	3.1022	0.001135	198.2051	62.0141
System	84.6660	9.4977	0.009692	1041.3383	145.6391

The state sampling MCS was also performed for 500 simulations years with a chronological HPL model. Table 4.19 presents the estimates of the bus and system indices. The CVs of the indices are provided in Appendix IX, where the CV of the system EENS index has a value of 1.48 %. A comparison against the estimates obtained with the CYPL model shows that the estimates of the system indices are considerably smaller. It can be observed, by a closer look at the bus indices, that the lower values of the system indices are mostly due to the changes of the bus 3 indices. The other buses have approximately equal estimates.

A comparison against the estimates of the HLI indices in Table 4.1 - Table 4.2, shows that the estimates of the system LOLE and EENS have approximately 10 times and 13 times larger values respectively. The inclusion of the transmission network into the assessment gives a lower reliability expectation of the system. It should, however, be noted that the lower reliability of the system is almost only due to the radial connection of bus 6.

The CVs of the indices are provided in Table 7.17 of Appendix IX. They are slightly higher than the CVs of the indices that were obtained with the CYPL model. Thus, the estimates that were obtained with the HPL model have lower precision than the ones obtained with the CYPL model.

Table 4.19: The bus and system indices of the RBTS DC by state sampling with the HPL model.

Bus	LOLE [hours/year]	LOL SD [hours/year]	LOLP'	EENS [MWh/year]	ENS SD [MWh/year]
2	0	0	0	0	0
3	1.0780	1.0169	0.000123	9.7520	13.4661
4	0	0	0	0	0
5	0.0100	0.0996	0.000001	0.1255	1.2978
6	10.0300	3.2617	0.001148	123.1301	41.5478
System	11.108	3.4537	0.001272	133.0076	44.0147

4.3.1.1.2 State Transition

The state transition MCS with the HPL model was performed for a sample size of 15 000 years, where 15 parallel simulations of 1000 years were used. The estimates of the bus and system indices are provided in Table 4.20. A computation time of 1217 seconds was needed to perform the MCS. If a comparison is made against the estimates that were obtained by the state sampling method with the HPL model, it can be observed that they are approximately equal. A small difference, however, can be observed for the indices at bus 2. The state sampling estimates of the bus 2 indices indicate no observations of LOL at this bus, while the state transition estimate indicates that a LOL at this bus was observed at least once throughout the simulation.

Table 4.20: The bus indices of the RBTS DC by state transition with the HPL model.

Bus	LOLE [hours/year]	LOL SD [hours/year]	LOLP'	EENS [MWh/year]	ENS SD [MWh/year]
2	0.0016	0.1095	0.000000	0.0239	1.6807
3	1.1466	4.3826	0.000131	10.0265	55.1230
4	0	0	0	0	0
5	0.0115	0.3141	0.000001	0.1470	4.1678
6	9.9337	14.1458	0.001137	122.024	175.6766
System	11.0809	14.8507	0.001268	132.2213	184.5751

The larger sample size of the state transition MCS compared to the sample size of the state sampling MCS, yields smaller CVs of the estimates for the former than the latter, even though the samples of the former have larger SDs. A comparison of the CVs of the system EENS

indices gives a CV of 1.14 % for the state transition method and a CV of 1.48 % for the state sampling method.

The state transition estimate of the LOLF index is presented in Table 4.21. It can be noted, that the inclusion of the transmission network into the assessment leads to an increase of almost 1 occurrence/year of the LOLF index. The LOLF is increased from 0.2143 at HLI to 1.1726 at HLII, which is an increase of 447 %.

Table 4.21: The LOLF index of the RBTS DC by state transition with the HPL model.

Index	LOLF	LOLF SD	CV
System	1.1726	1.2045	0.0084

4.3.1.1.3 Benchmark Comparison

A comparison against the estimates of [37] was made to provide an indication of the accuracy level of the MCS methods of this thesis. Table 4.22 presents the estimates of the benchmark study together with the computed estimates. The benchmark study has estimates of the EENS index that have stated CVs below 2 %. Estimates of the LOLE index are not provided in the benchmark study, but the computed estimates are still included in the table.

Table 4.22: Comparison against the benchmark estimates of the RBTS DC.

Method	LOLE [hours/year]	LOLP'	EENS [MWh/year]	LOLF [occ./year]	CV EENS
Benchmark CYPL [37]	-	0.00991	1058.96	4.2138	< 0.02
Benchmark HPL [37]	-	0.00129	135.24	1.2145	< 0.02
State Sampling CYPL	84.6660	0.009692	1041.3383	-	0.0063
State Sampling HPL	11.1080	0.001272	133.0076	-	0.0148
State Transition HPL	11.0809	0.001268	132.2213	1.1726	0.0114

The differences in percentage from the benchmark results are provided in Table 4.23. The three MCS methods of this thesis provide estimates of the LOLP’ and EENS that are 1.40-2.23 % lower than the benchmark estimates. The estimate of the LOLF is 3.45 % lower than benchmark estimate.

Table 4.23: The differences from the benchmark estimates of the RBTS DC.

Method	LOLP' [%]	EENS [%]	LOLF [%]
State Sampling CYPL	2.20	1.66	-
State Sampling HPL	1.40	1.65	-
State Transition HPL	1.71	2.23	3.45

Table 4.24 and Table 4.25 present the approximate CIs of the EENS and the LOLF estimates. The CIs were calculated by (2.25), and included to provide additional information regarding the uncertainties of the estimates. The state sampling CYPL estimate of the EENS has a 99 % CI with an upper bound that is lower than the benchmark estimate. However, when the state sampling method is used with the HPL model, the 95 % CI of the EENS estimate contains the benchmark estimate. The state transition EENS estimate, on the other hand, has a 99 % CI that contains the benchmark estimate but not a 95 % CI that contains the benchmark estimate.

The 99 % CI of the state transition LOLF estimate has also an upper bound that is lower than the benchmark estimate. This was also observed in the HLI studies. In general, it may seem that the methods of this thesis provide estimates of the LOLF index that are lower than the estimates of the benchmark study.

Table 4.24: The approximate CIs of the RBTS DC EENS.

Method	95% CI [MWh/year]		99% CI [MWh/year]	
	Lower	Upper	Lower	Upper
State Sampling CYPL	1028.5725	1054.1041	1024.5604	1058.1162
State Sampling HPL	129.1495	136.8657	127.9370	138.0782
State Transition HPL	129.2675	135.1751	128.3391	136.1035

Table 4.25: The approximate CIs of the RBTS DC LOLF.

Method	95% CI [occ./year]		99% CI [occ./year]	
	Lower	Upper	Lower	Upper
State Transition HPL	1.1533	1.1919	1.1473	1.1979

4.3.1.2 RTS

The section starts with a presentation of the estimates of the bus and system indices, which were obtained by three methods of MCS on the RTS. Thereafter, a comparison of the estimates is made against the results of Geng, Zhao and Chen [37].

4.3.1.2.1 State Sampling

The state sampling MCS with a CYPL model was performed for 500 simulation years. A computation time of 1186 s was used to obtain the indices. Table 4.26 presents the bus and system indices. The CVs of the indices are provided in Appendix IX, where the CV of the system EENS has a value of 0.21 %.

From the discussion on the bus indices of the RBTS, it is expected that the buses with the lowest priorities have the highest LOLE and EENS. The three buses of the RTS with the lowest priorities are bus 9, bus 14 and bus 19, in the order specified. It can be observed that bus 9 has the highest LOLE of 738.6 hours/year, bus 14 has the second highest LOLE of 345.3 hours/year and bus 19 has the third highest LOLE of 81.9 hours/year. One would also expect that the buses with the highest priorities, namely bus 4, bus 5 and bus 1, will have lower values of the indices. The three buses have either low values or values of zero of the indices. The other buses, that have priorities in-between, have low values of the indices.

It was noted in the discussion on the bus indices of the RBTS that the reliability of a bus with a radial connection to the rest of the system, is strongly dependent on the FOR value of the line. The RTS system has only one bus with such a connection, namely bus 7. If a comparison is made of the LOLP' of this bus against the FOR value of the line, one can see that the LOLP' of 0.000338 is approximately equal to the FOR value of 0.000342.

Table 4.26: The bus and system indices of the RTS DC by state sampling with the CYPL model.

Bus	LOLE [hours/year]	LOL SD [hours/year]	LOLP'	EENS [MWh/year]	ENS SD [MWh/year]
1	0	0	0	0	0
2	0	0	0	0	0
3	0.0020	0.0447	0.000000	0.0769	1.7195
4	0.0020	0.0447	0.000000	0.1482	3.3139
5	0.0040	0.0632	0.000000	0.2850	4.5017
6	0.0080	0.0892	0.000001	1.0944	12.1989
7	2.9540	1.7771	0.000338	370.4316	222.8524
8	0.0020	0.0447	0.000000	0.3420	7.6474
9	738.6380	25.0341	0.084551	84460.5896	3291.9463
10	19.1500	4.4034	0.002192	1722.2522	482.6105
13	0	0	0	0	0
14	345.3080	17.2865	0.039527	34270.1001	2139.4545
15	0	0	0	0	0
16	0	0	0	0	0
18	3.5620	1.9426	0.000408	268.1685	200.5809
19	81.8660	8.7382	0.009371	7476.7370	989.0896
20	0.0460	0.2190	0.000005	2.0473	11.9684
System	740.8760	25.0252	0.084807	128572.2728	5898.2223

The state sampling MCS with the HPL model was performed for 500 simulation years. A computation time of 312 seconds was used to obtain the estimates. Table 4.27 presents the bus and system indices. The CVs of the indices are provided in Appendix IX, where the CV of the system EENS has a value of 1.7%.

Large reductions in the values of the indices can be observed for bus 9, bus 10, bus 14 and bus 19 compared to the MCS with the CYPL model. Bus 9 has still the largest value of the LOLE and the EENS indices. It can be noted that the LOLE of bus 7 is approximately equal to the LOLE when the CYPL model is used. This is in accordance with the observed dependency on a line's FOR value when a bus has a radial connection to the rest of the system. Bus 7 has a lower EENS when the HPL model is used, because the average load requirement during outages of the line is lower than the peak load.

Table 4.27: The bus and system indices of the RTS DC by state sampling with the HPL model.

Bus	LOLE [hours/year]	LOL SD [hours/year]	LOLP'	EENS [MWh/year]	ENS SD [MWh/year]
1	0	0	0	0	0
2	0	0	0	0	0
3	0	0	0	0	0
4	0	0	0	0	0
5	0.0020	0.0447	0.000000	0.1133	2.5325
6	0.0080	0.0892	0.000001	0.5459	6.1471
7	3.0120	1.6761	0.000345	230.7388	133.4598
8	0.0060	0.0773	0.000001	0.6889	9.0081
9	9.3960	2.9727	0.001076	855.5926	315.3829
10	0.1280	0.3576	0.000015	8.9412	31.6455
13	0	0	0	0	0
14	2.8560	1.6712	0.000327	259.7811	185.7677
15	0	0	0	0	0
16	0	0	0	0	0
18	0.0100	0.0996	0.000001	0.5988	6.6015
19	0.6740	0.8421	0.000077	55.0109	82.0184
20	0	0	0	0	0
System	12.4000	3.3302	0.001419	1412.0114	537.0696

4.3.1.2.2 State Transition

The state transition MCS was performed for 15 000 simulation years, where 15 parallel simulations of 1000 years were used. A computation time of 1451 seconds was used to obtain the estimates of the indices. Table 4.28 presents the estimates of the bus and system indices. The CVs of the indices are provided in Appendix IX, where the CV of the system EENS index has a value of 1.73 %.

The estimates of the indices are approximately equal to the indices that were obtained by the state sampling method. The sample SDs of the LOL, ENS and LOLF distributions, however, are larger than the ones of the state sampling method. Therefore, a larger sample size is needed when the method is sequential instead of non-sequential, if the same level of precision is desired.

An increase in the LOLF index can be observed, if the estimate of HLII is compared against the estimate of HLI. The estimate has increased to a value of 2.19 occurrences/year from the value of 1.90 occurrences/year, which is an increase of 14.8 %. A larger increase of 447 %, however, was observed for the RBTS. Thus, the LOLF of the RTS is less influenced by the reliability of the transmission system than the LOLF of the RBTS.

Table 4.28: The bus and system indices of the RTS DC by state transition with the HPL model.

Bus	LOLE [hours/year]	LOL SD [hours/year]	LOLP'	EENS [MWh/year]	ENS SD [MWh/year]
1	0	0	0	0	0
2	0	0	0	0	0
3	0	0	0	0	0
4	0.0015	0.1254	0.000000	0.0740	6.8796
5	0.0013	0.0716	0.000000	0.0558	3.2976
6	0.0056	0.2607	0.000001	0.4470	20.6495
7	2.9297	7.6931	0.000335	226.0708	599.0139
8	0.0039	0.2228	0.000000	0.4204	24.9178
9	9.3511	16.0687	0.001070	852.2960	1760.7197
10	0.1222	1.3267	0.000014	9.2223	136.2805
13	0	0	0	0	0
14	2.8693	7.9800	0.000328	257.7802	901.5327
15	0	0	0	0	0
16	0	0	0	0	0
18	0.0155	0.4536	0.000002	1.1220	49.0637
19	0.6383	3.3714	0.000073	52.6206	352.7908
20	0.0002	0.0245	0	0.0031	0.3850
System	12.2838	17.8750	0.001406	1400.1122	2967.2594

Table 4.29: The LOLF index of the RTS DC by state transition with the HPL model.

Index	LOLF	LOLF SD	CV
System	2.1859	2.7033	0.0101

4.3.1.2.3 Benchmark Comparison

The computed estimates are compared against the results of [37], to provide an indication on the accuracy level of the methods of MCS of this thesis. Table 4.30 presents the computed

estimates together with the estimates of the benchmark. The two EENS estimates of the benchmark study have stated CVs that are below 4 %. Estimates of the LOLE index are not included in the benchmark study. The computed LOLE estimates, however, are still included in Table 4.30 to provide a basis for comparison between the methods. The state sampling CYPL estimates of the indices are lower than the benchmark estimates. However, when the HPL model is used, the state sampling method provides estimates that are higher than the benchmark estimates. Higher estimates can also be observed for the state transition method. It can be noted that the two methods of this thesis provide estimates that are approximately equal when the HPL model is used.

Table 4.30: Comparison against the benchmark results of the RTS DC.

Method	LOLE [hours/year]	LOLP'	EENS [MWh/year]	LOLF [occ./year]	CV EENS
Benchmark CYPL [37]	-	0.08575	131395.6	19.6226	< 0.04
Benchmark HPL [37]	-	0.00123	1341.16	2.2562	< 0.04
State Sampling CYPL	740.8760	0.084807	128572.2728	-	0.0021
State Sampling HPL	12.4000	0.001419	1412.0114	-	0.0170
State Transition HPL	12.2838	0.001406	1400.1122	2.1859	0.0173

The differences in percentage between the estimates of this thesis and the benchmark estimates, are presented in Table 4.32. The LOLP’ index shows large differences of approximately 15 %, for the two methods of this thesis when the HPL model is used. The state sampling CYPL LOLP’ estimate, however, is only 1.1 % lower than the benchmark estimate. A small deviation of 2.2 % can also be seen for the state sampling CYPL estimate of the EENS. The two other MCS methods have estimates of the EENS that are 4.4-5.3 % higher.

The LOLF estimate of the state transition method is 3.12 % lower than the benchmark estimate, even though the two other estimates of the method, LOLP’ and EENS, are higher than the benchmark estimates.

Table 4.31: The differences from the benchmark estimates of the RTS DC.

Method	LOLP' [%]	EENS [%]	LOLF [%]
State Sampling CYPL	1.10	2.15	
State Sampling HPL	15.37	5.28	
State Transition HPL	14.31	4.40	3.12

Table 4.32 and Table 4.33 present the approximate CIs of the EENS and LOLF estimates. They were calculated by (2.25), and provide additional information regarding the uncertainty in the estimates. While the state transition estimate has a 99 % CI that contains the benchmark estimate, the two state sampling estimates have 99 % CIs that do not contain the benchmark estimate. The state transition method, however, has a 99 % CI of the LOLF estimate that has an upper bound which is lower than the benchmark estimate. This is in accordance with the previous observations of lower LOLF estimates than the benchmark studies.

The widths of the CIs in Table 4.32, indicate that the state sampling method and the state transition method have almost equal levels of precision. This can also be seen by comparing the two methods' CVs of the indices. It should however be noted that the state transition method needs a considerably larger sample size than the state sampling method to reach the same precision level.

A note should also be made on the precision level of the benchmark estimates. The CVs of the benchmark EENS estimates have values below 4 %, which are considerably larger than the EENS CVs of this thesis. Thus, the benchmark estimates have lower precision than the estimates of this thesis. If CIs are calculated for the benchmark estimates, they would have more than double the width of comparable CIs from this thesis. It is therefore difficult to conclude regarding the accuracy level of this thesis' estimates.

Table 4.32: The approximate CIs of the RTS DC EENS estimates.

Method	95% CI [MWh/year]		99% CI [MWh/year]	
	Lower	Upper	Lower	Upper
State Sampling CYPL	128055.2708	129089.2748	127892.7845	129251.7611
State Sampling HPL	1364.9352	1459.0876	1350.1398	1473.8830
State Transition HPL	1352.6262	1447.5982	1337.7020	1462.5224

Table 4.33: The approximate CIs of the RTS DC LOLF estimate.

Method	95% CI [occ./year]		99% CI [occ./year]	
	Lower	Upper	Lower	Upper
State Transition HPL	2.1426	2.2292	2.1290	2.2428

4.3.2 AC

This section presents estimates of the bus and system indices that are obtained by the AC based approach. The bus indices of the buses without connected loads are omitted from the presented tables. Throughout this section, sample SDs are used as the measure of the variance in the underlying distributions of the indices. The CVs of the bus and system indices are provided in Appendix X. In this section, the state sampling method and the state transition method were only tested with the HPL model.

4.3.2.1 RBTS

This section starts with a presentation of the bus and system indices of the two MCS methods. Thereafter, a comparison of the estimates is made against the results of Hou, Jia, Xiandong, Liu and Jiang [38].

4.3.2.1.1 State Sampling

The state sampling MCS was performed for 500 simulation years. A computation time of 2239 seconds was used to obtain the indices. Table 4.34 presents the bus and system estimates of the indices. The CVs of the indices are provided in Appendix X, where the CV of the system EENS has a value of 1.41 %.

A small increase can be observed in the values of the system indices, if the indices are compared against the indices of the DC based approach (Table 4.19). The bus with the largest LOLE and EENS, is still bus 6. This is principally because of the radial connection of the bus to the rest of the system. One can, however, see an increase in the LOLE and EENS of bus 6, which is the bus that is furthest away from the generation sources. The voltage at this bus may drop below the specified voltage limit if certain contingencies occur. Thus, it can be necessary to curtail load at the bus.

An increase in the estimates of the bus 3 indices can also be observed from the indices of the DC based approach. The increase is mainly due to two reasons. One, because the transmission losses are included, there is a higher generation requirement in the system to meet the load demand, which again gives more system states where the generation capacity is insufficient. The other reason is that voltage limits are considered. Since bus 3 is the bus with the lowest cost of load curtailment, load is often curtailed at this bus if there is a voltage limit violation in the system.

Table 4.34: The bus and system indices of the RBTS AC by state sampling.

Bus	LOLE [hours/year]	LOL SD [hours/year]	LOLP'	EENS [MWh/year]	ENS SD [MWh/year]
2	0	0	0	0	0
3	1.8220	1.3879	0.000209	15.6874	16.8520
4	0	0	0	0	0
5	0.0060	0.0773	0.000001	0.0736	0.9742
6	11.4620	3.4844	0.001312	127.6475	41.4935
System	12.5640	3.6332	0.001438	143.4085	45.3447

4.3.2.1.2 State Transition

The state transition MCS was performed for 15 000 simulation years with 15 parallel simulations of 1000 years. A computation time of 13 680 seconds was used to obtain the indices. Table 4.35 and Table 4.36 present the estimates of the bus and system indices. The CVs of the indices are provided in Appendix X, where the CV of the EENS has a value of 1.10 %.

The estimates of the state transition method are approximately equal to the estimates of the sampling method. The sample SDs of the state transition method, on the other hand, are considerably larger. This is in accordance with the previous observations of this thesis.

The estimate of the LOLF has a value of 1.5135 occurrences/year. It is 29 % larger than the estimate of the DC approach, where the estimate was 1.1726 occurrences/year. Thus, the AC based approach gives a higher expectation of system failures than the DC based approach.

Table 4.35: The bus and system indices of the RBTS AC by state transition.

Bus	LOLE [hours/year]	LOL SD [hours/year]	LOLP'	EENS [MWh/year]	ENS SD [MWh/year]
2	0.0016	0.1095	0.000000	0.0239	1.6807
3	1.9057	5.5928	0.000218	15.9304	71.1010
4	0.0001	0.0163	0.000000	0.0000	0.0057
5	0.0116	0.3145	0.000001	0.1476	4.1684
6	11.3599	14.6398	0.001300	125.4442	175.9578
System	12.4783	15.3555	0.001428	141.5461	191.1578

Table 4.36: The LOLF index of the RBTS AC by state transition.

Index	LOLF	LOLF SD	CV
System	1.5135	1.4174	0.0076

4.3.2.1.3 Benchmark Comparison

The estimates of this thesis are compared against the results of [38], to provide an indication of their accuracy level. Table 4.37 presents the estimates of this thesis together with the benchmark estimates. The Sample SDs of the ENS are also included. Additional data regarding the sample sizes, computation times and CVs of the EENS index are given in Table 4.38. An estimate of the LOLE index is not provided in the benchmark study. The LOLE estimates of this thesis are still included, to provide a basis for comparison between the two methods of this thesis.

Table 4.37: Comparison against the benchmark results of the RBTS AC.

Method	LOLE [hours/year]	LOLP'	EENS [MWh/year]	ENS SD [MWh/year]	LOLF [occ./year]
Benchmark [38]	-	0.001425	141.7000	189.9579	1.5910
State Sampling	12.5640	0.001438	143.4085	45.3447	-
State Transition	12.4783	0.001428	141.5461	191.1578	1.5135

Table 4.38: Additional data of the RBTS AC benchmark comparison.

Method	Sample size [years]	CPU [s]	CV EENS
Benchmark	10000	645235	0.0134
State Sampling	500	2239	0.0141
State Transition	15000	13680	0.0110

The differences in percentage between the estimates of this thesis and the benchmark estimates are presented in Table 4.39. The LOLP' and LOLE estimates of this thesis are close to the benchmark estimates. The state sampling method has the largest differences of the two methods, with differences of 0.91 % and 1.21 % for the two indices. A large difference of 4.87 % can also be observed for the state transition LOLF estimate. It is an underestimation of the index, in compliance with the observed trend throughout this thesis.

Table 4.39: The differences from the benchmark estimates of the RBTS AC.

Method	LOLP' [%]	EENS [%]	LOLF [%]
State Sampling	0.91	1.21	
State Transition	0.21	0.11	4.87

Table 4.40 and Table 4.41 present the approximate CIs of the EENS and the LOLF estimates. They were calculated by (2.25), and provide additional information regarding the uncertainty in the estimates. The EENS estimates of two methods have 95 % CIs that contain the benchmark estimate. The LOLF estimate of the state transition method, however, has a 99 % CI that does not contain the benchmark estimate of the LOLF index. Thus, it is likely that the state transition method of this thesis underestimates the LOLF index.

Table 4.40: The approximate CIs of the RBTS AC EENS estimates.

Method	95% CI [MWh/year]		99% CI [MWh/year]	
	Lower	Upper	Lower	Upper
State Sampling	139.4339	147.3831	138.1847	148.6323
State Transition	138.4869	144.6053	137.5255	145.5667

Table 4.41: The approximate CIs of the RBTS AC LOLF estimate.

Method	95% CI [occ./year]		99% CI [occ./year]	
	Lower	Upper	Lower	Upper
State Transition	1.4908	1.5362	1.4837	1.5433

4.3.2.2 RTS

This section presents the estimates of the RTS bus and system indices. The estimates are not compared against a benchmark result since no suitable benchmark could be found in the literature.

4.3.2.2.1 State Sampling

The state sampling MCS was performed for 500 simulation years. A computation time of 31 417 seconds was used to obtain the indices. Table 4.42 presents the estimates of the bus and system indices. The CVs of the indices are provided in Appendix X, where the CV of the system EENS has a value of 1.51 %.

The estimates of the system LOLE and EENS have increased compared to the estimates of the DC based approach (Table 4.27). The increases in percentage are 49 % for the LOLE and 24 % for the EENS. For the RBTS, the corresponding increases are 13 % for the LOLE and 8 % for the EENS. Thus, it seems that the DC approach provides estimates that are closer to the estimates of the AC approach for the RBTS than for the RTS. It can also be noted that the EENS index seems to be less influenced by the DC assumptions than the LOLE index.

The three buses with the lowest priorities, bus 9, bus 14 and bus 19, are also the buses with the highest estimates of the indices when the AC approach is used. There are also three other buses with noticeable values of the indices, namely bus 6, bus 7, and bus 10. Of these, bus 7 was the only bus that had similar values of the indices when the DC approach was used. As noted previously, this is because the LOL events of bus 7 are due to outages of the bus's connection to the rest of the system. Bus 6 and bus 10 have medium costs of load curtailment, and are also neighboring buses. Thus, it is possible that the load curtailments at these buses are necessary to avoid violations of the voltage limits.

Table 4.42: The bus and system indices of the RTS AC by state sampling.

Bus	LOLE [hours/year]	LOL SD [hours/year]	LOLP'	EENS [MWh/year]	ENS SD [MWh/year]
1	0	0	0	0	0
2	0	0	0	0	0
3	0.1600	0.3933	0.000018	0.4460	4.6563
4	0	0	0	0	0
5	0.0020	0.0447	0.000000	0.0969	2.1667
6	3.3880	1.8385	0.000388	45.1686	30.3473
7	3.4340	1.7675	0.000393	249.0532	132.5136
8	0.0080	0.0892	0.000001	0.2547	5.0825
9	11.6520	3.3089	0.001334	1060.7666	354.0881
10	3.5800	1.8907	0.000410	9.8586	31.7515
13	0	0	0	0	0
14	11.6340	3.3036	0.001332	320.4070	206.1912
15	0.1440	0.3736	0.000016	0.0148	0.0393
16	0	0	0	0	0
18	0.6980	0.8125	0.000080	1.0284	11.3237
19	11.5740	3.2873	0.001325	68.8798	89.0093
20	0.1440	0.3736	0.000016	0.0188	0.0676
System	18.4500	4.3124	0.002112	1755.9935	593.6755

4.3.2.2.2 State Transition

The state transition MCS was performed for 15 000 simulation years, where 10 parallel simulations of 1500 years were used. A computation time of 319 813 seconds was used to obtain the estimates of the indices. Table 4.43 and Table 4.44 present the estimates of the bus and system indices. The CVs of the indices are provided in Appendix X, where the CV of the system EENS has a value of 1.54 %.

The estimates of the LOLE and EENS system indices are slightly lower than the corresponding estimates of the state sampling method: 2.3 % for the LOLE and 3.4% for the EENS. There are, however, only minor differences between the bus indices of the two methods.

The state transition estimate of the LOLF index is 3.0893 occurrences/year. This is 41 % higher than the DC based state transition estimate of 2.1859 occurrences/year. Increases can also be observed for the LOLE and the EENS indices, where the LOLE index has an increase of 47 %

and the EENS index has an increase of 21 %. This indicates that the LOLE is more sensitive to the DC assumptions than the two other indices. The EENS is the index that is least sensitive to the DC assumptions.

Table 4.43: The bus and system indices of the RTS AC by state transition.

Bus	LOLE [hours/year]	LOL SD [hours/year]	LOLP'	EENS [MWh/year]	ENS SD [MWh/year]
1	0	0	0	0	0
2	0	0	0	0	0
3	0.1684	1.5012	0.000019	0.7422	24.3098
4	0.0015	0.0883	0.000000	0.0699	4.3463
5	0.0012	0.0683	0.000000	0.0548	3.2020
6	3.2545	9.9044	0.000373	41.9911	154.4861
7	3.3567	8.4323	0.000384	240.8605	615.8406
8	0.0115	0.2995	0.000001	0.2757	16.3532
9	11.4251	17.9098	0.001308	1033.9670	1944.1674
10	3.4419	8.7118	0.000394	9.8637	111.4384
13	0	0	0	0	0
14	11.4073	17.8847	0.001306	305.7622	971.5850
15	0.1363	1.2716	0.000016	0.0142	0.1357
16	0	0	0	0	0
18	0.6217	3.3717	0.000071	0.9422	27.5015
19	11.3370	17.8266	0.001298	61.0805	365.3822
20	0.1376	1.2768	0.000016	0.0516	3.1186
System	18.0254	22.1557	0.002063	1695.6756	3202.2057

Table 4.44: The LOLF index of the RTS AC by state transition.

Index	LOLF [occ./year]	LOLF SD [occ./year]	CV
System	3.0893	3.2365	0.0086

5 Conclusions and Further Work

5.1 Conclusions

The thesis examined three MCS methods of obtaining power system adequacy indices: the state sampling method, the state transition method and the state transition method. Necessary in-house MATLAB scripts were developed for the software implementation of these methods for HLI and HLII studies. While all the three methods were applied to the generation adequacy assessment, only the state sampling method and the state transition method were applied to the composite system adequacy assessment. A DC-based contingency solver and an AC-based contingency solver were implemented to handle the evaluation of system states in the composite system adequacy assessment.

A major part of the thesis work has been spent on understanding the small, but important, details which are required to implement the three MCS methods and the two contingency solvers. As a result, the thesis seeks to present the gained understanding in a transparent manner, where the necessary assumptions and nuances are highlighted. In chapter 3 the methodology has been presented in a step by step manner, where emphasis has been placed on making the implementations of the MCS methods and the state evaluation reproducible.

The scripts created in the thesis were tested on two test systems: the RBTS and the RTS. At HLI, the sample sizes of the three MCS methods were kept equal, to compare the three methods. It was observed, through inspection of the indices' CVs, that the state sampling method gives estimates with a higher precision than the two sequential methods when equal sample sizes are used. The result is in accordance with other literature [7]. The reason is that it is possible to observe large variations between consecutive system states when the state sampling method is used. These large variations, however, are not possible to observe for the sequential methods [39]. Because of this, the state sampling method requires a smaller sample size than the sequential methods, to provide estimates of the reliability indices with the same level of precision.

It was observed that the state sampling method is unable to provide the true distributions of the indices. The distributions of the indices that were obtained by the state sampling method, have forms similar in shape to the normal distribution. The sequential methods, however, provide distributions of the indices with negative exponential forms. This is in accordance with the observations of [36].

The tests of the three MCS methods suggest that the state transition method requires less computation time to simulate a year than the two other methods. This is because the method has a reduced need for generation of random numbers when a new system state is to be obtained [7].

It was also observed that the precision of MCS is dependent on the reliability of the system and not the size of the system. At HLI, this was seen by comparing the CVs of the indices for the RTS against the CVs of indices for the RBTS. This was also observed in the HLII studies, where it was noted that the reliable buses of the test systems have larger CVs of the indices than the less reliable buses. The MCS's dependency on the reliability of a system is also stated in [7].

In composite system adequacy assessment, it was observed that the bus indices are dependent on the applied load curtailment philosophy. The buses with the lowest priorities had the highest expectations of LOL. It was also observed that the buses that have a radial connection to the rest of the system, are strongly dependent on the reliability of this connection.

It was observed that the RBTS showed a smaller percentage difference of the indices between the DC-based approach and the AC-based approach than the RTS. The EENS index was less sensitive to the choice of approach, DC based or AC based, than the LOLE and LOLF indices for both test systems. The LOLE index was most sensitive to the choice of approach for both test systems.

The use of same load curves at all buses of the test systems in the composite system adequacy assessment, is a limitation to the work of this thesis. A more realistic approach would be to use individual load curves at the different buses. Other studies like [14], have used such an approach.

Regarding the accuracy levels of the developed scripts, it is difficult to state a definite conclusion. It may seem that the sequential methods of this thesis provide underestimations of the LOLF index. The estimates of the other indices are in general closer to the benchmark estimates, even though some simulations have provided deviating estimates. Repeated trials of the methods should, however, be conducted to be certain if the deviations are due to random errors or systematical errors.

5.2 Future Work

During the thesis work, a choice was made to have a DC based approach and an AC based approach for the composite system adequacy assessment. It was observed that the estimates obtained by the DC based approach are lower than the estimates that include all the AC considerations into the assessment. The AC based approach, however, has a large computation time associated with the evaluation of system states, due to OPF solutions. Thus, it would be interesting to look at a decoupled approach, where voltage limits and reactive power generation are considered, to see what gains could be achieved in terms of reduced computation time, and how estimates of the indices are affected. It should, however, be noted that a decoupled OPF approach is different from a decoupled power flow approach, because decoupled OPF is approximate [28]. Therefore, it could be interesting to examine both approaches and their differences.

Optimization of the software codes can also be looked into.

It could also be interesting to examine the effect of using the "branch flow model" instead of the "bus injection model" to represent the system in the AC OPF problems [29], [30]. As stated by Frank and Rebennack in [28], it has gained recent interest because it offers advantages for convex relaxation of OPF problems.

Another interesting topic to examine further, is the use of variance reduction techniques. By reducing the sample variance, the required sample size to obtain precise estimates of the indices is reduced, thus reducing the computational burden. A variety of different methods exist. Among the variance reduction techniques that would be interesting to look into are the importance sampling method [40] and the Latin hypercube sampling method [41].

Further work could also examine the topics of using pattern classifiers instead of OPF for evaluation of system state samples. Thus, simplifying the system state evaluation from mathematical programming solving to solving by simple algebra. Among the interesting classifier methods are Bayes classifier, Support Vector Machine, Self-organizing Map, Multi-Layer Neural Network and Learning Vector Quantization [42].

The pseudo-sequential MCS for PSR was introduced in [43] "*based on the nonsequential sampling of system states and on the chronological simulation of only the sub-sequences associated with failed states*". This is an improvement over the sequential MCS in terms of required computational resources, which combines selectively the concepts of both sequential

MCS and non-sequential MCS. Extending the present framework of composite system adequacy assessment to include pseudo-sequential MCS would be a natural extension of the thesis work.

6 Bibliography

[1] R. Billinton and R. Mo, “Deterministic/Probabilistic Contingency Evaluation in Composite Generation and Transmission Systems,” *IEEE Power Eng. Soc. Gen. Meet.*, vol. 2, pp. 2232–2237, 2004.

[2] W. Wangdee and R. Billinton, “Bulk electric system well-being analysis using sequential Monte Carlo simulation,” *IEEE Trans. Power Syst.*, vol. 21, no. 1, pp. 188–193, 2006.

[3] T. K. Vrana and E. Johansson, “Overview of Power System Reliability Assessment Techniques,” in *CIGRE Colloquium Recife*, 2011, p. 12.

[4] R. Billinton and R. N. Allan, *Reliability Evaluation of Power Systems*, 2nd ed. New York: Plenum Press, 1996.

[5] R. Billinton and R. N. Allan, “Power-system reliability in perspective,” *Electron. Power*, vol. 30, no. 3, pp. 231–236, 1984.

[6] E. Zio, *The Monte Carlo Simulation Method for System Reliability and Risk Analysis*. London: Springer, 2013.

[7] R. Billinton and W. Li, *Reliability Assessment of Electric Power Systems Using Monte Carlo Methods*. New York: Springer Science, 1994.

[8] M. Rausand and A. Høyland, *System Reliability Theory: Models, Statistical Methods, and Applications*, 2nd ed. Hoboken, New Yersey: Wiley, 2004.

[9] M. P. Bhavajaru, R. Billinton, N. D. Reppen, R. J. Ringlee, and P. F. Albrecht, “Requirements for composite system reliability evaluation models,” *IEEE Trans. Power Syst.*, vol. 3, no. 1, pp. 149–157, 1988.

[10] R. Billinton and E. Khan, “A security based approach to composite power system reliability evaluation,” *IEEE Trans. Power Syst.*, vol. 7, no. 1, pp. 65–72, 1992.

[11] X. Luo, C. Singh, and A. D. Patton, “Loss-of-Load State Identification Using Self-organizing Map,” in *1999 IEEE Power Engineering Society Summer Meeting.*, 1999, pp. 670–675.

[12] C. Singh, X. Luo, and H. Kim, “Power System Adequacy and Security Calculations Using Monte Carlo Simulation incorporating Intelligent System Methodology,” in *International Conference on Probabilistic Methods Applied to Power Systems*, 2006, pp. 1–9.

[13] M. R. Bhuiyan and R. N. Allan, “Modelling multistate problems in sequential simulation of power system reliability studies,” *IEE Proc. - Gener. Transm. Distrib.*, vol. 142, no. 4, pp. 343–349, 1995.

[14] A. Sankarakrishnan and R. Billinton, “Sequential Monte Carlo simulation for composite power system reliability analysis with time varying loads,” *IEEE Trans. Power Syst.*, vol. 10, no. 3, pp. 1540–1545, 1995.

[15] M. B. Guertin *et al.*, “Reliability Indices for Use in Bulk Power Supply Adequacy Evaluation,” *IEEE Trans. Power Appar. Syst.*, vol. PAS-97, no. 4, pp. 1097–1103, 1978.

[16] A. Jonnavithula, “Composite System Reliability Evaluation using Sequential Monte Carlo Simulation.” PHD Thesis, University of Saskatchewan, Saskatoon, 1997.

[17] R. Billinton and D. Huang, “Basic concepts in generating capacity adequacy evaluation,” in *International Conference on Probabilistic Methods Applied to Power Systems*, 2006, pp. 1–6.

[18] Mathworks, *MATLAB Mathematics R2018a*. Natick, Massachusetts: The MathWorks, Inc, 2018.

[19] Mathworks, *Parallel Computing Toolbox User’s Guide R2018a*. Natick, Massachusetts: The MathWorks, Inc, 2018.

[20] R. Billinton and W. Li, “A system state transition sampling method for composite system reliability evaluation,” *IEEE Trans. Power Syst.*, vol. 8, no. 3, pp. 761–770, 1993.

[21] W. L. Dunn and J. K. Shultis, *Exploring Monte Carlo Methods*. Amsterdam: Elsevier, 2012.

[22] R. E. Walpole, R. H. Myers, S. L. Myers, and K. Ye, *Probability and Statistics for Engineers & Scientists*, 9th ed. Harlow, Essex: Pearson Education, 2016.

[23] M. Amelin, “Monte Carlo Simulation in Engineering,” Course Compendium, KTH Royal Institute of Technology, Stockholm, 2015.

[24] E. L. Lehmann and J. P. Romano, *Testing Statistical Hypotheses*, 3rd ed. New York: Springer Science, 2005.

[25] J. D. Glover, M. S. Sarma, and T. J. Overbye, *Power System Analysis and Design*, 5th ed. Stamford: Nelson Education, 2011.

[26] L. L. Garver, P. R. Horne, and K. A. Wirgau, “Load Supplying Capability of Generation-Transmission Networks,” *IEEE Trans. Power Appar. Syst.*, vol. PAS-98, no. 3, pp. 957–962, 1979.

[27] W. Wangdee and R. Billinton, “Impact of load shedding philosophies on bulk electric system reliability analysis using sequential Monte Carlo simulation,” *Electr. Power Components Syst.*, vol. 34, no. 3, pp. 355–368, 2006.

[28] S. Frank and S. Rebennack, “An introduction to optimal power flow: Theory, formulation, and examples,” *IIE Trans.*, vol. 48, no. 12, pp. 1172–1197, 2016.

[29] B. Subhonmesh, S. H. Low, and K. M. Chandy, “Equivalence of Branch Flow and Bus Injection models,” in *50th Annual Allerton Conference on Communication, Control, and Computing (Allerton)*, 2012, pp. 1893–1899.

[30] M. Farivar and S. H. Low, “Branch Flow Model: Relaxations and Convexification (Parts I, II),” in *51st IEEE Conference on Decision and Control December 10-13*, 2012, pp. 3672–3679.

[31] H. Dommel and W. Tinney, “Optimal Power Flow Solutions,” *IEEE Trans. Power Appar. Syst.*, vol. PAS-87, no. 10, pp. 1866–1876, 1968.

[32] Mathworks, *Optimization Toolbox User’s Guide R2018a*. Natick, Massachusetts: The MathWorks, Inc, 2018.

[33] N. Gubbala and C. Singh, “Models and considerations for parallel implementation of monte carlo simulation methods for power system reliability evaluation,” *IEEE Trans. Power Syst.*, vol. 10, no. 2, pp. 779–787, 1995.

[34] P. M. Subcommittee, “IEEE Reliability Test System,” *IEEE Trans. Power Appar. Syst.*, vol. PAS-98, no. 6, pp. 2047–2054, 1979.

[35] K. Koldingsnes, “Reliability-based Derating Approach for Interconnectors,” Master thesis, NTNU, 2017.

[36] R. Billinton and A. Jonnavithula, “Application of sequential Monte Carlo simulation to evaluation of distributions of composite system indices,” *IEE Proc. - Gener. Transm. Distrib.*, vol. 144, no. 2, pp. 87–90, 1997.

[37] L. Geng, Y. Zhao, and G. Chen, “Simplified Sequential Simulation of Bulk Power System Reliability Via Chronological Probability Model of Load Supplying Capability,” *IEEE Trans. Power Syst.*, vol. 33, no. 3, pp. 2349–2358, 2018.

[38] K. Hou, H. Jia, X. Xiandong, Z. Liu, and Y. Jiang, “A Continuous Time Markov Chain Based Sequential Analytical Approach for Composite Power System Reliability Assessment,” *IEEE Trans. Power Syst.*, vol. 31, no. 1, pp. 738–748, 2016.

[39] C. L. T. Borges, D. M. Falcao, J. C. O. Mello, and A. C. G. Melo, “Concurrent composite reliability evaluation using the state sampling approach,” *Electr. Power Syst. Res.*, vol. 57, no. 3, pp. 149–155, 2001.

[40] E. Tomasson and L. Soder, “Improved Importance Sampling for Reliability Evaluation of Composite Power Systems,” *IEEE Trans. Power Syst.*, vol. 32, no. 3, pp. 2426–2434, 2017.

[41] P. Jirutitijaroen and C. Singh, “Comparison of Simulation Methods for Power System Reliability Indexes and Their Distributions,” *IEEE Trans. Power Syst.*, vol. 23, no. 2, pp. 486–493, 2008.

[42] B. Bordeerath and P. Jirutitijaroen, “Techniques for improving precision and construction efficiency of a pattern classifier in composite system reliability assessment,” *Electr. Power Syst. Res.*, vol. 88, pp. 33–41, 2012.

[43] J. C. O. Mello, M. V. F. Pereira, and a. M. Leite da Silva, “Evaluation of reliability worth in composite systems based on pseudo-sequential Monte Carlo simulation,” *IEEE Trans. Power Syst.*, vol. 9, no. 3, pp. 1318–1326, 1994.

[44] R. Billinton *et al.*, “A reliability test system for educational purposes - basic data,” *IEEE Trans. Power Syst.*, vol. 4, no. 3, pp. 1238–1244, 1989.

7 Appendices

Appendix I RBTS

The system consists of 11 generators. Bus 1 has all the thermal-generators connected, and bus 2 has all the hydro-generators connected. The capacities of the generators have a range from 5 MW to 40 MW. The total generation capacity of the system is 240 MW. The peak load of the system is 185 MW. The size of the system is smaller than the commonly used RTS system. It was created for educational purposes at the University of Saskatchewan. Included in the system description, are the data that are needed to perform studies at HLI and HLII [44]. Table 7.1 gives the data of the generators. The network data are provided in Table 7.2 and Table 7.3. The load requirements at the buses and other bus specifications that are relevant for composite system analysis, are provided in Table 7.4. Figure 7.1 shows the connections of the system.

Table 7.1: The generator data of the RBTS test system.

Capacity [MW]	Bus	Min Reactive [MVAr]	Max Reactive [MVAr]	FOR	Failure rate [1/year]	Repair rate [1/year]
10	1	0	7	0.020	4.0	196.0
20	1	-7	12	0.025	5.0	195.0
40	1	-15	17	0.030	6.0	194.0
40	1	-15	17	0.030	6.0	194.0
5	2	0	5	0.010	2.0	198.0
5	2	0	5	0.010	2.0	198.0
20	2	-7	12	0.015	2.4	157.6
20	2	-7	12	0.015	2.4	157.6
20	2	-7	12	0.015	2.4	157.6
20	2	-7	12	0.015	2.4	157.6
40	2	-15	17	0.020	3.0	147.0

Table 7.2: The outage data of the RBTS network.

Line	From	To	Failure rate [1/year]	MTTR [hours]	FOR
1	1	3	1.5	10	0.00171
2	2	4	5.0	10	0.00568
3	1	2	4.0	10	0.00455
4	3	4	1.0	10	0.00114
5	3	5	1.0	10	0.00114
6	1	3	1.5	10	0.00171
7	2	4	5.0	10	0.00568
8	4	5	1.0	10	0.00114
9	5	6	1.0	10	0.00114

Table 7.3: The network parameters of the RBTS.

Line	From	To	Resistance [pu]	Reactance [pu]	B/2 [pu]	Current Rating [pu]
1	1	3	0.0342	0.18	0.0106	0.85
2	2	4	0.1140	0.60	0.0352	0.71
3	1	2	0.0912	0.48	0.0282	0.71
4	3	4	0.0228	0.12	0.0071	0.71
5	3	5	0.0228	0.12	0.0071	0.71
6	1	3	0.0342	0.18	0.0106	0.85
7	2	4	0.1140	0.60	0.0352	0.71
8	4	5	0.0228	0.12	0.0071	0.71
9	5	6	0.0228	0.12	0.0071	0.71

Table 7.4: The bus specifications of the RBTS.

Bus	Share of Load	Min Voltage [pu]	Max Voltage [pu]	Curtailment Cost [$/kWh]
1	0	0.97	1.05	0
2	0.1081	0.97	1.05	9.6325
3	0.4595	0.97	1.05	4.3769
4	0.2162	0.97	1.05	8.0267
5	0.1081	0.97	1.05	8.6323
6	0.1081	0.97	1.05	5.5132

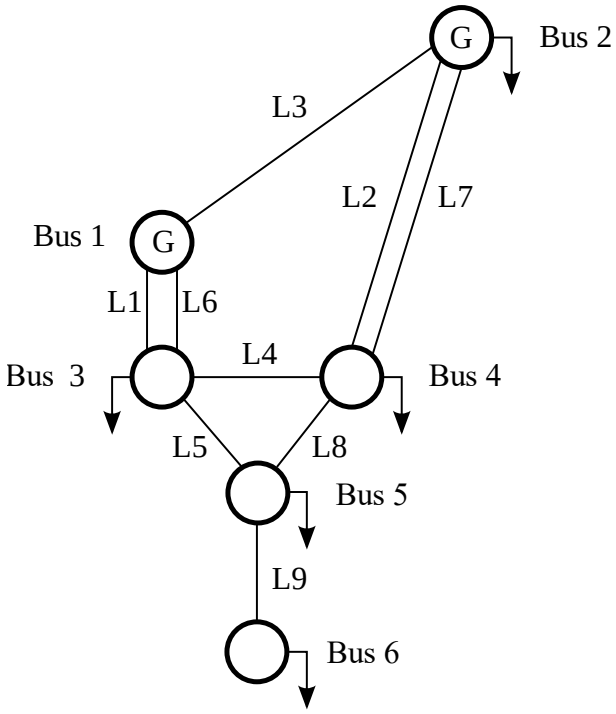

Figure 7.1: The network of the RBTS.

Appendix II IEEE-RTS

The system consists of 32 generators, that have a range from 12 MW to 400 MW. The total installed capacity of the system is 3405 MW. The system has a peak load of 2850 MW. Complete system data, which are necessary to perform reliability studies at HLI and HLII, are provided in [34], where an illustration of the network can be found. Table 7.5 gives the generator data, and the network data are provided in Table 7.6 and Table 7.7. The load shares of the buses and other bus specifications are given in Table 7.8. The last column of Table 7.8 gives the new numbering scheme, that are used to re-number the buses to make the slack bus (bus 13) the first bus.

TRMs with included state capacities for the de-rated 350 and 400 MW generators, are provided in Table 7.9 and Table 7.10. These are in accordance with the ones given in [13].

Table 7.5: The generator data of the IEEE-RTS.

Capacity [MW]	Bus	Min Reactive [MVAr]	Max Reactive [MVAr]	FOR	MTTF	MTTR
12	15	0	6	0.02	2940	60
12	15	0	6	0.02	2940	60
12	15	0	6	0.02	2940	60
12	15	0	6	0.02	2940	60
12	15	0	6	0.02	2940	60
20	1	0	10	0.10	450	50
20	1	0	10	0.10	450	50
20	2	0	10	0.10	450	50
20	2	0	10	0.10	450	50
50	22	-10	16	0.01	1980	20
50	22	-10	16	0.01	1980	20
50	22	-10	16	0.01	1980	20
50	22	-10	16	0.01	1980	20
50	22	-10	16	0.01	1980	20
50	22	-10	16	0.01	1980	20
76	1	-25	30	0.02	1960	40
76	1	-25	30	0.02	1960	40
76	2	-25	30	0.02	1960	40
76	2	-25	30	0.02	1960	40
100	7	0	60	0.04	1200	50
100	7	0	60	0.04	1200	50
100	7	0	60	0.04	1200	50
155	15	-50	80	0.04	960	40
155	16	-50	80	0.04	960	40
155	23	-50	80	0.04	960	40
155	23	-50	80	0.04	960	40
197	13	0	80	0.05	950	50
197	13	0	80	0.05	950	50
197	13	0	80	0.05	950	50
350	23	-25	150	0.08	1150	100
400	18	-50	200	0.12	1100	150
400	21	-50	200	0.12	1100	150
0	14	-50	200	0	-	-
0	6	-100	0	0	-	-

Table 7.6: The outage data of the RTS network.

Line	From	To	FOR	Failure Rate [1/year]	MTTR [hours]
1	1	2	0.000438164	0.24	16
2	1	3	0.000581853	0.51	10
3	1	5	0.000376570	0.33	10
4	2	4	0.000445007	0.39	10
5	2	6	0.000547645	0.48	10
6	3	9	0.000433602	0.38	10
7	3	24	0.001750356	0.02	768
8	4	9	0.000410790	0.36	10
9	5	10	0.000387977	0.34	10
10	6	10	0.001316757	0.33	35
11	7	8	0.000342349	0.30	10
12	8	9	0.000502031	0.44	10
13	8	10	0.000502031	0.44	10
14	9	11	0.001750356	0.02	768
15	9	12	0.001750356	0.02	768
16	10	11	0.001750356	0.02	768
17	10	12	0.001750356	0.02	768
18	11	13	0.000502031	0.40	11
19	11	14	0.000489486	0.39	11
20	12	13	0.000502031	0.40	11
21	12	23	0.000652542	0.52	11
22	13	23	0.000614918	0.49	11
23	14	16	0.000476941	0.38	11
24	15	16	0.000414212	0.33	11
25	15	21	0.000514575	0.41	11
26	15	21	0.000514575	0.41	11
27	15	24	0.000514575	0.41	11
28	16	17	0.000439305	0.35	11
29	16	19	0.000426758	0.34	11
30	17	18	0.000401665	0.32	11
31	17	22	0.000677623	0.54	11
32	18	21	0.000439305	0.35	11
33	18	21	0.000439305	0.35	11
34	19	20	0.000476941	0.38	11
35	19	20	0.000476941	0.38	11
36	20	23	0.000426758	0.34	11
37	20	23	0.000426758	0.34	11
38	21	22	0.000564749	0.45	11

Table 7.7: The network parameters of the RTS.

Line	From	To	Resistance [pu]	Reactance [pu]	B/2 [pu]	Current rating [pu]
1	1	2	0.0026	0.0139	0.23055	1.93
2	1	3	0.0546	0.2112	0.0286	2.08
3	1	5	0.0218	0.0845	0.01145	2.08
4	2	4	0.0328	0.1267	0.01715	2.08
5	2	6	0.0497	0.1920	0.0260	2.08
6	3	9	0.0308	0.1190	0.0161	2.08
7	3	24	0.0023	0.0839	0	5.1
8	4	9	0.0268	0.1037	0.01405	2.08
9	5	10	0.0228	0.0883	0.01195	2.08
10	6	10	0.0139	0.0605	1.2295	1.93
11	7	8	0.0159	0.0614	0.0083	2.08
12	8	9	0.0427	0.1651	0.02235	2.08
13	8	10	0.0427	0.1651	0.02235	2.08
14	9	11	0.0023	0.0839	0	5.1
15	9	12	0.0023	0.0839	0	5.1
16	10	11	0.0023	0.0839	0	5.1
17	10	12	0.0023	0.0839	0	5.1
18	11	13	0.0061	0.0476	0.04995	6
19	11	14	0.0054	0.0418	0.04395	6
20	12	13	0.0061	0.0476	0.04995	6
21	12	23	0.0124	0.0966	0.1015	6
22	13	23	0.0111	0.0865	0.0909	6
23	14	16	0.0050	0.0389	0.0409	6
24	15	16	0.0022	0.0173	0.0182	6
25	15	21	0.0063	0.0490	0.0515	6
26	15	21	0.0063	0.0490	0.0515	6
27	15	24	0.0067	0.0519	0.05455	6
28	16	17	0.0033	0.0259	0.02725	6
29	16	19	0.0030	0.0231	0.02425	6
30	17	18	0.0018	0.0144	0.01515	6
31	17	22	0.0135	0.1053	0.1106	6
32	18	21	0.0033	0.0259	0.02725	6
33	18	21	0.0033	0.0259	0.02725	6
34	19	20	0.0051	0.0396	0.04165	6
35	19	20	0.0051	0.0396	0.04165	6
36	20	23	0.0028	0.0216	0.02275	6
37	20	23	0.0028	0.0216	0.02275	6
38	21	22	0.0087	0.0678	0.0712	6

Table 7.8: The bus specifications of the RTS.

Bus	Share of load	Min Voltage [pu]	Max Voltage [pu]	Curtailment Cost [$/kWh]	Number
1	0.038	0.95	1.05	8.9815	13
2	0.034	0.95	1.05	7.3606	12
3	0.063	0.95	1.05	5.8990	11
4	0.026	0.95	1.05	9.5992	10
5	0.025	0.95	1.05	9.2323	9
6	0.048	0.95	1.05	6.5238	8
7	0.044	0.95	1.05	7.0291	7
8	0.06	0.95	1.05	7.7742	6
9	0.061	0.95	1.05	3.6623	5
10	0.068	0.95	1.05	5.1940	4
11	0	0.95	1.05	0	3
12	0	0.95	1.05	0	2
13	0.093	0.95	1.05	7.2813	1
14	0.068	0.95	1.05	4.3717	20
15	0.111	0.95	1.05	5.9744	18
16	0.035	0.95	1.05	7.2305	17
17	0	0.95	1.05	0	21
18	0.117	0.95	1.05	5.6149	22
19	0.064	0.95	1.05	4.5430	16
20	0.045	0.95	1.05	5.6836	15
21	0	0.95	1.05	0	23
22	0	0.95	1.05	0	24
23	0	0.95	1.05	0	14
24	0	0.95	1.05	0	19

Table 7.9: TRM, with rates per year, of the 350 MW generator.

State	1	2	3	[MW]
1	-13	6	7	350
2	115	-115	0	175
3	115	0	-115	0

Table 7.10: TRM, with rates per year, of the 400 MW generators.

State	1	2	3	[MW]
1	-8	4	4	400
2	44	-44	0	200
3	44	0	-44	0

Appendix III Load Data

Load data of the RBTS and IEEE-RTS system

Table 7.11: The variation of peak load through the days of a week.

Day	Peak Load [%]
Monday	93
Tuesday	100
Wednesday	98
Thursday	96
Friday	94
Saturday	77
Sunday	75

Table 7.12: Weekly variations of the peak load.

Week	Peak Load [%]	Week	Peak Load [%]	Week	Peak Load [%]	Week	Peak Load [%]
1	86.2	14	75.0	27	75.5	40	72.4
2	90.0	15	72.1	28	81.6	41	74.3
3	87.8	16	80.0	29	80.1	42	74.4
4	83.4	17	75.4	30	88.0	43	80.0
5	88.0	18	83.7	31	72.2	44	88.1
6	84.1	19	87.0	32	77.6	45	88.5
7	83.2	20	88.0	33	80.0	46	90.9
8	80.6	21	85.6	34	72.9	47	94.0
9	74.0	22	81.1	35	72.6	48	89.0
10	73.7	23	90.0	36	70.5	49	94.2
11	71.5	24	88.7	37	78.0	50	97.0
12	72.7	25	89.6	38	69.5	51	100
13	70.4	26	86.1	39	72.4	52	95.2

Table 7.13: The variation of peak load in percent through the hours of a day, for different weeks depending on whether it is a weekday or a weekend.

	Winter weeks 1-8 & 44-52		Summer weeks 18-30		Spring/fall weeks 9-17 & 31-43	
Hour	Wkdy	Wknd	Wkdy	Wknd	Wkdy	Wknd
0-1	67	78	64	74	63	75
1-2	63	72	60	70	62	73
2-3	60	68	58	66	60	69
3-4	59	66	56	65	58	66
4-5	59	64	56	64	59	65
5-6	60	65	58	62	65	65
6-7	74	66	64	62	72	68
7-8	86	70	76	66	85	74
8-9	95	80	87	81	95	83
9-10	96	88	95	86	99	89
10-11	96	90	99	91	100	92
11-12	95	91	100	93	99	94
12-13	95	90	99	93	93	91
13-14	95	88	100	92	92	90
14-15	93	87	100	91	90	90
15-16	94	87	97	91	88	86
16-17	99	91	96	92	90	85
17-18	100	100	96	94	92	88
18-19	100	99	93	95	96	92
19-20	96	97	92	95	98	100
20-21	91	94	92	100	96	97
21-22	83	92	93	93	90	95
22-23	73	87	87	88	80	90
23-24	63	81	72	80	70	85

Appendix IV MATLAB Codes

(Restricted Access)

Appendix V 3-Bus example DC

The OPF problem with L1 on outage

The equations that are used to obtain the OPF formulation, are equal to the ones that are used when all the components are available. When line L1 is on outage, the susceptance of the line is set equal to zero. Thus, the susceptance matrix changes.

Step 1:

$$B = \begin{bmatrix} 5 & 0 & -5 \\ 0 & 5 & -5 \\ -5 & -5 & 10 \end{bmatrix}$$

$$B' = \begin{bmatrix} 5 & -5 \\ -5 & 10 \end{bmatrix}$$

Step 2:

$$[B']^{-1} = \begin{bmatrix} 0.4 & 0.2 \\ 0.2 & 0.2 \end{bmatrix}$$

$$Z = \begin{bmatrix} 0 & 0 & 0 \\ 0 & 0.4 & 0.2 \\ 0 & 0.2 & 0.2 \end{bmatrix}$$

Step 3: Calculate the power transfer distribution factors:

a) Line 1:

$$P_{12} = 0 \cdot P_1 + 0 \cdot P_2 + 0 \cdot P_3$$

b) Line 2:

$$\begin{aligned} P_{13} &= \frac{z_{11} - z_{31}}{X_{13}} \cdot P_1 + \frac{z_{12} - z_{32}}{X_{13}} \cdot P_2 + \frac{z_{13} - z_{33}}{X_{13}} \cdot P_3 \\ &= \frac{0-0}{0.2} \cdot P_1 + \frac{0-0.2}{0.2} \cdot P_2 + \frac{0-0.2}{0.2} \cdot P_3 \\ &= 0 \cdot P_1 - 1 \cdot P_2 - 1 \cdot P_3 \end{aligned}$$

c) Line 3:

$$\begin{aligned} P_{23} &= \frac{z_{21}-z_{31}}{X_{23}}\cdot P_1 + \frac{z_{22}-z_{32}}{X_{23}}\cdot P_2 + \frac{z_{23}-z_{33}}{X_{23}}\cdot P_3 \\ &= \frac{0-0}{0.2}\cdot P_1 + \frac{0.4-0.2}{0.2}\cdot P_2 + \frac{0.2-0.2}{0.2}\cdot P_3 \\ &= 0\cdot P_1 + 1\cdot P_2 + 0\cdot P_3 \end{aligned}$$

d) Obtain the sensitivity matrix:

$$A = \begin{bmatrix} 0 & 0 & 0 \\ 0 & -1 & -1 \\ 0 & 1 & 0 \end{bmatrix}$$

Step 4: Obtain Tlim1 and Tlim2:

a) Tlim1:

$$\begin{aligned} T_{Line1} &= T_{lim} + 0\cdot P_{L1} + 0\cdot P_{L2} + 0\cdot P_{L3} \\ &= 0.5 + 0\cdot 0 + 0\cdot 0.3 + 0\cdot 0.4 = 0.5 \\ T_{Line2} &= T_{lim} + 0\cdot P_{L1} - 1\cdot P_{L2} - 1\cdot P_{L3} \\ &= 0.5 + 0\cdot 0 - 1\cdot 0.3 - 1\cdot 0.4 = -0.2 \\ T_{Line3} &= T_{lim} + 0\cdot P_{L1} + 1\cdot P_{L2} + 0\cdot P_{L3} \\ &= 0.5 + 0\cdot 0 + 1\cdot 0.3 + 0\cdot 0.4 = 0.8 \end{aligned}$$

b) Tlim2:

$$\begin{aligned} T_{Line1} &= T_{lim} - 0\cdot P_{L1} + 0\cdot P_{L2} + 0\cdot P_{L3} \\ &= 0.5 - 0\cdot 0 - 0\cdot 0.3 - 0\cdot 0.4 = 0.5 \\ T_{Line2} &= T_{lim} - 0\cdot P_{L1} + 1\cdot P_{L2} + 1\cdot P_{L3} \\ &= 0.5 - 0\cdot 0 + 0\cdot 0.3 + 0\cdot 0.4 = 1.2 \\ T_{Line3} &= T_{lim} - 0\cdot P_{L1} - 1\cdot P_{L2} + 0\cdot P_{L3} \\ &= 0.5 - 0\cdot 0 - 1\cdot 0.3 + 0\cdot 0.4 = 0.2 \end{aligned}$$

c) The final vector form:

$$T_{lim,1} = \begin{bmatrix} 0.5 \\ -0.2 \\ 0.8 \end{bmatrix} \text{ and } T_{lim,2} = \begin{bmatrix} 0.5 \\ 1.2 \\ 0.2 \end{bmatrix}$$

Step 5) The final OPF formulation:

$$\text{Min } Z = 0 \cdot P_{g1} + 1 \cdot C_2 + 1 \cdot C_3$$

$$1 \cdot P_{g1} + 1 \cdot C_2 + 1 \cdot C_3 = 0.7$$

$$0 \cdot P_{g1} + 0 \cdot C_2 + 0 \cdot C_3 \le 0.5$$

$$0 \cdot P_{g1} - 1 \cdot C_2 - 1 \cdot C_3 \le -0.2$$

$$0 \cdot P_{g1} + 1 \cdot C_2 + 0 \cdot C_3 \le 0.8$$

$$0 \cdot P_{g1} + 0 \cdot C_2 + 0 \cdot C_3 \le 0.5$$

$$0 \cdot P_{g1} + 1 \cdot C_2 + 1 \cdot C_3 \le 1.2$$

$$0 \cdot P_{g1} - 1 \cdot C_2 + 0 \cdot C_3 \le 0.2$$

$$P_{g1} \le 1$$

$$C_2 \le 0.3$$

$$C_2 \le 0.4$$

$$P_{g1}, C_2, C_3 \ge 0$$

Appendix VI 3-Bus Example AC

OPF problem with L1 on outage

The equations that are used to obtain the problem formulation are equal to the ones that are used when all components are available.

Step 1: Obtain the conductance and susceptance matrices of (3.65):

a) Calculate the series admittance of the lines by (3.59):

$$y_{12} = 0$$
$$y_{13} = \frac{1}{0.04 + j0.2} = \frac{0.04}{0.04^2 + 0.2^2} - j\frac{0.2}{0.04^2 + 0.2^2} = 0.9615 - j4.8077$$
$$y_{23} = y_{13}$$

b) Calculate the elements of the conductance matrix, G_{bus}:

$$G_{11} = g_{13} = 0.9615$$
$$G_{22} = g_{23} = 0.9615$$
$$G_{33} = g_{13} + g_{23} = 0.9615 + 0.9615 = 1.9231$$
$$G_{12} = G_{21} = 0$$
$$G_{13} = G_{31} = -g_{13} = -0.9615$$
$$G_{23} = G_{32} = -g_{23} = -0.9615$$

c) Calculate the elements of the susceptance matrix, B_{bus}:

$$B_{11} = b_{13} + b_{10}^{L2} = -4.8077 + 0.02 = -4.7877$$
$$B_{22} = b_{23} + b_{20}^{L3} = -4.8077 + 0.02 = -4.7877$$
$$B_{33} = b_{13} + b_{23} + b_{30}^{L2} + b_{30}^{L3} = -4.8077 - 4.8077 + 0.02 + 0.02 = -9.5754$$
$$B_{12} = B_{21} = 0$$
$$B_{13} = B_{31} = -b_{13} = 4.8077$$
$$B_{23} = B_{32} = -b_{23} = 4.8077$$

d) Create the conductance matrix, G_{bus}:

$$G_{bus} = \begin{bmatrix} 0.96 & 0 & -0.96 \\ 0 & 0.96 & -0.96 \\ -0.96 & -0.96 & 1.92 \end{bmatrix}$$

e) Create the susceptance matrix, B_{bus}:

$$B_{bus} = \begin{bmatrix} -4.79 & 0 & 4.81 \\ 0 & -4.79 & 4.81 \\ 4.81 & 4.81 & -9.58 \end{bmatrix}$$

Step 2: Set up the AC power flow equations, (3.66) and (3.67), for each of the three buses:

a) Active power:

$$\begin{aligned} P_1(V,\delta) &= V_1V_1\left[G_{11}\cos(\delta_1-\delta_1)+B_{11}\sin(\delta_1-\delta_1)\right] \\ &+V_1V_2\left[G_{12}\cos(\delta_1-\delta_2)+B_{12}\sin(\delta_1-\delta_2)\right] \\ &+V_1V_3\left[G_{13}\cos(\delta_1-\delta_3)+B_{13}\sin(\delta_1-\delta_3)\right] \\ &= 0.96\cdot V_1^2 - 0.96\cdot V_1V_3\cos(\delta_1-\delta_3)+4.81\cdot V_1V_3\sin(\delta_1-\delta_3) \end{aligned}$$

$$\begin{aligned} P_2(V,\delta) &= V_2V_1\left[G_{21}\cos(\delta_2-\delta_1)+B_{21}\sin(\delta_2-\delta_1)\right] \\ &+V_2V_2\left[G_{22}\cos(\delta_2-\delta_2)+B_{22}\sin(\delta_2-\delta_2)\right] \\ &+V_2V_3\left[G_{23}\cos(\delta_2-\delta_3)+B_{23}\sin(\delta_2-\delta_3)\right] \\ &= 0.96\cdot V_2^2 - 0.96\cdot V_2V_3\cos(\delta_2-\delta_3)+4.81\cdot V_2V_3\sin(\delta_2-\delta_3) \end{aligned}$$

$$\begin{aligned} P_3(V,\delta) &= V_3V_1\left[G_{31}\cos(\delta_3-\delta_1)+B_{31}\sin(\delta_3-\delta_1)\right] \\ &+V_3V_2\left[G_{32}\cos(\delta_3-\delta_2)+B_{32}\sin(\delta_3-\delta_2)\right] \\ &+V_3V_3\left[G_{33}\cos(\delta_3-\delta_3)+B_{33}\sin(\delta_3-\delta_3)\right] \\ &= -0.96\cdot V_3V_1\cos(\delta_3-\delta_1)+4.81\cdot V_3V_1\sin(\delta_3-\delta_1) \\ &-0.96\cdot V_3V_2\cos(\delta_3-\delta_2)+4.81\cdot V_3V_2\sin(\delta_3-\delta_2)+1.92\cdot V_3^2 \end{aligned}$$

b) Reactive Power:

$$\begin{aligned} Q_1(V,\delta) &= V_1V_1\left[G_{11}\sin(\delta_1-\delta_1)-B_{11}\cos(\delta_1-\delta_1)\right] \\ &+V_1V_2\left[G_{12}\sin(\delta_1-\delta_2)-B_{12}\cos(\delta_1-\delta_2)\right] \\ &+V_1V_3\left[G_{13}\sin(\delta_1-\delta_3)-B_{13}\cos(\delta_1-\delta_3)\right] \\ &= 4.79\cdot V_1^2 - 0.96\cdot V_1V_3\sin(\delta_1-\delta_3)-4.81\cdot V_1V_3\cos(\delta_1-\delta_3) \end{aligned}$$

$$
\begin{aligned}
Q_2(V,\delta) &= V_2V_1\left[G_{21}\sin(\delta_2-\delta_1)-B_{21}\cos(\delta_2-\delta_1)\right] \\
&\quad +V_2V_2\left[G_{22}\sin(\delta_2-\delta_2)-B_{22}\cos(\delta_2-\delta_2)\right] \\
&\quad +V_2V_3\left[G_{23}\sin(\delta_2-\delta_3)-B_{23}\cos(\delta_2-\delta_3)\right] \\
&= 4.79\cdot V_2^2-0.96\cdot V_2V_3\sin(\delta_2-\delta_3)-4.81\cdot V_2V_3\cos(\delta_2-\delta_3)
\end{aligned}
$$

$$
\begin{aligned}
Q_3(V,\delta) &= V_3V_1\left[G_{31}\sin(\delta_3-\delta_1)-B_{31}\cos(\delta_3-\delta_1)\right] \\
&\quad +V_3V_2\left[G_{32}\sin(\delta_3-\delta_2)-B_{32}\cos(\delta_3-\delta_2)\right] \\
&\quad +V_3V_3\left[G_{33}\sin(\delta_3-\delta_3)-B_{33}\cos(\delta_3-\delta_3)\right] \\
&= -0.96\cdot V_3V_1\sin(\delta_3-\delta_1)-4.81\cdot V_3V_1\cos(\delta_3-\delta_1) \\
&\quad -0.96\cdot V_3V_2\sin(\delta_3-\delta_2)-4.81\cdot V_3V_2\cos(\delta_3-\delta_2)+9.58\cdot V_3^2
\end{aligned}
$$

Step 3: Set up the power balance equations for each bus, by using the AC power flow equations from step 2 and the net injection equations of (3.25) and (3.68). The nonlinear line current constraints are set up by using (3.83):

a) The power balance at each bus:

$$
\begin{aligned}
&P_{g1}+C_{P1}-P_{load,1}-P_1(V,\delta)=P_{g1}+C_{P1}-P_1(V,\delta)=0 \\
&P_{g2}+C_{P2}-P_{load,2}-P_2(V,\delta)=P_{g2}+C_{P2}-P_2(V,\delta)-0.3=0 \\
&P_{g3}+C_{P3}-P_{load,3}-P_3(V,\delta)=P_{g3}+C_{P3}-P_3(V,\delta)-0.4=0 \\
&Q_{g1}+C_{Q1}-Q_{load,1}-Q_1(V,\delta)=Q_{g1}+C_{Q1}-Q_1(V,\delta)=0 \\
&Q_{g2}+C_{Q2}-Q_{load,2}-Q_2(V,\delta)=Q_{g2}+C_{Q2}-Q_2(V,\delta)-0.06=0 \\
&Q_{g3}+C_{Q3}-Q_{load,3}-Q_3(V,\delta)=Q_{g3}+C_{Q3}-Q_3(V,\delta)-0.08=0
\end{aligned}
$$

b) The current constraints of the three lines:

i) Line L1: Outage

ii) Line L2:

$$
\begin{aligned}
&(V_1\cos\delta_1-V_3\cos\delta_3)^2+(V_1\sin\delta_1-V_3\sin\delta_3)^2-\left(\frac{I_{13}^{max}}{\sqrt{g_{13}^2+b_{13}^2}}\right)^2\le 0 \\
&(V_1\cos\delta_1-V_3\cos\delta_3)^2+(V_1\sin\delta_1-V_3\sin\delta_3)^2-\frac{0.5^2}{0.96^2+4.81^2}\le 0 \\
&(V_1\cos\delta_1-V_3\cos\delta_3)^2+(V_1\sin\delta_1-V_3\sin\delta_3)^2-0.010392\le 0
\end{aligned}
$$

iii) Line L3:

$$\left(V_2\cos\delta_2 - V_3\cos\delta_3\right)^2 + \left(V_2\sin\delta_2 - V_3\sin\delta_3\right)^2 - \left(\frac{I_{23}^{max}}{\sqrt{g_{23}^2 + b_{23}^2}}\right)^2 \le 0$$

$$\left(V_2\cos\delta_2 - V_3\cos\delta_3\right)^2 + \left(V_2\sin\delta_2 - V_3\sin\delta_3\right)^2 - \frac{0.5^2}{0.96^2 + 4.81^2} \le 0$$

$$\left(V_2\cos\delta_2 - V_3\cos\delta_3\right)^2 + \left(V_2\sin\delta_2 - V_3\sin\delta_3\right)^2 - 0.010392 \le 0$$

Step 4: Set up the equations that maintain the power factor of the loads at each load bus:

$$0.2\cdot C_{P2} - C_{Q2} = 0$$
$$0.2\cdot C_{P3} - C_{Q3} = 0$$

Step 5: Set up the final OPF problem, recognizing that bus 1 is a generator bus without connected loads and bus 2 and 3 have no connected generators. Thus, the number of decision variables could be reduced. The angle of the slack bus is the reference angle of the system; thus, it is fixed at zero radians.

$$\begin{aligned}\text{Min } f = {} & 0\cdot P_{g1} + 0\cdot Q_{g1} + 1\cdot C_{P2} + 1\cdot C_{P3} + 1\cdot C_{Q2} + 1\cdot C_{Q3} \\ & + 0\cdot V_1 + 0\cdot V_2 + 0\cdot V_3 + 0\cdot\delta_1 + 0\cdot\delta_2 + 0\cdot\delta_3\end{aligned}$$

$$P_{g1} - 0.96\cdot V_1^2 + 0.96\cdot V_1V_3\cos\left(\delta_1 - \delta_3\right) - 4.81\cdot V_1V_3\sin\left(\delta_1 - \delta_3\right) = 0$$

$$C_{P2} - 0.96\cdot V_2^2 + 0.96\cdot V_2V_3\cos\left(\delta_2 - \delta_3\right) - 4.81\cdot V_2V_3\sin\left(\delta_2 - \delta_3\right) - 0.3 = 0$$

$$\begin{aligned}& C_{P3} + 0.96\cdot V_3V_1\cos\left(\delta_3 - \delta_1\right) - 4.81\cdot V_3V_1\sin\left(\delta_3 - \delta_1\right) \\ & + 0.96\cdot V_3V_2\cos\left(\delta_3 - \delta_2\right) - 4.81\cdot V_3V_2\sin\left(\delta_3 - \delta_2\right) - 1.92\cdot V_3^2 - 0.4 = 0\end{aligned}$$

$$Q_{g1} - 4.79\cdot V_1^2 + 0.96\cdot V_1V_3\sin\left(\delta_1 - \delta_3\right) + 4.81\cdot V_1V_3\cos\left(\delta_1 - \delta_3\right) = 0$$

$$C_{Q2} - 4.79\cdot V_2^2 + 0.96\cdot V_2V_3\sin\left(\delta_2 - \delta_3\right) + 4.81\cdot V_2V_3\cos\left(\delta_2 - \delta_3\right) - 0.06 = 0$$

$$\begin{aligned}& C_{Q3} + 0.96\cdot V_3V_1\sin\left(\delta_3 - \delta_1\right) + 4.81\cdot V_3V_1\cos\left(\delta_3 - \delta_1\right) \\ & + 0.96\cdot V_3V_2\sin\left(\delta_3 - \delta_2\right) + 4.81\cdot V_3V_2\cos\left(\delta_3 - \delta_2\right) - 9.58\cdot V_3^2 - 0.08 = 0\end{aligned}$$

$$\left(V_1\cos\delta_1 - V_3\cos\delta_3\right)^2 + \left(V_1\sin\delta_1 - V_3\sin\delta_3\right)^2 - 0.010392 \le 0$$
$$\left(V_2\cos\delta_2 - V_3\cos\delta_3\right)^2 + \left(V_2\sin\delta_2 - V_3\sin\delta_3\right)^2 - 0.010392 \le 0$$

$$0.2 \cdot C_{P2} - C_{Q2} = 0$$
$$0.2 \cdot C_{P3} - C_{Q3} = 0$$

$$0 \le P_{g1} \le 1.0$$
$$-0.2 \le Q_{g1} \le 0.4$$
$$0 \le C_{P2} \le 0.3$$
$$0 \le C_{P3} \le 0.4$$
$$0 \le C_{Q2} \le 0.06$$
$$0 \le C_{Q3} \le 0.08$$

$$0.95 \le V_1 \le 1.05$$
$$0.95 \le V_2 \le 1.05$$
$$0.95 \le V_3 \le 1.05$$
$$0 \le \delta_1 \le 0$$
$$-\pi \le \delta_2 \le \pi$$
$$-\pi \le \delta_3 \le \pi$$

Appendix VII Simulation Results HL1 RBTS

State Transition Method: The Distributions of the Indices

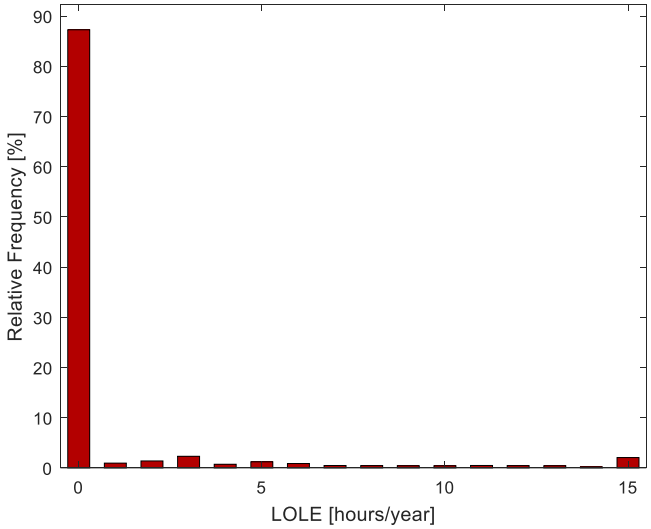

Figure 7.2: The LOLE distribution by the state transition method.

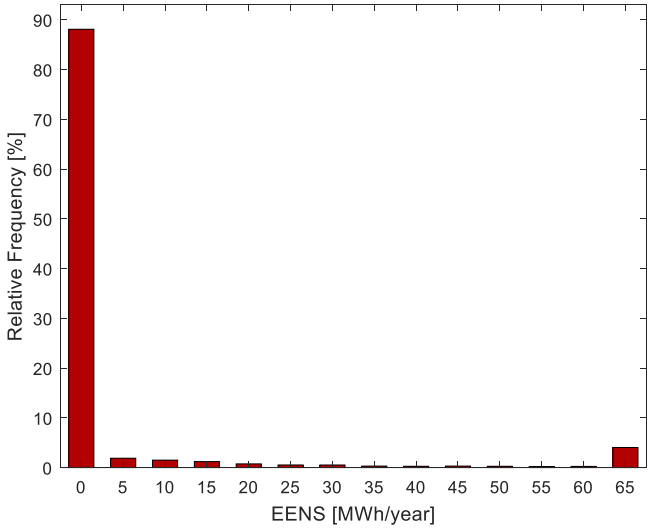

Figure 7.3: The EENS distribution by the state transition method.

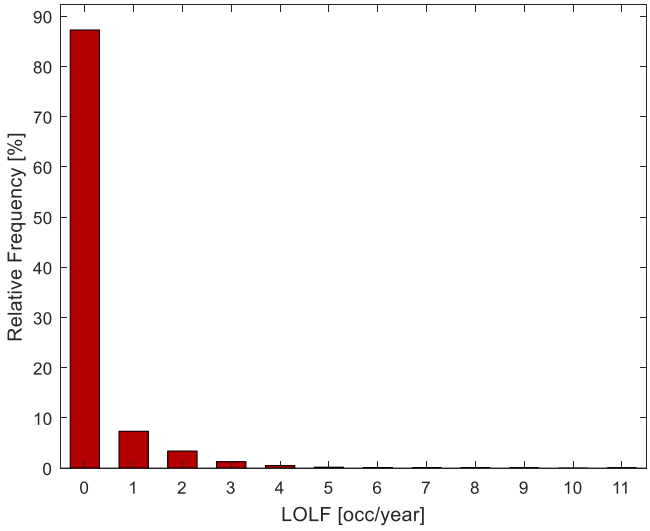

Figure 7.4: The LOLF distribution by the state transition method.

Convergence processes of the state transition method indices

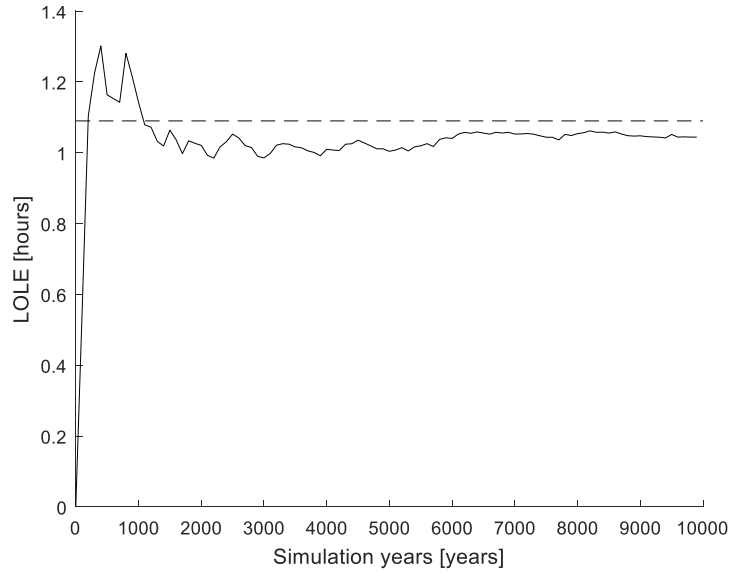

Figure 7.5: The convergence process of the LOLE index plotted together with the benchmark result of Billinton and Huang.

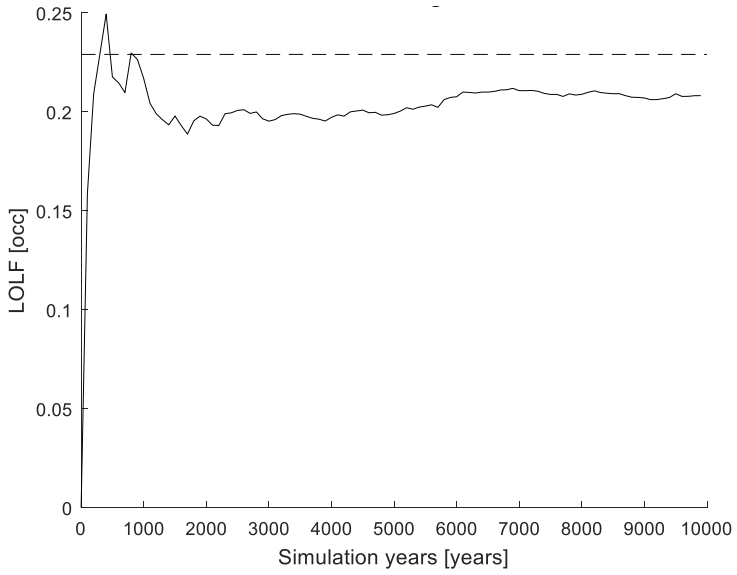

Figure 7.6: The convergence process of the LOLF index plotted together with the benchmark result of Billinton and Huang.

Table 7.14: The indices and the CVs of the RBTS convergence example.

N=10 000 years	LOLE [hours/year]	EENS [MWh/year]	LOLF [#/year]
Value	1.0372	9.5473	0.2074
CV	0.0391	0.0553	0.0315

Appendix VIII Simulation Results HLI RTS

State Sampling

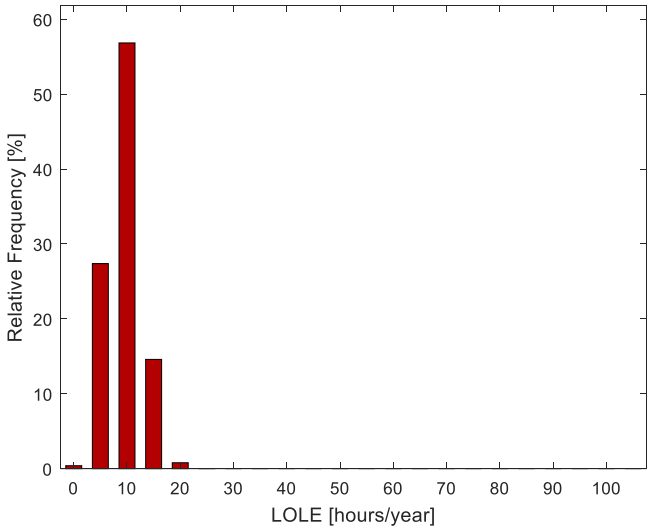

Figure 7.7: The LOLE distribution by the state sampling method.

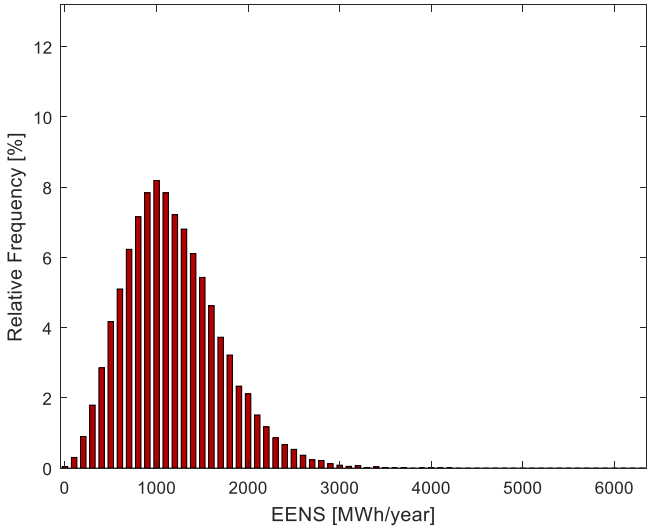

Figure 7.8: The EENS distribution by the state sampling method.

State Transition

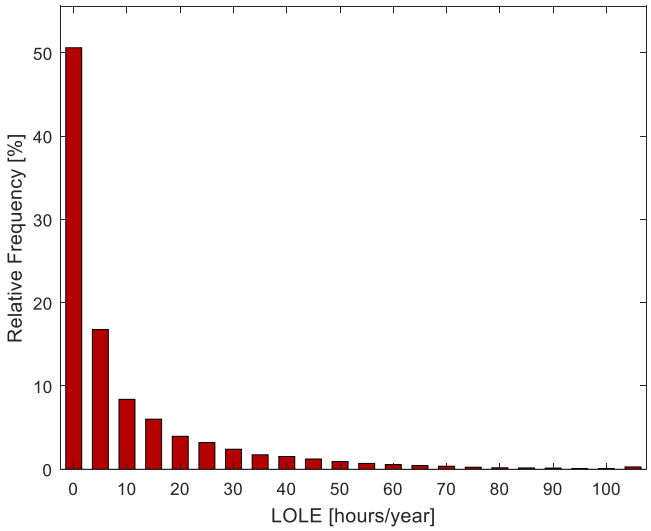

Figure 7.9: The LOLE distribution by the state transition method

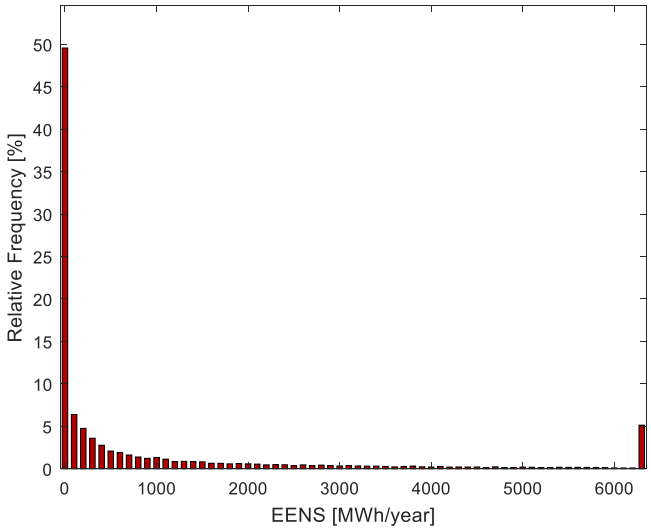

Figure 7.10: The EENS distribution by the state transition method.

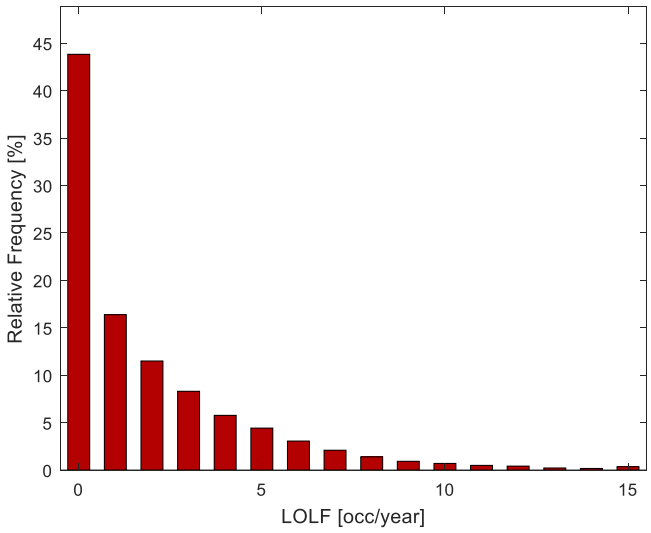

Figure 7.11: The LOLF distribution by the state transition method.

State Duration, Large Units with De-Rated States

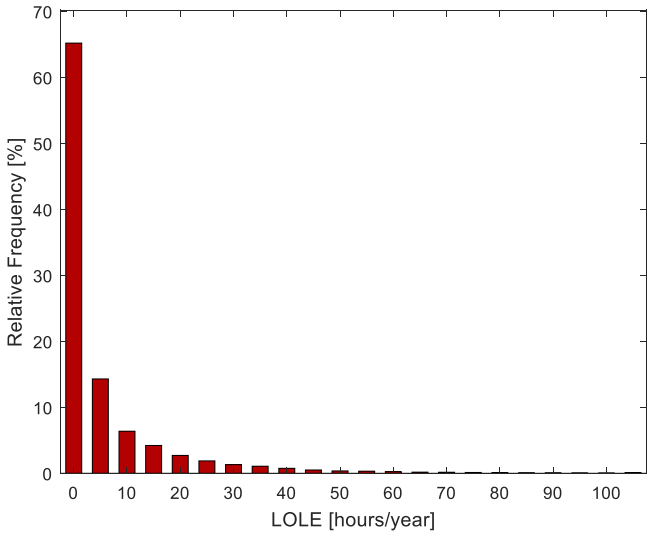

Figure 7.12: The LOLE distribution by the state duration method.

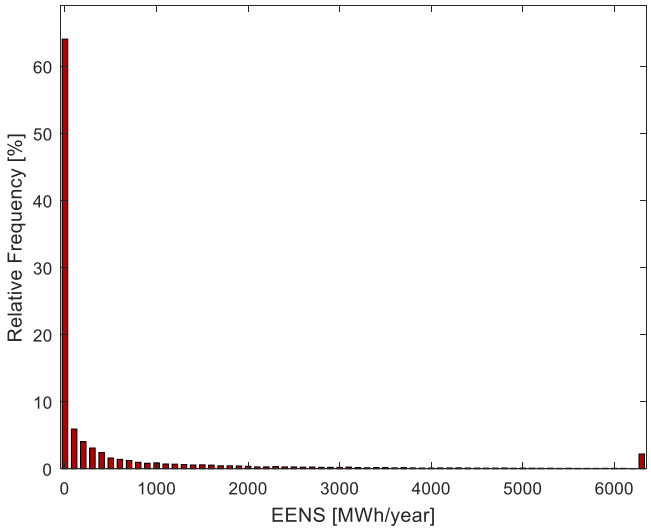

Figure 7.13: The EENS distribution by the state duration method.

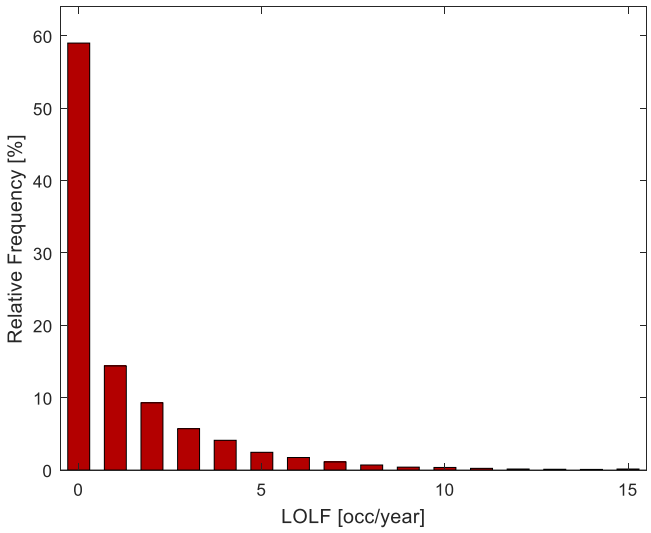

Figure 7.14: The LOLF distribution obtained by the state duration method.

Convergence processes of the state duration method indices

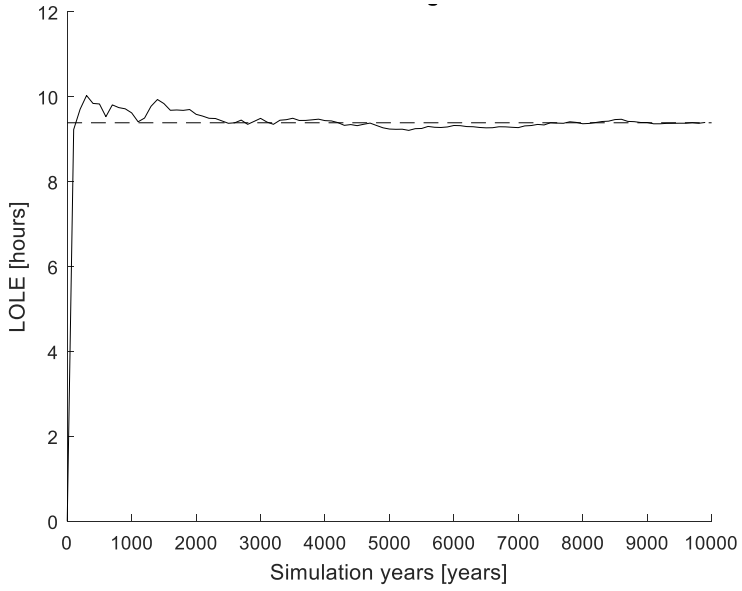

Figure 7.15: The convergence process of the LOLE index plotted together with the benchmark result of Billinton and Huang.

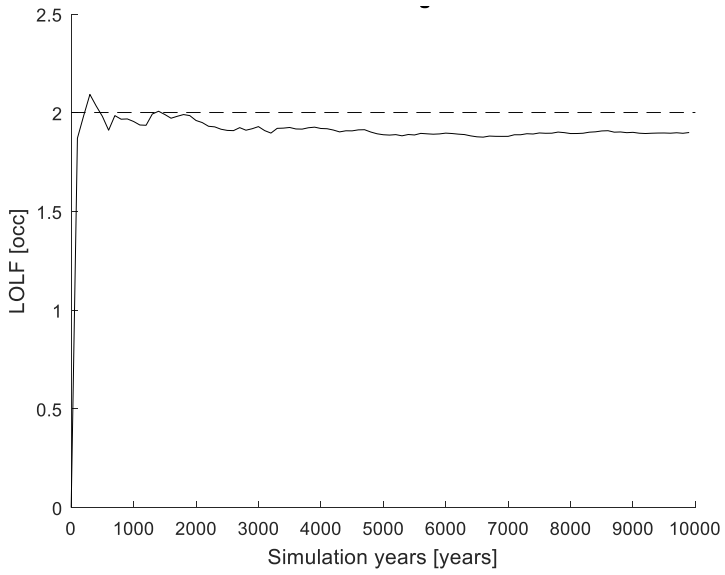

Figure 7.16: The convergence process of the LOLF index plotted together with the benchmark result of Billinton and Huang.

Table 7.15: The indices and the CVs of the RTS convergence example.

N=10 000 years	LOLE [hours/year]	EENS [MWh/year]	LOLF [#/year]
Value	9.4527	1193.3287	1.9066
CV	0.0174	0.0252	0.0140

Appendix IX HLII DC

RBTS State Sampling

Table 7.16: The CVs of the RBTS DC CYPL indices by state sampling.

Bus	LOLE	EENS
2	-	-
3	0.0054	0.0071
4	-	-
5	0.4454	0.4454
6	0.0140	0.0140
System	0.0050	0.0063

Table 7.17: The CVs of the RBTS DC HPL indices by state sampling.

Bus	LOLE	EENS
2	-	-
3	0.0422	0.0618
4	-	-
5	0.4454	0.4625
6	0.0145	0.0151
System	0.0139	0.0148

RBTS State Transition

Table 7.18: The CVs of the RBTS DC HPL indices by state transition.

Bus	LOLE	EENS
2	0.5590	0.5748
3	0.0312	0.0449
4	-	-
5	0.2237	0.2315
6	0.0116	0.0118
System	0.0109	0.0114

RTS State Sampling

Table 7.19: The CVs of the RTS DC CYPL indices by state sampling.

Bus	LOLE	EENS
1	-	-
2	-	-
3	1.0000	1.0000
4	1.0000	1.0000
5	0.7064	0.7064
6	0.4985	0.4985
7	0.0269	0.0269
8	1.0000	1.0000
9	0.0015	0.0017
10	0.0103	0.0125
13	-	-
14	0.0022	0.0028
15	-	-
16	-	-
18	0.0244	0.0335
19	0.0048	0.0059
20	0.2130	0.2614
System	0.0015	0.0021

Table 7.20: The CVs of the RTS DC HPL indices by state sampling.

Bus	LOLE	EENS
1	-	-
2	-	-
3	-	-
4	-	-
5	1.0000	1.0000
6	0.4985	0.5036
7	0.0249	0.0259
8	0.5762	0.5848
9	0.0141	0.0165
10	0.1249	0.1583
13	-	-
14	0.0262	0.0320
15	-	-
16	-	-
18	0.4454	0.4930
19	0.0559	0.0667
20	-	-
System	0.0120	0.0170

RTS State Transition

Table 7.21: The CVs of the RTS DC HPL indices by state transition.

Bus	LOLE	EENS
1	-	-
2	-	-
3	-	-
4	0.6983	0.7589
5	0.4618	0.4824
6	0.3801	0.3772
7	0.0214	0.0216
8	0.4626	0.4839
9	0.0140	0.0169
10	0.0886	0.1207
13	-	-
14	0.0227	0.0286
15	-	-
16	-	-
18	0.2395	0.3571
19	0.0431	0.0547
20	1.0000	1.0000
System	0.0119	0.0173

Appendix X HLII AC

RBTS State Sampling

Table 7.22: The CVs of the RBTS AC indices by state sampling.

Bus	LOLE	EENS
2	-	-
3	0.0341	0.0480
4	-	-
5	0.5762	0.5919
6	0.0136	0.0145
System	0.0129	0.0141

RBTS State Transition

Table 7.23: The CVs of the RBTS AC indices by state transition.

Bus	LOLE	EENS
2	0.5590	0.5748
3	0.0240	0.0364
4	1.0000	1.0000
5	0.2214	0.2306
6	0.0105	0.0115
System	0.0100	0.0110

RTS State Sampling

Table 7.24: The CVs of the RTS AC indices by state sampling.

Bus	LOLE	EENS
1	-	-
2	-	-
3	0.1099	0.4669
4	-	-
5	1.0000	1.0000
6	0.0243	0.0300
7	0.0230	0.0238
8	0.4985	0.8922
9	0.0127	0.0149
10	0.0236	0.1440
13	-	-
14	0.0127	0.0288
15	0.1160	0.1187
16	-	-
18	0.0521	0.4924
19	0.0127	0.0578
20	0.1160	0.1609
System	0.0105	0.0151

RTS State Transition

Table 7.25: The CVs of the RTS AC indices by state transition.

Bus	LOLE	EENS
1	-	-
2	-	-
3	0.0728	0.2674
4	0.4702	0.5075
5	0.4648	0.4770
6	0.0248	0.0300
7	0.0205	0.0209
8	0.2120	0.4844
9	0.0128	0.0154
10	0.0207	0.0922
13	-	-
14	0.0128	0.0259
15	0.0762	0.0783
16	-	-
18	0.0443	0.2383
19	0.0128	0.0488
20	0.0758	0.4935
System	0.0100	0.0154